10-22-2020 1:30 PM

Hargraves Crater Ejecta and Implications for Impact Processes

Leah E. Sacks, *The University of Western Ontario*

Supervisor: Osinski, Gordon R., *The University of Western Ontario*
Co-Supervisor: Tornabene, Livio L., *The University of Western Ontario*
A thesis submitted in partial fulfillment of the requirements for the Master of Science degree in Geology
© Leah E. Sacks 2020

Abstract

Impact craters and their ejecta deposits offer insights into the structure and composition of planet crusts. Hargraves Crater, Mars, demonstrates an unusual balance of exposure and preservation in its ejecta. Analysing its morphologic, morphometric, thermophysical, and stratigraphic characteristics, we interpret two predominant units: an underlying ballistic lithic breccia and an overlying impact melt-bearing deposit. The lower unit is a lithic breccia composed of sub-angular, unsorted clasts (~10-12 m mean diameter), while the overlying unit is a smooth, dark toned, smaller clast-bearing (~1 m diameter at image resolution) impact melt-bearing unit with polygonal fracturing. There appears to be a sharp contact between these units visible through "windows" in the overlying unit that reveal the underlying breccia. These orbital observations link well with terrestrial field observations. Future study of this "Hargraves-type" ejecta, which reveals the stratigraphy and structure of ejecta deposits, will improve our understanding of ejecta and ejecta emplacement processes.

Keywords

Summary for Lay Audience

Impact craters are windows into the insides of planets. When an asteroid collides with a planet, the resulting pit is called a crater. The debris around the crater from the impact is termed the ejecta blanket. We study ejecta to learn about the inside of the impacted planet as well as the surface of the planet. One of the topics we do not fully understand about ejecta is how it moves from inside the crater to its final position around the outside of the crater. To study this question, this thesis focuses on the ejecta blanket of a crater on Mars, known as Hargraves Crater. Hargraves Crater offers unusual access to the interior of the ejecta. Using close-up images of the ejecta, we study the shapes, sizes, positions, and rate of temperature change of visible rocks. From the results, we determine that the ejecta is primarily two units: a lower unit called a lithic breccia made of broken rock fragments (~10 m average diameter) with no structure thrown from the crater, and an upper unit, an impact melt-bearing rock, made of a combination of rock fragments (~1 m average diameter) and melted rock that flowed out of the crater. These units show that there are at least two parts to how the ejecta blanket forms, one for each unit. We are able to examine how these two units relate to each other due to holes in the top unit that allow us to observe the lower unit. This unusual visibility of the inside of the ejecta at Hargraves Crater facilitated the observation of both units and how they relate, thus we suggest studying other examples of crater ejecta with interior units visible in order to learn more about the ways that ejecta leaves the crater and forms the ejecta blanket. We also suggest that it may be important to try to understand why only a few craters show the visibility we see at Hargraves Crater. By studying these types of craters, we may be better prepared for future space missions and studies of craters and of Mars.

Co-Authorship Statement

Chapter 1. Chapter 1 of this thesis was written by Leah Sacks with edits and advice from Gordon Osinski and Livio Tornabene. Some images within the chapter were modified from or taken from papers belonging to other authors, all of which are attributed to those authors within the captions.

Chapter 2. Chapter 2 is a co-authored manuscript written by Leah Sacks with edits and advice from Gordon Osinski and Livio Tornabene. Mapping of the full Hargraves Crater ejecta blanket was completed by Leah Sacks. Mapping of the focused exposure to the south was completed by Racel Sopoco and slightly adjusted by Leah Sacks. Mapping and analysis of clast content was completed by Leah Sacks. Interpretations of the units were completed with input from Livio Tornabene, Gordon Osinski, and Racel Sopoco.

Chapter 3. Chapter 3 was written by Leah Sacks with edits and advice from Gordon Osinski and Livio Tornabene. Additional Hargraves-type craters were identified, and images suggested by Livio Tornabene, Racel Sopoco, and Leah Sacks.

All three chapters were adjusted for final submission after edits and suggestions from Phil McCausland, Phil Stooke, and Cindy Mora-Stock.

Acknowledgments

Table of Contents

List of Tables

List of Figures

List of Appendices

Chapter 1

1   Introduction

As one of the few surface features common to almost every planetary body in our solar system, impact craters are a significant topic within planetary science. Understanding, and studying the ways that craters form and their effects on the surrounding surface is integral to our exploration of the solar system. Impact craters provide insights into astrobiology, planetary surfaces, inner planetary structures, and much more. This information provides much of the basis for exploration missions and future study of planetary bodies.

Impact craters are formed from the collision of two planetary objects. Commonly, smaller bodies, such as asteroids, collide with the surface of a planet or larger asteroid. The resulting forces and shock waves displace material from the location of the impact, leaving behind a depression, commonly surrounded by some of the excavated material. This material is known as the ejecta blanket. This study explores the ejecta deposits at Hargraves Crater, Mars in order to investigate impact ejecta processes. The unusual exposure and preservation of the ejecta blanket observed at this crater provides a unique opportunity to examine the characteristics of the inner structure of the ejecta deposits. By mapping the Hargraves Crater ejecta and then investigating some of the best exposures at the crater in high-resolution, we can constrain ejecta emplacement mechanisms on Mars. This thesis interprets the findings of mapping, clast measurement, and morphologic and stratigraphic analysis at Hargraves Crater with the purpose of understanding the origins, nature, and emplacement methods of the units. We will then place the findings within the context of the current literature to further our understanding of ejecta emplacement processes on Mars as well as throughout the solar system.

1.1   Impact Cratering

1.1.1   Craters and the Impact Cratering Process

Impact craters are typically classified based on morphology. Structures termed "simple" craters have a simple bowl shape and range from centimetres to tens of kilometres,

depending on the gravity, and composition of the planetary surface they form on. In contrast, craters known as "complex" craters range up to hundreds of kilometres in size and show signs of collapse which forms a flatter infilled crater floor, terraces in the crater walls, and a central topographic high termed as central uplift. The crater diameter at which point complex craters form rather than simple craters depends on the target material as well as surface gravity (Pike, 1980; Boyce and Garbeil, 2007; Robbins and Hynek, 2012; Osinski et al., 2019). When the diameter of a crater is near the transition between a simple and complex crater morphology, it may exhibit some of the signs of a complex crater, but not all, which are classified as "transitional" craters. These craters commonly show signs of collapse and terracing but may not develop all of the characteristics of a complex crater (Tornabene et al., 2018). At large crater diameters, multiple concentric crater rings may form a structure termed a "multi-ring basin."

The impact cratering process is divided into three stages, contact and compression, excavation, and modification, but crater formation happens over a very short period of time and the stages are not entirely temporally distinct. An impactor collides with a surface, initiating the contact and compression stage. The momentum of the impactor transfers into the ground as the object compresses against the target surface. The object continues into the surface to a depth of about 1.5 times the radius of the object (Kieffer and Simonds, 1980), where a shock wave radiates spherically outward into the ground from the impactor (Melosh, 1989). During this stage, part of the shock wave reflects back up through the impactor as a rarefaction wave (Ahrens and O'Keefe, 1972). The shock wave, the rarefaction wave, the surface of the ground and the physical impacting body all interact to displace material downward and outward from the impactor, forming a bowl-shaped depression that is referred to as the "transient cavity" (Fig. 1, first frame).
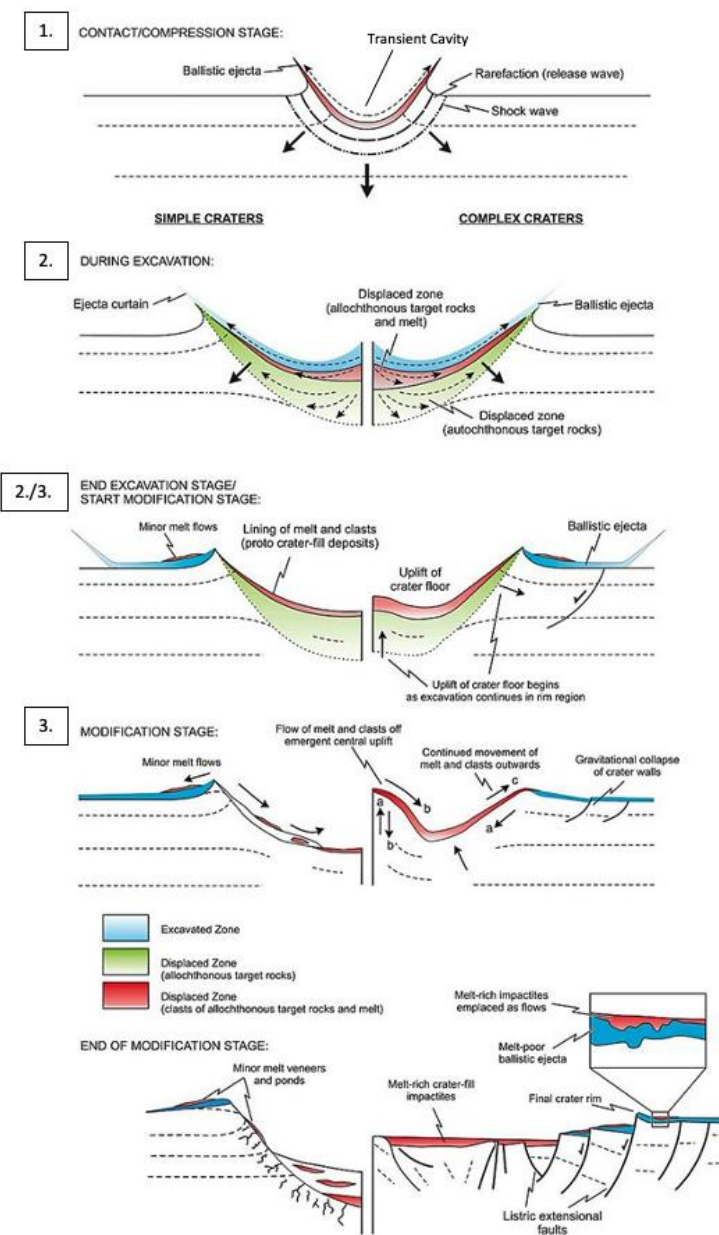
Figure 1 The stages of the impact cratering process. Left sides of the figures show a simple crater, right sides of the figures show a complex crater. (1) The contact and compression stage. (2) The excavation stage. (2/3) The excavation stage and the beginning of the modification stage. (3) The modification stage in process. Blue colours show excavated material, greens show displaced rock and rock fragments, reds show displaced melt and rock fragments. Arrows indicate the direction of movement. Figure modified from (Osinski and Pierazzo, 2012, which is modified from Osinski et al., 2011).

The excavation stage of crater formation is considered to begin somewhere between the generation of the shock wave and the formation of the transient cavity. The force, pressure, and shock wave of the impact cause the immediate surrounding target material to vaporize (Melosh, 1989). At the highest shock levels, >>50GPa (Osinski et al., 2018 and references therein), where 1 GPa is 9869.23 times the pressure of a standard atmosphere (atm), melting and vaporization occur. Outside the vaporized and melted material, and beyond the Hugoniot elastic limit, but at shock pressures greater than ~5 GPa, material may be crushed, and shock metamorphosed. At levels less than 5 GPa, the material is fractured (Osinski and Pierazzo, 2012). Some of the material is displaced downward in the crater and much of it is moved out beyond the rim of the transient cavity (Fig. 1, second and third frames). The collective term for any rock and impact melt transported beyond the transient cavity rim is ejecta (Osinski and Pierazzo, 2012; Osinski et al., 2012). The subsurface interaction between the rarefaction wave from the front of the shock wave as it refracts off the surface and the parts of the shock wave that have yet to reach the surface launches surficial crustal material off the surface at high velocities, meters to thousands of meters per second, depending on the impacted planetary body (Melosh, 1989).

As the shockwave moves beyond the transient cavity and excavation of material slows, the walls and floor of the transient cavity collapse due to gravity. The following period of crater collapse is known as the modification stage (Fig. 1, fourth and fifth frames). The extent of modification and collapse with respect to the so-called transient cavity is generally minimal for simple craters and progressively becomes more extensive as crater diameter generally increases moving into transitional and then complex craters. Indeed, when a crater is large enough with respect to the mass/gravity of the body, the strength of the target materials is insufficient to oppose the force of gravity, resulting in extensive collapse and the final crater will take the form of a complex crater (Fig. 1). In these craters, grabens may form along the walls of the crater as material collapses back inward along listric faults. The floor of the crater is uplifted to accommodate material moving back into the centre of the impact. The force involved with the collapse of the crater walls and the formation of a central uplift may also initiate a second round of target rock displacement just as the excavation stage is ending. In some cases, momentum from

collapse and uplift may be transferred to impact melt deposits settled on the floor of the crater transporting some of these materials beyond the rim of the transient cavity, and thereby emplacing melt as veneers, ponds and flows (e.g., Osinski et al., 2011). The modification stage does not have a defined termination point (French, 1998). Ongoing collapse and crater degradation continue to change the crater in perpetuity.

1.1.2 Impact Crater Ejecta

Impact crater ejecta, the material moved beyond the rim of the transient cavity, is an important resource for understanding impact cratering and the impact crater emplacement process. As craters displace material from significant depths within the surface of a planet, that material contains samples from many layers of the surface. Using orbiters, we can then study those different layers. As much of planetary science happens remotely and we cannot yet travel to the planets to view those layers in place, this access to the inner structures of the planet is significant and valuable. Studying ejecta allows researchers to take advantage of the access to the subsurface provided by an ejecta blanket. From examining ejecta blankets, we know that ejecta more distal to the crater rim is from more surficial layers, while material closer to the rim comes from deeper in the subsurface (Oberbeck et al., 1975; Osinski et al., 2012). Similarly, deeper ejecta material is often found overlying surficial ejecta material as it is ejected slightly later than that from the surface, inverting the stratigraphy. The continuous ejecta is the term given to material closer to the crater that prior to erosion forms an uninterrupted swath of material radiating form the crater centre and extending for 1-2 crater radii (Melosh, 1989). In contrast, discontinuous ejecta is the term used to describe the patchy areas of ejecta that are distal to the crater rim and not connected to the main body of ejected material. In order to make the most of our knowledge of ejecta blankets, however, it is first necessary to understand how ejecta blankets form following an impact.

While the crater formation process has a commonly accepted set of stages, the understanding of ejecta emplacement is less complete. Both surface properties and impactor properties can affect ejecta. The presence of water, the impactor velocity, or significant topography are thought to have an effect, particularly on the distribution of the ejecta. However, outside of these specific circumstances, there is debate over the actual

depositional mechanisms of ejecta for craters throughout the Solar System. To begin with, a number of early crater and ejecta studies were performed on explosion and nuclear tests. Roberts (1966) studied thermo-nuclear explosions and a number of small craters to learn about basic characteristics of ejecta blankets and to propose explanations for impact processes. This and other early studies were then complemented by what became the foundation of ejecta emplacement studies: a study of lunar craters and ballistic ejecta emplacement by Verne Oberbeck (1975).

Oberbeck's (1975) seminal work both assessed potential emplacement mechanisms, specifically for the Moon, and developed the resulting mechanism based on his findings. For the study, Oberbeck examined two proposed theories for ejecta emplacement: overland base-surge and ballistic sedimentation. Essentially, he questioned whether the ejecta was emplaced across the surface from the base of the explosive cloud or aerially as ballistics. In appearance, ballistic sedimentation would look more like a "splash" of falling material while base surge would have a similar appearance to a ground-hugging pyroclastic flow, incorporating atmosphere as it expanded radially. Determining that base-surge would require an atmosphere, Oberbeck noted that as the Moon lacks an atmosphere, base-surge must be ruled out for the deposition of lunar ejecta blankets. Studying the ejecta blanket on the Moon, Oberbeck (1975) presented a model for ballistic sedimentation that is largely unchanged today (Fig. 2). Target material is ejected in ballistic trajectories of varying angles and velocities related to location relative to the impactor and the depth of excavation. Smaller target fragments travel further with higher velocities while larger ones obtain lower velocities and remain proximal to the rim of the transient cavity. As part of the theory of ballistic sedimentation, Oberbeck (1975) additionally presented the idea that secondary impacts from the ballistically emplaced material hitting the surface causes the surrounding materials to be displaced and incorporated into the evolving ejecta deposit. These incorporated materials are known as secondary ejecta. Foundationally, the total amount of ejecta material decreases with distance from the crater. Similarly, the ratio of primary ejecta (material originating from the formation of the transient cavity) to secondary ejecta (target material mobilized by the interaction of the primary ejecta with the target surface) varies with distance from the crater. At distal locations, primary ejecta is < 5% of the total ejecta (Hörz et al., 1983).

Hörz et al. (1983) and Chao (1976) debated this theory of ballistic sedimentation and secondary material incorporation as the emplacement mechanism for the Bunte Breccia ejecta layer of the Ries impact structure in Germany. As one of the few terrestrial craters with preserved ejecta deposits, the Ries crater provides important insight. Hörz et al. (1983) validated the ideas of incorporated secondary material posited by Oberbeck (1975) by examining cores at the Ries crater. Chao (1976) argued that the Bunte Breccia was emplaced as an overland flow that was not airborne. Hörz et al. (1983) refuted these interpretations and held that the same observations used to support the argument, mainly striations that shows overland movement, were easily explained by the debris flows that are part of the turbulent emplacement of ejecta as a result of ballistic sedimentation and secondary cratering. The incorporation of large amounts of secondary material, one of Chao's (1976) pieces of evidence, is consistent with Hörz's argument (Oberbeck, 1975; Horz et al., 1983), though some incorporation is possible in both explanations. Going forward, ballistic sedimentation and incorporated secondary ejecta were commonly accepted as the primary depositional mechanisms associated with crater ejecta deposits. Notably, this process did not attempt to explain impact melt or impact melt-bearing deposits, which are discussed later in this chapter.
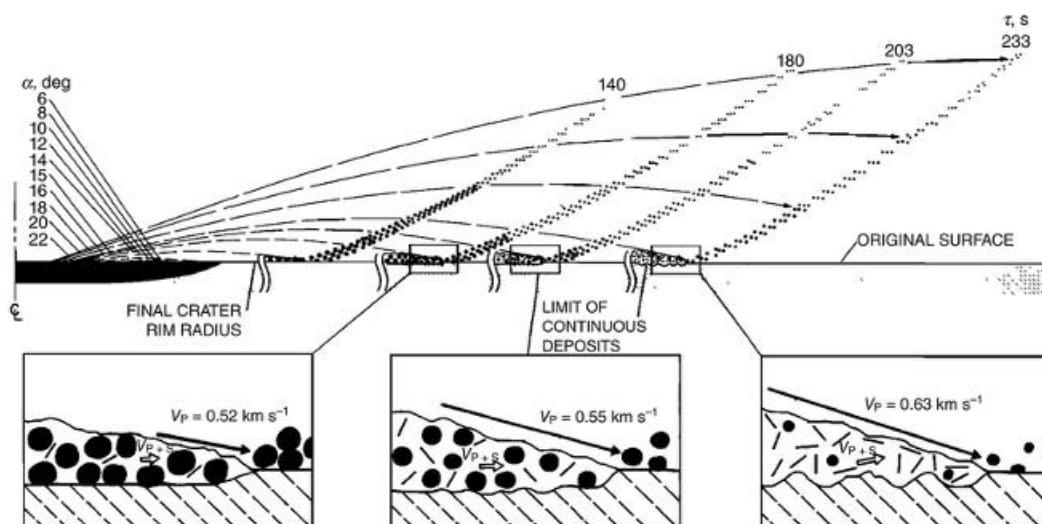
Figure 2 Oberbeck's (1975) model of ballistic sedimentation and the incorporation of increasing amount of secondary material with increased distance from the crater. Figure from Oberbeck 1975.

Many ejecta studies focused on the very visible ejecta blankets on the Moon and the few available on Earth, prior to good images from Mars. Once ejecta studies began on Mars, understanding of ejecta emplacement developed further. Carr et al. (1977) noted a morphologic distinction between lunar craters and what were termed martian rampart (McCauley, 1973; Carr et al., 1977) and martian radial craters (Carr et al., 1977), while acknowledging the presence of some lunar-like craters on Mars as well. For rampart and radial craters, though the craters themselves are relatively similar, the ejecta blankets were observed to be quite different in appearance. Carr et al. (1977) contrasted the sometimes multi-layered "lobate" ejecta with distant thick edged "ramparts" with the "rubbled" lunar ejecta blankets that pinch out at their distal edges. Barlow et al. (2000; 2005) would later classify specific "layered" morphologies within the total set of martian craters. To explain the distinction between martian and lunar craters, Carr et al. (1977) proposed that "radial flow" or large mass movements during emplacement helped to build the thicker edges of what they termed "rampart" craters. Essentially, with enough velocity and momentum ejecta material continues to flow away from the crater after hitting the ground, an effect that is termed "radial flow." Obvious flow directions away from the crater were cited as the evidence for radial flow while solely aerial emplacement was eliminated as ejecta moved around obstacles rather than draping them (Carr et al., 1977). These signs of flow and resulting ramparts can be likened to the types of secondary debris flows Hörz et al. (1983) described at the Ries impact crater and used to refute the idea of simple overland flow. Thus, providing further support for ballistic sedimentation with incorporation of secondary material as an emplacement mechanism, while also identifying an important distinguishing feature between lunar and martian craters.

While Carr et al. (1977) proposed one explanation for the rampart morphology, the signs of flow, multiple layers of ejecta, and other morphologic differences prompted several other emplacement theories involving atmosphere, volatiles, and grain flow. Schultz and Gault (1979) built on the work of Carr et al. (1977) and proposed that the layered structure of martian craters came from ballistic emplacement followed by additional stages of emplacement of a set of particles that were small enough to be subject to atmospheric drag force that initially kept them airborne. Barnouin-Jha et al. (1999) and

then Barnouin-Jha and Schultz (1999) continued to develop the idea of atmospheric incorporation into the ejecta plume as a means of producing the layered morphology seen in the ejecta blankets of Mars. A further study by Wada and Barnouin-Jha (2006) focused on the fact that unlike the Moon, Mars does have an atmosphere and has volatiles in the crust and argued that this distinguishing characteristic is likely an influential factor in the unique layering observed on Mars. The study determined simple granular flow over an unconsolidated, or eroded surface would be difficult without some element of volatile or atmospheric incorporation. Boyce et al. (2010) furthered this discussion by showing that on an icy planet lacking an atmosphere, layered ejecta blankets were still possible, though they did not rule out the inclusion of volatiles that originated from the impact itself. Barlow (2005) and Komatsu et al. (2007) proposed an emplacement mechanism that combined many of these aspects. They argued that there would be largely ballistic sedimentation emplacement, but that near-surface water, liquefaction and/or the incorporation of atmospheric particles would all be factors in the ejecta, resulting in the layered rampart structure of Martian craters (Komatsu et al., 2007). The High-Resolution Stereo Camera, on the Mars Express mission, was used in the study and as supporting evidence, the authors noted that the profile resulting from the formation of ramparts did not match a solely ballistic emplacement style (Komatsu et al., 2007).

Beyond these explanations for the overall morphology of Martian craters, a more expanded look at layered ejecta on other planets provided further insight. The martian crater morphology was classified by Barlow (2000, 2005) into Single Layered Ejecta (SLE), Double Layered Ejecta (DLE), and Multiple Layered Ejecta (MLE), but while identified and categorized on Mars, the layered morphology is not unique to Mars. Osinski et al. (2011) proposed that the impact ejecta emplacement process is essentially the same process on multiple planets, with extenuating factors affecting the visual results. Along with the icy planet layered craters discussed previously (Boyce et al. 2010), Osinski et al. (2011) noted that the presence of impact melt deposits on the ejecta blankets of craters on Mercury, Venus, Earth, and the Moon suggests that ejecta deposition cannot be explained by ballistic emplacement of fragmental materials alone and has multiple stages. Osinski et al. (2011) suggested that during the end of the excavation stage and the beginning of the modification stage, momentum from the crater

collapse and the formation of a central uplift is imparted to impact melt deposits transporting them beyond the transient cavity rim to be emplaced as "ground hugging flows" atop the ballistic ejecta emplaced during the excavation stage. Osinski et al. (2011) posited that these stages and the resulting units could contribute to the layered morphology of some craters.

Osinski et al. (2011) were not alone in consideration of mechanisms for depositing impact melt bearing units. The emplacement mechanisms for an impact melt-bearing unit of ejecta has been thoroughly debated. Stoffler (1977) suggested the addition of an impact melt-bearing layer through ejection and aerial emplacement rather than via ground-hugging flow. Following works developed a plume model to support aerial deposition (Engelhardt and Graup, 1984; Engelhardt, 1990; Engelhardt et al., 1995). However, Osinski et al. (2004) refuted this model, citing evidence that melt-bearing deposits were not consistent with volcanic airborne deposits, including shaping and sorting characteristics. Notably, aerial plume deposits should be well-sorted and display normal grading. Samples of impact melt-bearing deposits do not support this observation, nor do they display aerodynamically shaped characteristics consistent with aerial deposition (Osinski et al., 2016). Artemieva et al. (2013) countered this theory arguing that impact deposits would not necessarily be comparable to volcanic deposits and the characteristics noted in Osinski et al. (2004) were explainable through known volcanic phenomena. Instead, Artemieva et al. (2013) proposed a version of the theory including a phenomenon known as fuel coolant interaction (FCI) in which surface water or water incorporated into the target rocks reacts with impact-generated melt. These FCI reactions are then responsible for the multiple layers of ejecta seen on Mars and other planetary bodies. This emplacement mechanism has been used to explain the characteristics of deposits at some terrestrial impact structures, including the Onaping Formation at the Sudbury impact structure in Ontario, Canada (Grieve et al., 2010). Artemieva et al. (2013) also proposed that FCI deposits were present at the Ries impact structure. However, Osinski et al. (2016) refuted the possibility of FCI emplacement at the Ries impact structure through a comparison of the Sudbury and Ries structures. Among other evidence, Osinski et al. (2016) noted that FCI units contain only less than centimetre scale lithic fragments, while the impact melt-bearing unit at the Ries impact structure has

a much larger lithic component of up to a 1m in diameter, excluding even larger megablock units. Osinski et al. (2020) noted that there are significant visual differences between deposits from an FCI and those at the Ries. Thus, while useful to explain some location-specific units at impact craters, FCI emplacement still cannot explain the morphology of many impact melt-bearing deposits. Recent work suggests that the Ries impact structure suevite, the melt-bearing unit, may have been emplaced by a density current (Siegert et al., 2017), contributing to the growing number of potential emplacement theories. Even so, both the Ries structure and the Mistastin Lake impact structure in Canada provide insight into the layered ejecta discussion. The Ries impact structure is composed of two general layers or units of ejecta materials. The lower layer is the Bunte Breccia, which is always superposed by the so-called "suevite" or impact melt-bearing layer (Hörz, 1982). Field observations of a consistently sharp contact between the two facies of ejecta, flow morphologies, and temperature indicators all suggest the suevite layer was emplaced as a hot ground-hugging flow. Similarly, at the Mistastin Lake Impact structure, outcrops of ejecta deposits show the same distinctive two units of ejecta. In contrast to the Ries crater, Mistastin Lake shows evidence of full impact melt layer outcrops (Mader and Osinski, 2018). The Discovery Hill locality of the Mistastin Lake structure shows a layer of impact melt-bearing deposit overlying a lithic breccia interpreted to be the ballistically emplaced ejecta (Mader and Osinski, 2018).

These proposals, that suggest an impact melt layer may be contributing to the layered morphology, are supported by examples on Earth such as the afore mentioned Ries and Mistastin Lake impact structures, which continue to be important to impact cratering studies. On Earth, there are approximately 201 confirmed impact craters (Impact Earth, 2020). Many of these craters are difficult to identify because they have been eroded, buried, overgrown with vegetation, or otherwise obscured. Seventy percent of the surface of the Earth is also covered with oceans, which retain little to no structure from impacts. Of the craters on the Earth, very few of them retain exposed craters structures or ejecta deposits for study (11 as of Osinski et al., 2012). However, the work on these terrestrial impact structures, despite their non-pristine state, provides much insight into the ejecta process. The Ries impact structure in Germany and the Mistastin Lake impact structure in

Canada have been extensively studied to understand ejecta emplacement processes, ejecta distribution, and other features.

Moving forward in studying impact melt and layered ejecta on planetary bodies, it is necessary to constrain the appearance of both ejecta as a whole and of the impact melt. Howard and Wilshire (1975) provided significant evidence early in ejecta studies to support the idea that the material observed around lunar craters was of impact origin rather than volcanic, as was commonly believed. The lack of a volcanic source and the distribution of melt-like materials originating from the crater, as well as the relative age-dating of the materials led to these conclusions. They also provided suggestions for the emplacement of melt, which have since evolved into those mentioned previously. Hawke and Head (1977) built on the observations made by Howard and Wilshire (1975) to provide further characteristics used to identify impact melt and different melt morphologies. Some of the diagnostic characteristics of melt from Howard and Wilshire (1975) include: signs of flow (channels, ponding, lineation), cooling cracks, tension cracks, gradational changes in morphology, and lower albedo relative to underlying ejecta materials. Hawke and Head (1977) also identified different types of melt morphologies correlated to different lunar crater sizes including veneers, ponds, thin flows, and thick lobes. More extensive and further reaching melt and ejecta deposits were associated with larger craters (Hawke and Head, 1977). Other authors (e.g. Bray et al., 2010; Osinski et al., 2011) added observations with the Lunar Reconnaissance Orbiter Camera that used features similar to Hawke and Head (1977) and Howard and Wilshire (1975) to identify impact melt (Figure 3). Both studies added that the digitate, lobed shape of melt flows (Figure 3 A, B, D) can be modelled with fractals at a level that is consistent with lava and melt flows on Earth rather than grain flows, which have a much higher fractal measurement (Bray et al., 2010, 2018). In addition to the morphologies described by Hawke and Head (1977), more recent studies such as Tornabene et al. (2012) have shown that crater-related pitted materials are consistent with impact melt, suggesting that the presence of pitted materials may be used as an indicator of impact melt, though their absence does not exclude an identification as impact melt. Crater-related pitted materials are polygonal, quasi-circular depressions that commonly share sides and are found in groupings (Boyce et al., 2012; Tornabene et al., 2012). They have

been observed within crater fill, rim, and ejecta deposits and are consistent with a melt-bearing unit (Tornabene et al., 2012). Pitted materials are useful as an orbital indicator of melt-bearing units.
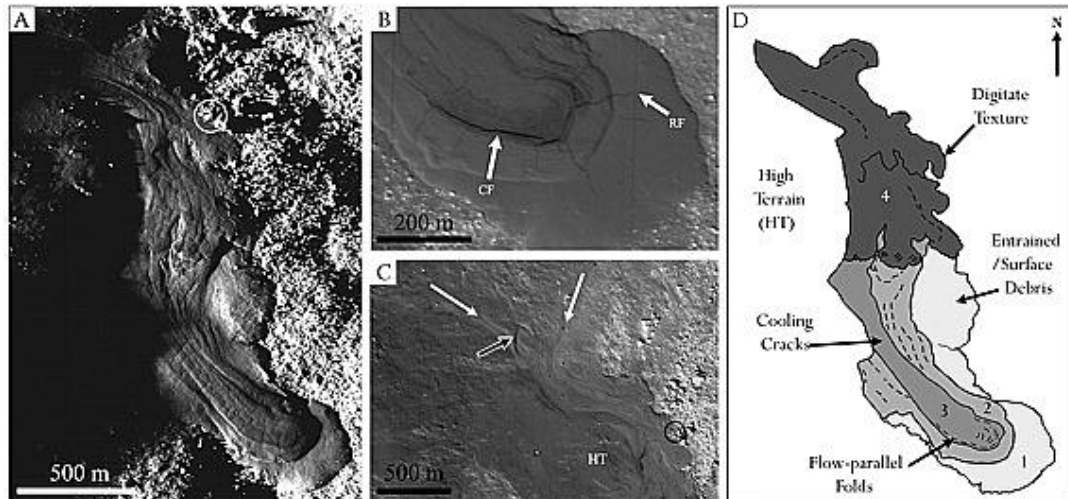
Figure 3 Example of a lunar melt flow showing melt textures. 3A is image M101476840L of a melt flow outside the rim of Giordano Bruno crater. 3B is of the main toe of that lobe and is image M106209806R. White arrows indicate CF (cooling fractures) and RF (radial fractures). 3C is a zoomed-out version of the scene in A where the circles in both images indicate the same rock cluster. White arrow show melt flows while HT and the black arrow indicate high terrain influencing the flow. 3D shows a sketch of 3A with notable features indicated. Figure and caption information from Bray et al. (2010). Courtesy Wiley/Geophysical Research Letters.

To understand and study the layered morphology seen on both Earth and Mars, it is important to continue to connect the two locations and use them as analogues for each other. Sturm et al. (2013, 2015) proposed that the Ries impact structure is similar to a martian DLE crater. "Suevite" at the Ries impact structure is an impact melt bearing breccia, which shows that if indeed Ries is consistent with a DLE, then impact melt must be involved in the formation of this morphology. The characterization and identification of melt from orbit allows for exploration of layered ejecta with further observations. Both Howard and Wilshire (1975) and Hawke and Head (1977) identified impact melt deposits overlying other ejecta materials, frequently proximal to the crater rim. As previously

mentioned, Osinski et al. (2011) and Mader and Osinski (2018) identified examples of impact melt overlying ejecta deposits on Earth to corroborate these orbital observations as well as those found within Osinski et al (2011). This study at Hargraves Crater seeks to further explore the relationship between units of ejecta, including impact melt rock.

1.2 Mars

Mars is the fourth (and farthest) terrestrial planet out from the Sun. The planet is particularly interesting because it is both close to and most similar to Earth of all the planets. Both planets have atmospheres, rocky compositions, active erosion and weather, and evidence of water. Mars is half the size of the Earth in terms of radius (3,389.5 km) and has consequently smaller gravitational acceleration of ~3.72 m/s^2 (Hirt et al., 2012) which is a little over one third of Earth's. Mars has two small moons, Phobos and Deimos, and has days that are approximately 24 hours and 37 minutes long. Several large impact basins mark the surface of Mars and attest to past heavy cratering activity. Currently, there is no known evidence of active plate tectonics or volcanism (Edgett et al., 2010), though there is evidence of past activity in volcanoes and lava flows on the surface. As a result, the planet itself is relatively cold. Mars maintains an atmosphere only about 0.6% of the thickness of that of the Earth, ~0.0061 bars on average. The surface of the planet is largely composed of basaltic sand and dust (e.g. Szwast et al., 2006; Berger et al., 2016), with oxidized iron components giving the planet the red colour it is known for. Though currently there is no liquid water on the surface of the planet, many surface features and the similarities between Earth and Mars have led to the interpretation that there may be subsurface water on Mars, and that there may once have been liquid water on the surface. The visible channel features on Mars (Carr, 1995), sandstones, and H$_2$O ice at the poles contribute to this interpretation. The possibility of past liquid water, and thus the possibility of past or current life on Mars, increases the interest in Mars for planetary study.

The northern hemisphere of the planet, known as the northern lowlands or plains, is comparatively smooth and low-lying with relatively few craters. In comparison, the southern hemisphere of the planet, known as the southern highlands, is heavily cratered. This boundary between northern and southern hemispheres is known as the crustal

dichotomy. The southern highlands area is topographically much higher than the northern lowland plains (Frey et al., 1998). While the thickness of the crust varies and does not entirely line up with the crustal dichotomy (Zuber et al., 2000), the northern lowlands have a lower mean thickness of 32 km while the southern highlands have an average thickness of 58 km (Neumann et al., 2004). The planet also hosts two polar ice caps and there is evidence for glacial and permafrost activity down to mid latitudes (e.g. Head et al., 2003; Levy et al., 2009, 2014). Very notable in a topographic image of the martian surface are the, now inactive, Tharsis volcanoes and Olympus Mons, the tallest and one of the largest known volcanoes in the solar system (Fig. 4). Large ergs, dune fields, are also present on the surface. Occasional dust storms cross the surface of the planet and emphasize the presence of active erosional and atmospheric processes. As Mars has active dunes, dust, and wind, the surface features on the planet change with time as they are eroded, exhumed, or buried and obscured.
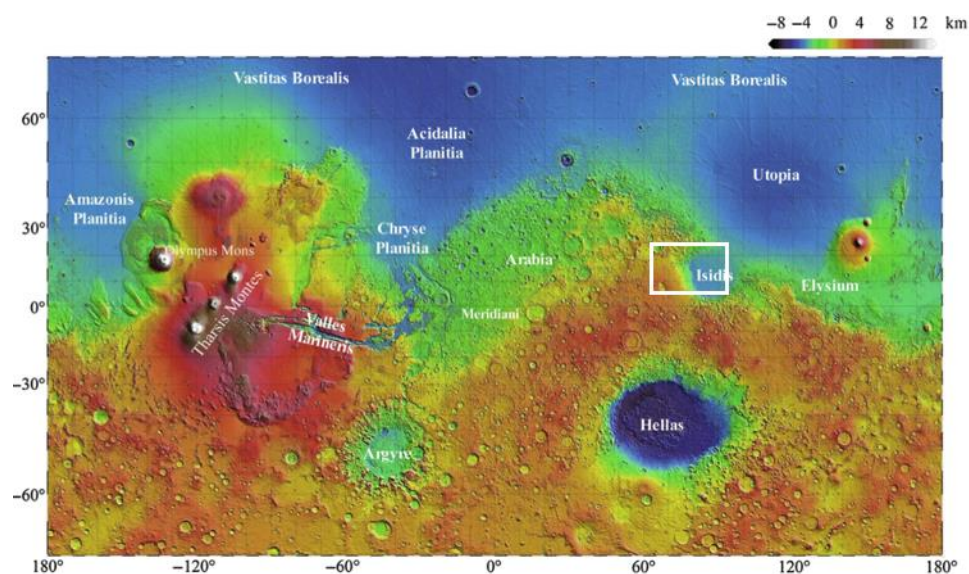
Figure 4 Colourized topography map of Mars from the MOLA instrument (NASA/MOLA Science Teams). Colours denote different levels of topography. White names label notable location on the martian surface. Of note for this study is the Isidis Basin, which is a light blue colour, and the orange/yellow/red area to the west of that Basin, which is known as Syrtis Major, and contains the region Nili Fossae. White box indicates location of Figure 6. Modified figure from the Encyclopedia of the Solar System, Chapter 16 (Catling, 2014).
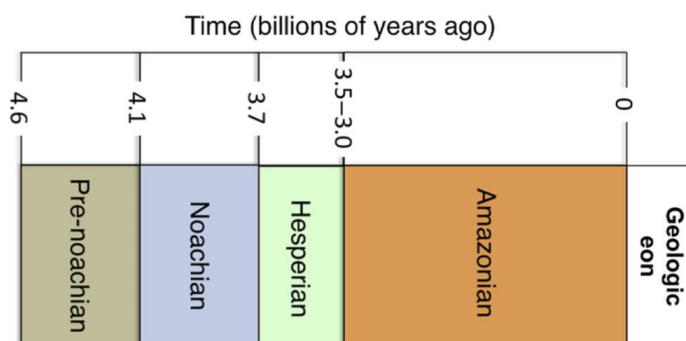
Figure 5 The breakdown of the martian geologic time scale into eons with approximate time points in billions of years. Figure modified from the Encyclopedia of the Solar System, Chapter 16 (Catling, 2014).

The geologic timescale of Mars is divided into periods, much the same as Earth, but there is much less available information for Mars and most information is orbital rather than in-situ or ground-based. Broadly, they are the Pre-Noachian, the Noachian, the Hesperian, and the Amazonian eons (Fig. 5); although finer divisions (periods) and divisions by mineralogy also exist. Comparatively little is known about the pre-Noachian, though the global dichotomy is the oldest visible known surface feature and is associated with pre-Noachian times. The formation of Hellas Basin is a common marker for the beginning of the Noachian period (Carr and Head, 2010 and sources therein). The Noachian is associated with periods of high cratering followed by and in conjunction with the formation of valley networks. During this period, large amount of mineral alteration and possible aqueous erosion and weathering are also thought to have occurred (Carr and Head, 2010 and sources therein). The beginning of the Hesperian period is marked by a change from the patterns of the Noachian period. There was a lower cratering rate and there is thought to be a decrease in the amount of erosion and alteration, both aqueous and otherwise. Instead, the period is marked by volcanic eruptions, including the beginnings of the Tharsis volcanoes and Olympus Mons as well as canyon formation, including potentially Valles Marineris (Carr and Head 2010 and sources therein). Finally, the Amazonian period is largely associated with fewer large-scale surface processes and more with aeolian, periglacial, and glacial processes, though there likely continued to be

episodic volcanism as well (Carr and Head, 2010 and therein). This period includes the deposition of layered deposits at the poles (Carr and Head, 2010 and therein).

1.2.1   The Nili Fossae Region of Mars and Hargraves Crater

1.2.1.1   Nili Fossae
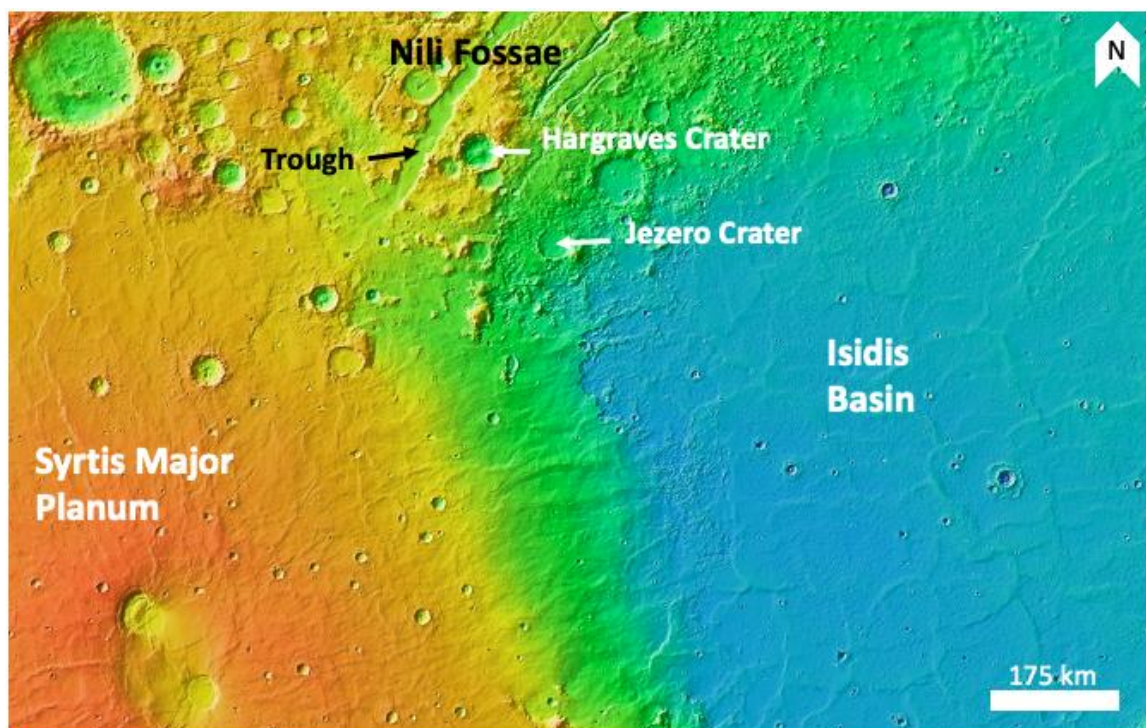
Figure 6 Significant locations labelled on a Mars Orbiter Laser Altimeter shaded relief and colorized elevation mosaic.

The Nili Fossae region of Mars hosts some of the oldest surface materials and stratigraphy on Mars (Fig. 6). Much of the area is comprised of the Noachian Basement group and overlying units, representing the oldest established eon of geologic time on Mars and anything that came before it (pre-Noachian) (e.g. Scheller and Ehlmann, 2020). As such, the location and its geology are important to understanding the overall geology and history of Mars. Jezero Crater, the focus of the Mars 2020 Perseverance rover mission, is located on the south-eastern border of Nili Fossae (Fig. 6) and showcases the local stratigraphy. The area additionally contains Hargraves Crater, the main focus of

Chapter 2 of this thesis. Thus, the geology of Nili Fossae, located just off of Syrtis Major Planum (Fig. 6), is important contextual knowledge.

The third largest known impact basin on Mars, located directly on the border between the northern and southern hemispheres, is the Isidis Basin (1900 km diameter). The Isidis Basin, located on the south-eastern border of the Nili Fossae region (Fig. 6), is superposed by Jezero Crater and is thought to have formed at ~3.96 Ga. (Werner, 2005). As a large-scale impact, the material excavated and then deposited as an ejecta blanket would have extended continuously for at least 1-2 crater radii (950-1900 km) and likely contributed to the stratigraphy of the surrounding area. The geology of the Nili Fossae region is thus rightfully largely associated with this impact. Stratigraphically, the Noachian-aged crust in which the basin is located is the lowest known layer and appears to be a mix of low calcium pyroxene-bearing rocks and alteration in the form of Fe smectite phyllosilicates (Mangold et al. 2007) (Fig. 7). Shortly thereafter (Goudge et al., 2015; Kremer et al., 2019), an olivine-bearing unit, or a unit bearing a strong olivine signature, was deposited atop the excavated material (Mustard et al., 2007). This unit has a number of interpretations, including that of an impact melt sheet related to the formation of Isidis (Mustard et al., 2007) or of an unrelated lava flow post impact. This unit is still widespread in the northeast portion of Syrtis Major. This olivine-bearing unit is cross-cut by the grabens of Nili Fossae – a graben system northwest of Isidis Basin that is linked to the formation of the basin (Mangold et al., 2007, Mustard et al., 2007). It is thought that tensional forces related to the impact created the series of crests and troughs that marks the region. Post tectonic deformation, from impacts and otherwise, channels cut the Noachian surface and altered the surface depositing clays and carbonates, followed by sulphates, particularly in topographic lows (Ehlmann and Mustard, 2012; Bramble et al., 2017)(Fig. 7). Following all of these events, which occurred during the Noachian period of Martian geologic history, is the emplacement of the Syrtis volcanic group, essentially a series of lava flows which both partially infill and embay the Nili Fossae and is thought to cross into the Early Hesperian period of Martian geologic history.
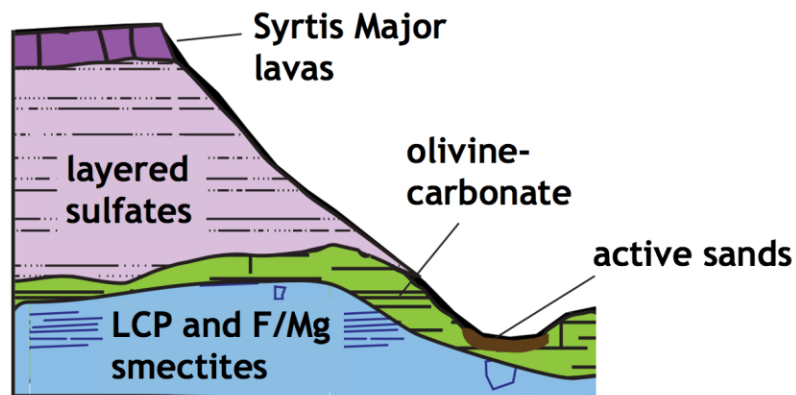
Figure 7 Approximate stratigraphy of the Nili Fossae region of Syrtis Major Planum with major units denoted. Figure modified from Ehlmann et al. (2009). Figure is not to scale, nor linked to a specific geologic location in this paper.

1.2.1.2   Hargraves Crater

Hargraves Crater and its ejecta blanket are the main foci of this study. They are located just east-southeast of the Nili Fossae "trough," an unofficial name for one of the grabens in the Nili Fossae Graben system (Fig. 8). As discussed, the crater is located near both the large Isidis Basin and the well-known Jezero Crater. The crater is ~68 km in diameter and the surrounding area is mainly Noachian in age. The impact likely occurred after the emplacement of the Syrtis Volcanics, as ejecta in the "trough" overlies the lavas embaying the trough floor. The impact also overprints two older remnant craters that now border the crater to the south and west-southwest (Fig. 8). The crater itself is a complex crater with a central uplift and visible terracing in the crater walls. Very little of the central uplift shows exposed bedrock. Ejecta from the crater is observed in thermal and visual orbital datasets flowing into and over these pre-existing craters and radially outward from the Hargraves Crater centre. Previous peer-reviewed published work on the crater is limited. The well-exposed nature of the ejecta of the crater was noted in early HiRISE results (McEwen et al., 2010). More recently, Ryan et al. (2017, 2016) presented conference abstract mapping results for small portions of Hargraves Crater ejecta present in one of the Nili Fossae grabens specifically focused on Hargraves Crater ejecta promoting Nili Fossae trough as a potential landing site for the Mars 2020 rover mission. Tornabene et al. (2017) also presented some of the information covered in Chapter 2 of

this thesis at a Mars 2020 landing site workshop. The Hargraves Crater ejecta blanket has been presented as exceptionally well-exposed and well-preserved ejecta blanket. Other presented results are covered within this thesis.
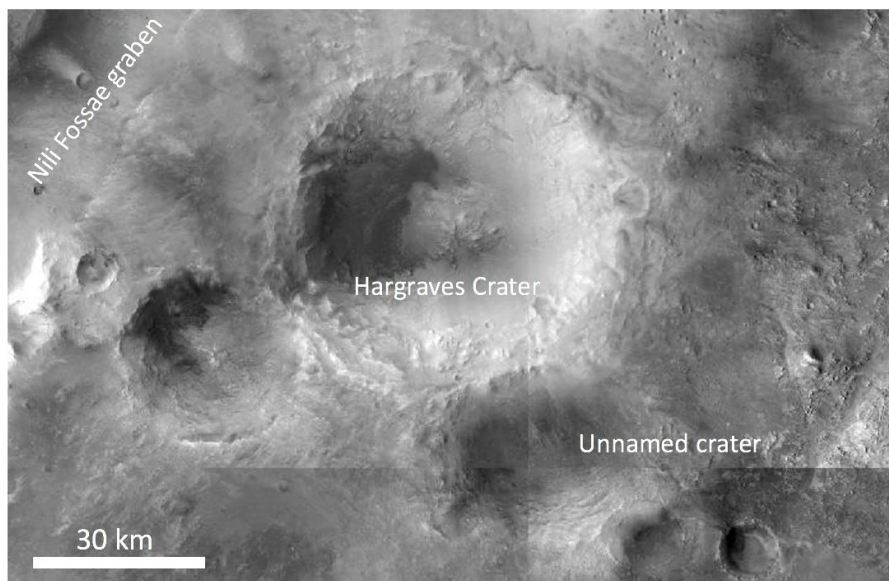
Figure 8 Hargraves Crater in Nili Fossae. One of the Nili Fossae grabens is noted as well as an older unnamed crater that contains ejecta from Hargraves Crater. The image is the CTX (Context Camera) beta mosaic from the Murray Lab.

1.3   Instrumentation

1.3.1   Mars Reconnaissance Orbiter (MRO)

The Mars Reconnaissance Orbiter (MRO) is a science-focused spacecraft orbiting Mars. MRO began science operations in 2006 and contains six instruments, operated cooperatively by individual instrument teams (Zurek and Smrekar, 2007). The orbiter expands upon the abilities of existing satellites around Mars, including acting as a relay for the Curiosity rover mission. Some of the main science goals of MRO include understanding the history and role of water on Mars and the Martian surface, acting as a relay between landed missions and Earth, as well as identifying and studying critical sites for further human exploration and study (Zurek and Smrekar, 2007). Currently, the orbiter is approximately 300 km above the martian surface in a sun-synchronous orbit.

1.3.1.1   HiRISE

One of the instruments aboard MRO and utilized within this study is the High-Resolution
Imaging Science Experiment (HiRISE). HiRISE began its primary science phase in 2006
capturing high resolution images of the Martian surface and continues to the present. The
camera is composed of fourteen CCDs (charge-couple devices). Ten 10 red filter CCDs
form a line across the instrument and capture a swath approximately 6 kilometres wide
(Fig. 9). An additional two near-infrared filter CCDS and two blue-green filter CCDS
overlap the centre of the instrument (Fig. 9) (McEwen et al., 2007, 2010). A three-colour
composite strip is produced, using these CCDs, for the centre of each HiRISE image that
is two CCDs wide (~1.2 km at full resolution). This colour strip is composed of the three
different CCD channels, the RED (red) channel, the BGR (blue-green) channel, and the
NIR (near infrared) channel and is available in two different RGB composites. HiRISE
currently has a maximum resolution of ~25 cm per pixel and objects around 1 m in size
are resolvable. The instrument operates as a push-broom imaging system where it
captures one horizontal strip of the landscape at a time as the orbiter moves and then
mosaics the rows together to form the final image. Later processing stages map-project
the images and correct for noise and variation across CCDs (McEwen et al., 2010).
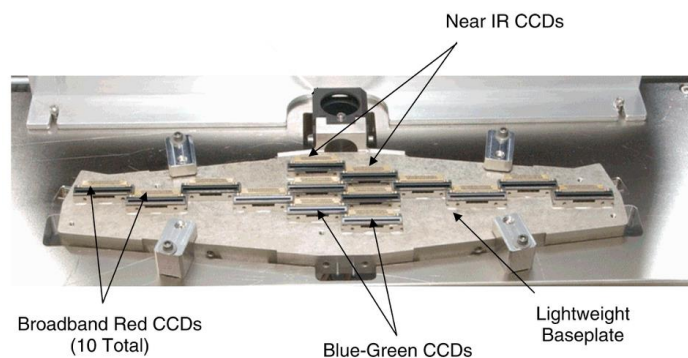
**Figure 9 This image shows the HiRISE instrument face. The 14 CCDS are indicated
with the type of light they are centred on. The middle 6 CCDS form the colour strip
of HiRISE images. All CCDS are mounted on a baseplate. Image modified from
Delamere et al. (2010).**

1.3.1.2　CTX

The CTX (Context Camera) instrument (Malin et al., 2007) is also aboard MRO. The imagers main function in to provide higher resolution images of the full surface of Mars in order to explore types of landforms identified from earlier imaging missions (Malin et al., 2007). Imaging at ~5-6 m/px from ~300 km above the surface, CTX has provided new images of much the surface. They images have been combined into the current highest resolution visible light mosaic of Mars (Dickson et al., 2018). The imager functions across a 500-700 nm band pass and produces grey-scale images as products. In addition to imaging the full surface, CTX takes targeted images of specific features, sometimes in conjunction with other MRO instruments such as HiRISE or other orbital instruments such as CaSSIS (see below). Much like HiRISE, CTX is also capable of taking images from two angles that can be used together to produce a stereo image. Anaglyphs and DEMs produced from CTX images are useful for studying the features that are part of the main science goals of CTX.

1.3.2　THEMIS

The THEMIS instrument (Thermal Emission Imaging System), unlike HiRISE and CTX, is aboard the Mars Odyssey Orbiter. The instrument is a multi-spectral imager with 9 thermal infrared (TIR) wavelengths between 6.8 and 14.9 µm and 5 visible/near-infrared wavelengths between 0.42 and 0.86 µm. With these capabilities, THEMIS mapped the full surface of Mars at 100 m/px at both day and night-time periods at TIR wavelengths. The resulting night and day mosaics use brightness as an equivalent of temperature to represent the TIR data (Edwards et al., 2011). THEMIS also captures more targeted images at higher resolutions (~18 m/px) for compositional study in visible/near-infrared wavelengths.

1.3.3　CaSSIS

The CaSSIS instrument (Color and Stereo Surface Imaging System) is aboard the ExoMars Trace Gas Orbiter (TGO). Equipped with panchromatic (PAN), blue (BLU), red (RED), and near-infrared (NIR) filters, CaSSIS can capture images in up to 4 colors at a time. Images have approximately 4.6 m/px resolution (Thomas et al., 2017). CaSSIS is a

push-frame imaging system. Frames are captured as the instrument moves along the orbit and then stitched together to form the full image (Thomas et al., 2017). As designed, CaSSIS regularly takes one stereo image per orbit (Thomas et al., 2017). One of the primary advantages of CaSSIS as an imager is that the stereo images are captured in one pass over. The image is captured as the orbiter approaches, then the instrument rotates to capture the image again as the orbiter departs. These two angles of imaging (on approach and on departure) provide enough of a parallax angle to generate a stereo image.

1.4   Summary

This first chapter of the thesis provided background information necessary to understand this study as well as a review of the literature relevant to placing this study in context. It explained the stages of the impact process and covered the work already completed on ejecta studies. An overview of Martian geology as a whole was complemented by a review of the geology near Hargraves Crater. Finally, an introduction to the instruments utilized within Chapters 2 and 3 provides good groundwork for the coming study. Chapter 2 focuses on a morphological and morphometric analysis of the best ejecta exposure at Hargraves Crater. A context mapping of the whole crater and a focused mapping of an exposure south of the crater were imperative to the study. Observations from the mapping and the image are used to identify and interpret the ejecta units at Hargraves, highlighting the unique qualities showcased at this particular site. The third and final chapter of this thesis defines Hargraves-type ejecta, looks at additional examples, and places the results of the study in Chapter 2 within the context of Chapter 1. The chapter closes by proposing starting places for future work and identifying the main questions still to be answered about Hargraves Crater.

Chapter 2

2 Hargraves Crater Ejecta and Implications for Impact Processes

This chapter is the current manuscript of a paper that will be submitted to a journal in the coming months.

2.1 Introduction

The prevalence of impact craters throughout the Solar System correlates with their importance in the study of planetary surface processes, providing insights into the nature of surface materials, crustal structures, surface age, stratigraphy, and astrobiology. Impact craters are found on the Earth, covering the surface of the Moon and nearby asteroids, and over most of the surface of Mars. Cratering studies have focused on both the Moon and Mars due to the exceptional preservation of these structures when compared to those of Earth. Erosion, active tectonics, plant life, and habitation on Earth are detrimental to the preservation of craters, many of which formed during the first billion years of the Solar System. The Moon has little to no atmosphere and no erosion, preserving craters for study. However, in contrast to the Moon, the presence of an atmosphere and volatile-rich target rocks make Mars a compelling comparison to terrestrial craters that may contribute to understanding impact cratering on planetary surfaces with an atmosphere, such as Earth. The assorted well-preserved craters and the extensive coverage of the surface with high-resolution images and datasets strengthen the value of studying impacts on Mars.

A prominent feature of impact craters is the presence of ejecta deposits within and around the host crater (e.g. Melosh, 1989; Osinski et al., 2012). Because impact craters excavate and deposit material from a range of depths, they provide information about the subsurface of planets with solid surfaces. The study and optimal sampling of these deposits relies on an accurate understanding of crater excavation, ejecta emplacement and distribution processes.

Understanding the deposition of ejecta is an active field of study. The current understanding of ejecta emplacement focuses on ballistic sedimentation. Ballistic

sedimentation is the name given to the mechanism dominated by the emplacement of airborne ejecta that radiates outward from the crater centre along ballistic trajectories, which subsequently impacts the surfaces and flows radially outward (Oberbeck, 1975). The mechanism was derived from studies of the Moon and of explosions and nuclear tests (Roberts, 1966; Oberbeck, 1975). While this model accounts for most of the observed ejecta deposits, namely, fragmental brecciated and transported target materials, a separate mechanism must be used to emplace the overlying melt-bearing unit that has been observed both in the field terrestrially (e.g., Osinski et al., 2011) and in high resolution images of the best-preserved craters in the Solar System (e.g., Hawke and Head, 1977; Osinski et al. 2011; Tornabene et al., 2012, etc.).

On Earth, our observations are limited as there are very few impact structures which have an exposed and preserved ejecta blanket. In particular, the Ries impact structure (~24 km diameter) in Germany is an important site for understanding ejecta blankets as it is one of the best-studied and best-preserved complex craters on Earth (e.g., Osinski et al. 2011). The eroded remnants of the Ries impact ejecta preserve impact melt-bearing rocks (a.k.a., "Suevite") and a stratigraphically lower unit or "layer" of melt-poor brecciated materials termed "Bunte Breccia." Oberbeck's (1975) method of ejecta emplacement, ballistic sedimentation, adequately explains the Bunte Breccia (Hörz et al.1983), but not the layered morphology and impact-melt bearing unit observed at the Ries Impact Structure and other terrestrial and extra-terrestrial craters (Hawke and Head, 1977; Bray et al., 2010; Osinski et al., 2011; Mader and Osinski, 2018).

As mentioned, the melt-bearing ejecta seen at the Ries impact structure is not unique to Earth but can also be observed in high-resolution images of the best-preserved craters in the Solar System. Early recognition of the associations of impact melt deposits on the Moon served to visually separate lunar impact melts from volcanic deposits. Hawke and Head (1977) and Howard and Wilshire (1975) recognized distinctive morphologic features indicative of impact melts such as flows, ponds, veneers, and cooling-contraction fractures. Additionally, on Mars, crater related pitted materials are consistent with these morphologic characteristics of impact melt deposits (Tornabene et al. 2012). However, many Martian craters possess ejecta blankets that are distinct from lunar craters due their

lobate, rampart or so-called layered morphology (Carr et al. 1977, Barlow et al. 2000, 2005).

Our studies of craters on both Earth and Mars and the connections between them inform our understanding of the impact cratering process as a whole. For example, high-resolution images of Martian craters may help to explain impact melt observations as well as the layered structure observed at the Ries impact structure. The HiRISE (High Resolution Imaging Science Experiment) instrument (McEwen et al., 2007) on the Mars Reconnaissance Orbiter (MRO) continues to reveal an abundance of morphological information on Martian ejecta blankets at meter-scales and in various states of preservation and exposure. Notably, even at the highest spatial resolution, most ejecta deposits do not provide sufficient preservation and exposure to study the detailed stratigraphy and internal structure of ejecta blankets. However, HiRISE images show that, unlike many martian craters, Hargraves Crater exhibits a balance of preservation and erosion, which has exposed some of the internal structures, diverse compositions, and stratigraphy of the ejecta (McEwen et al. 2010). As such, the study of Hargraves Crater may place further constraints on ejecta formation and emplacement models, as well as provide a template for locating additional examples for further study.

In this work, we present the results of a detailed analysis of the Hargraves Crater ejecta blanket based on orbital datasets mainly derived from HiRISE (McEwen et al. 2007), CTX (Context Camera) (Malin et al. 2007), and THEMIS (Thermal Emission Imaging Spectrometer) (Christensen et al. 2004). This study begins with a morphologic and morphometric characterization of observed ejecta features to complement and expand on previous preliminary works on Hargraves Crater (McEwen et al. 2010) that include focused studies of the exposed ejecta as part of the "Nili Fossae trough" candidate landing site for the Mars 2020 Perseverance Rover (Ryan et al., 2016, Tornabene et al. 2017). Due to a balance of preservation and excavation, Hargraves Crater represents a unique opportunity to study and understand the inner morphologic structures and stratigraphy of ejecta for comparison against terrestrial field observations and current emplacement mechanisms.

2.2   Geologic Setting-Hargraves Crater
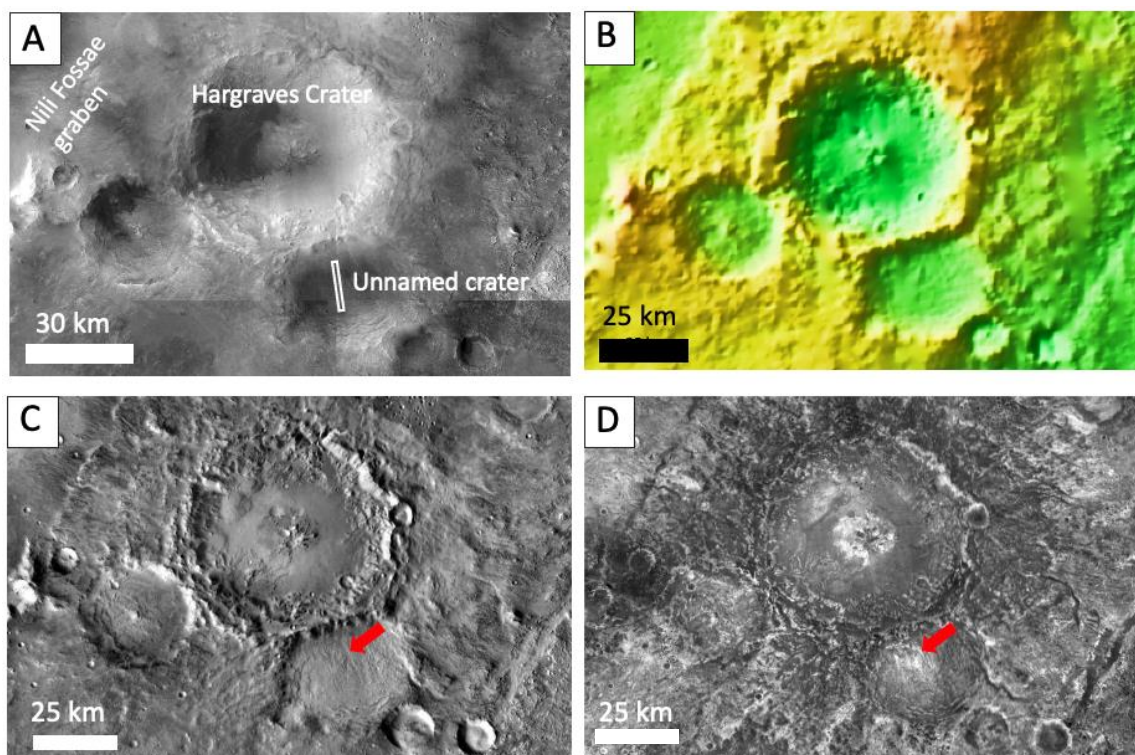
Figure 10 A) **Hargraves Crater is shown as the largest circular depression in the centre of the image, with location of Figure 11, ESP_044161_2005_COLOR, indicated by the white box to the southeast of the crater. The base image is a CTX mosaic from the Murray Lab available through JMARS, (Christensen et al. 2009; Dickson et al. 2018). B) Mars Orbiter Laser Altimeter topography map. Greens show areas of lower elevation while yellow and browns show comparatively higher elevations. C) Base map is the THEMIS Day Infrared mosaic with the area of interest indicated by a red arrow. Note the brightness difference in this area from C to D, demonstrating a change in the signature. D) Base map is the THEMIS Night Infrared derived brightness temperature mosaic with the area of interest indicated by a red arrow. Note the bright signature contrasted with the darker signature of C. Images courtesy: CTX- NASA/JPL-Caltech/MSSS, THEMIS - NASA/JPL-Caltech/Arizona State University.**

Hargraves Crater is located in the Nili Fossae region of Mars at 20.76°N 284.36°W (Fig. 10). The Nili Fossae region is comprised of several notable surface features and a significant stratigraphy. The name of the region comes from the graben system of the same name that consists of a set of concentric arced "troughs," which are most likely related to the stress and tension release from the impact that formed the ~1900-km Isidis Basin (Wichman and Schultz, 1989; Kraal et al., 1998). Isidis Basin is located southeast of Nili Fossae. South-southwest of the Nili Fossae and west of Isidis Basin is Syrtis Major Planum, a dark albedo feature, comprised predominately of the Syrtis Major Volcanic Complex containing two caldera complexes: Nili and Meroe Patera.

The surface rocks the Nili Fossae incise into are predominately Noachian in age (Tanaka et al., 2005; Mangold et al., 2007; Mustard et al., 2007; Scheller and Ehlmann, 2020). Based on visible/near-infrared spectral studies, the region hosts significant amounts of low-calcium pyroxene, olivine, and Fe- and Mg-smectite clay bearing materials (Ehlmann and Mustard 2012, Ehlmann et al., 2009, Mustard et al. 2007, Mangold et al. 2007). The Nili Fossae region also contains what is referred to as a "megabreccia" unit located in a number of areas around Isidis Basin (Mustard et al. 2009, Weiss et al., 2018). These units are defined in Weiss et al. (2018) as "cataclastic deposit[s] of large… typically angular blocks set within a finer-grained matrix" greater than or equal to 10 meters in size and are theorized to be related to the Isidis Basin impact". Regionally, the Noachian terrain is affected most prominently by the formation of the Isidis Basin. Either simultaneous or immediately following the deposition of Isidis Basin ejecta, an olivine-rich unit was deposited, followed by the formation of the aforementioned Nili Fossae graben system (Mangold et al., 2007, Mustard et al., 2007). Channel systems, either fluvial or possibly glacial or subglacial (Grau Galofre et al., 2020) altered the Noachian surface and olivine layer and deposited clays, carbonates, and sulphates (Ehlmann and Mustard, 2012). Later, the graben system was embayed by the emplacement of the Syrtis Major Volcanics (Mustard et al., 2009)

Hargraves Crater is located just southeast of one of the troughs of the Nili Fossae (Fig. 10), and northwest of Isidis Basin. The crater is ~68 km in diameter with a central uplift and collapsed walls indicative of a complex crater morphology. Ejecta from Hargraves is

found radially beyond the crater rim, including in other nearby pre-existing topographic lows, which provide some of the clearest and best exposures of ejecta. These topographic structures include: a segment of the Nili Fossae graben system located to the northwest of Hargraves; and an older and degraded ~38 km diameter crater immediately south of Hargraves where the most diverse and best-exposed ejecta features are observed to date are revealed (white box in Fig. 10A, Fig. 11). The southern exposure of the Hargraves ejecta (within ~10 km of the rim) is closer to the rim Hargraves Crater than the deposits on the floor of the "trough" (within ~30 km of the rim) and appears to be better preserved and both spectrally and morphologically diverse. Based on stratigraphic relations, the Hargraves ejecta is currently thought to have been deposited sometime after the Syrtis volcanic lavas.
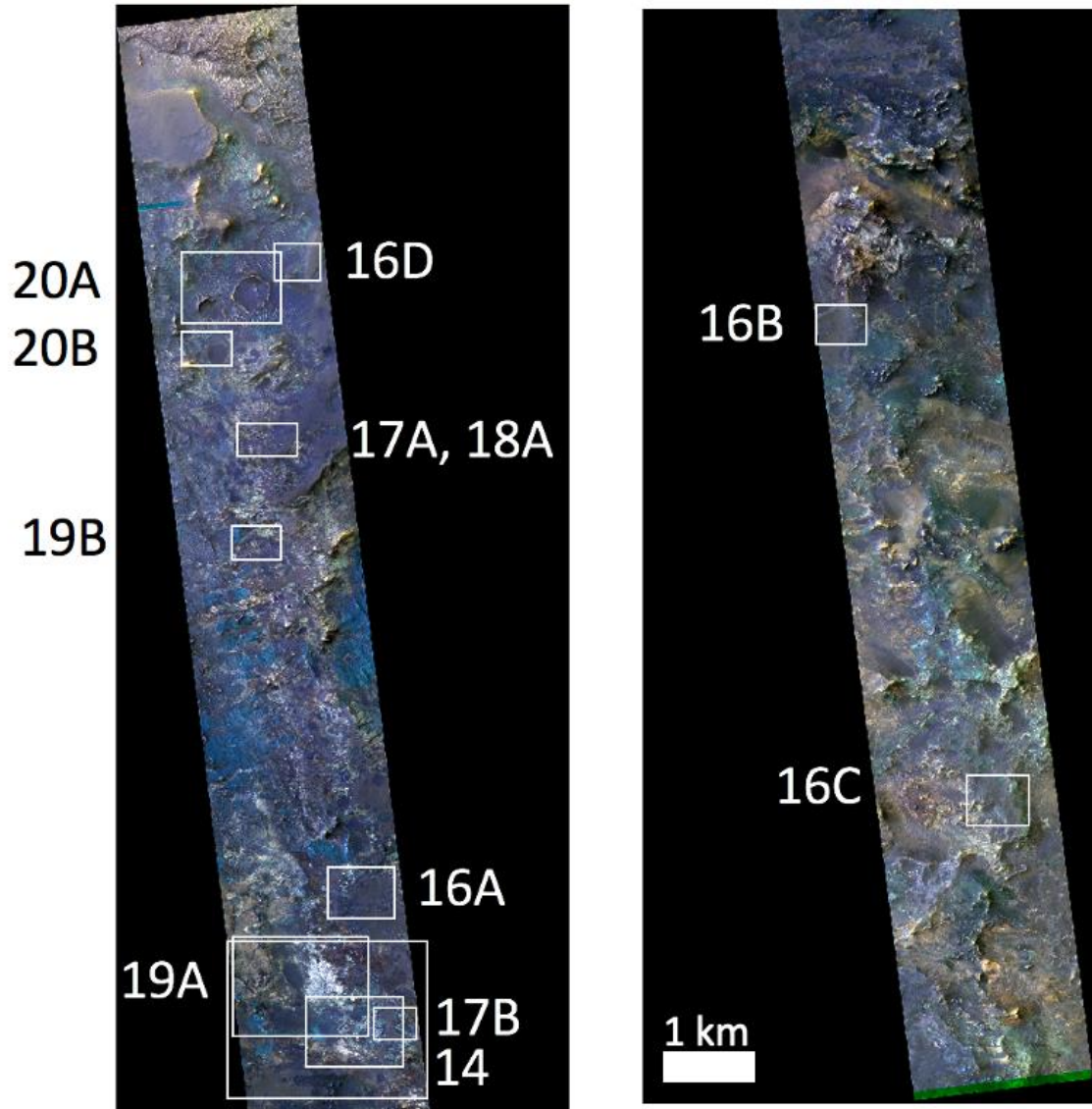
Figure 11 Image ESP_044161_2005_COLOR as an IRB colour composite (Infrared, RED and Blue-Green) product. (Shown outlined in white in Figure 10A). White numbered boxes indicate locations of future figures in this text.

This study focuses on the southern exposure of the Hargraves Crater ejecta in HiRISE image ESP_044161_2005_COLOR (Fig. 11) as it is entirely within the observable continuous ejecta (Fig. 10A) and showcases the best preservation, colour diversity and exposure thus far recognized in ejecta with HiRISE.

2.3   Methods

2.3.1   Instruments

2.3.1.1   HiRISE

The HiRISE instrument aboard the Mars Reconnaissance Orbiter (MRO) obtained the main images used in this study. The camera has a maximum spatial resolution of up to ~25 centimetres per pixel. HiRISE, a push broom imaging system, has a row of 10 red-filter ("RED") CCDs (charge couple devices) with two blue-green ("BGR") and two near-infrared (NIR) CCDs positioned at the centre of the array of 10 RED CCDs (see McEwen et al. 2007; Delamere et al. 2010). By virtue of the overlap of BGR, NIR and the middle two RED CCDs, a centre strip representing 20% of the overall HiRISE image width (~1 to 1.2 km and 5 to 6 km, respectively) can be combined into a colour-infrared image. The three colour filters provide three data points within the visible/near-infrared spectrum for cursory 3-band spectral analysis. HiRISE R-G-B (Red, Green, Blue)-colour composites are produced in a simulated "true colour" format ("RGB") as well as a colour-infrared product (i.e., combining NIR, RED and BGR ["IRB" which stands for Infrared-Red-Blue/Green]) (McEwen et al. 2007).

Additionally, the HiRISE team can produce stereo images. Two HiRISE images which are taken at different times and from different angles are used to produce anaglyphs and digital terrain models (DTMs) as higher-level data products (Kirk et al. 2007). When both images are combined into R-G-B channels and each coloured differently, the parallax angle between the two images allows topography to be inferred by the brain using 3D glasses and classic stereoscopy. For DTMs, the ISIS 3 processing system is used on the images to calculate and orthorectify the model (Kirk et al. 2007). The HiRISE system is able to correct the data on a high precision level, to produce orthorectified, undistorted, high-resolution DTMs (Kirk et al. 2007, McEwen et al. 2010). These products are used to understand stratigraphic and topographic relationships. HiRISE images are uniquely suited to studying the well-exposed Hargraves Crater ejecta blanket due to the high resolution, stereo capability and colour-infrared capabilities.

2.3.1.2   CTX

The CTX (Context Camera) instrument is also aboard MRO and in this study was used primarily for context in mapping and understanding the HiRISE images seen at Hargraves Crater. The instrument captures targeted images up to ~5 meters per pixel. CTX is a panchromatic imager with a 7-micron pixel CCD detector (Malin et al. 2007). The response of the instrument filter is focused on a 500-700 nm band pass and it takes one image at a time but may also build a stereo image pair for 3D context in the same manner as HiRISE does (Malin et al. 2007).

2.3.1.3   THEMIS

THEMIS (Thermal Emission Imaging System) is on the Mars Odyssey Orbiter. The instrument is a two-component multi-spectral push broom imager covering both the visible/near-infrared and thermal segments of the electromagnetic spectrum (Christensen et al., 2004). There are 10 channels (9 wavelengths) that range from 0.42 μm to 0.86 μm in the thermal wavelengths and 5 that range from 6.8 μm to 14.9 μm in the visible/near-infrared. This study used the thermal infrared (TIR) wavelengths of the instrument which imaged the total surface of Mars at 100 m/px (Edwards et al., 2011). These mosaics of night and day TIR temperature signatures of the surface are a qualitative proxy for thermal inertia and thereby their thermophysical properties. Surface units that are cool during the day and bright during the night are commonly tied to bedrock exposures, while the reverse, day bright and night cool, are tied to less coherent features such as sand or dunes. The consolidated bedrock retains heat from the day into the night because it has higher thermal inertia, while loose sand has low thermal inertia and loses the heat of the day quickly, resulting in a dark night TIR signature. Due to these indicators of potential exposed bedrock, the THEMIS mosaics were used in this study to determine areas of the crater that would have the best exposures of ejecta layers, showcasing rock within the ejecta.

2.3.2   Morphologic Mapping

As context for this study, the full ejecta blanket of Hargraves Crater was mapped at ~5-6 m/px on CTX images; however, the study site, the southern ejecta exposure, is comprised

of the colour strip of HiRISE image ESP_044161_2005. In both cases, units were identified largely according to morphology and tonality. Unfortunately, there is no current coverage of the location covered by this image with CRISM (Compact Reconnaissance Imaging Spectrometer for Mars) or any other spectral or colour dataset at a spatial scale that is useful for our mapping purposes (Appendix 1A shows the existing HiRISE coverage at Hargraves Crater as well as the existing CRISM coverage). The image is a stereo pair with ESP_051321_2005 which allows for an anaglyph image to be produced and used for understanding stratigraphic relationships in the mapping. Units were distinguished largely by texture (smooth or fragmented), relative stratigraphic position (above or below), and colour. Colour information was determined from the HiRISE IRB composite as well as tonal differences in the greyscale RED mosaic image.

2.3.3   Quantitative Measure of Fragment Distribution

The southern exposure of the Hargraves Crater ejecta is representatively captured in HiRISE image ESP_044161_2005, which has a resolution of ~25 cm/px. This image was analysed to obtain a size frequency distribution of ejecta fragments as they relate to distance from the crater. As the image is aligned south of the crater, the top of the image is proximal to the crater, while the southern, bottom portion of the image is more distal. Fragments in the image that were observed to be discrete clasts, where exposed, were outlined and analysed. The image was binned into ten sections of ~1445 m long top to bottom, with increasing radial distance from the crater for analysis, from zone 1, closest to the crater, to zone 10, furthest from the crater. These measured clasts were analysed after the procedure followed by Sturm et al. (2015) where each clast polygon area was converted to an area equivalent circle, and the radius of that circle used to calculate diameter, which was termed the "block size" for this analysis. Apparent sphericity, often confused with roundness, was also calculated for these measured clasts. Given the nature of the data in this study, only two dimensions of clasts are visible while sphericity is calculated with three. Thus, we calculated what we termed "apparent sphericity" from the two dimensions visible in the data. Apparent sphericity is calculated as a ratio of the area of the clast over the area of a hypothetical circle with the major axis of the clast as the

diameter. This calculation, given by the equation $4 * \frac{Area}{\pi * (Major\ Axis)^2}$, was done automatically using ImageJ software (Schneider et al., 2012).

2.4 Results

The Hargraves ejecta blanket shows an uncommon diversity of colour and a distinctive stratigraphy. The full ejecta blanket is shown mapped at ~5-6 m/px in Figure 12, and this study highlights the southern exposure shown in HiRISE image ESP_044161_2005_COLOR (Fig. 11) where the ejecta is best exposed in high resolution with colour capabilities. The studied image is located such that the northern edge of the image (top of the image in figures) is close to the southern rim of the crater, and the bottom of the image extends to the south (Fig. 11, 13). From top to bottom, the HiRISE image notably parallels the approximate radial flow of the ejecta. The ejecta is comprised of two general morphologic units with consistent stratigraphic relationships throughout our detailed and contextual mapping areas and has distinct correlations with THEMIS thermophysical signatures (*c.f.* Figs. 10 and 12). THEMIS signatures give a relative sense of thermal inertia. Within a scene, areas that are brighter during the day and cooler at night have a lower thermal inertia and change temperature quickly. In contrast, areas that are cool during the day and brighter at night have high thermal inertia and change temperature more slowly. At Hargraves, the two units are: a stratigraphically lower fragmental, brightly and diversely coloured unit (mapped in greens in Fig. 12 and Fig. 13) that correlates with the brighter portion of the night TIR THEMIS mosaic and a stratigraphically higher dark toned smooth unit (mapped in pink and purple in Fig. 12 and 13) that correlates with the darker portion of the night TIR THEMIS mosaic. The units were also analysed for clast content. In addition to these two main units, smaller craters, either superposed or pre-existing, are visible as dark circular features, while blue (in colour-infrared) aeolian dune forms cover smaller areas.

Legend

🟩 Fragmental	🟧 Unclassified	🟦 Interior Smooth		
🟪 Smooth	🟪 Possible Smooth	Terraces		
🟦 Uplift		60 Km		
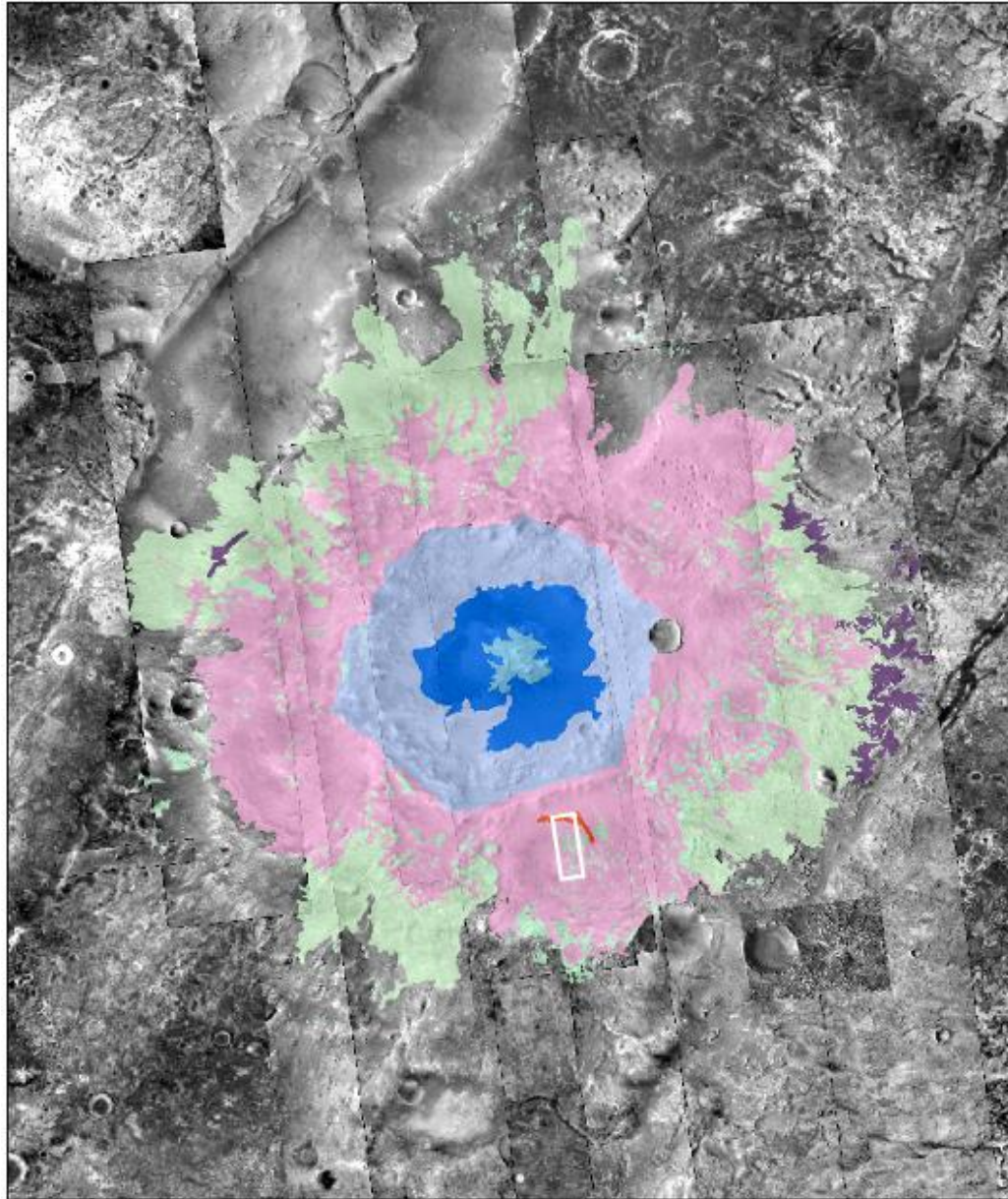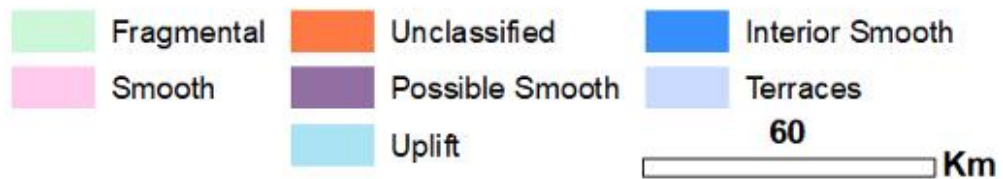
Figure 12 Full map of Hargraves Crater ejecta. See legend for units. Mapped on CTX images at 5-6 m/px, overlaid on THEMIS nights TIR mosaic. White box indicates location of Figure 13.
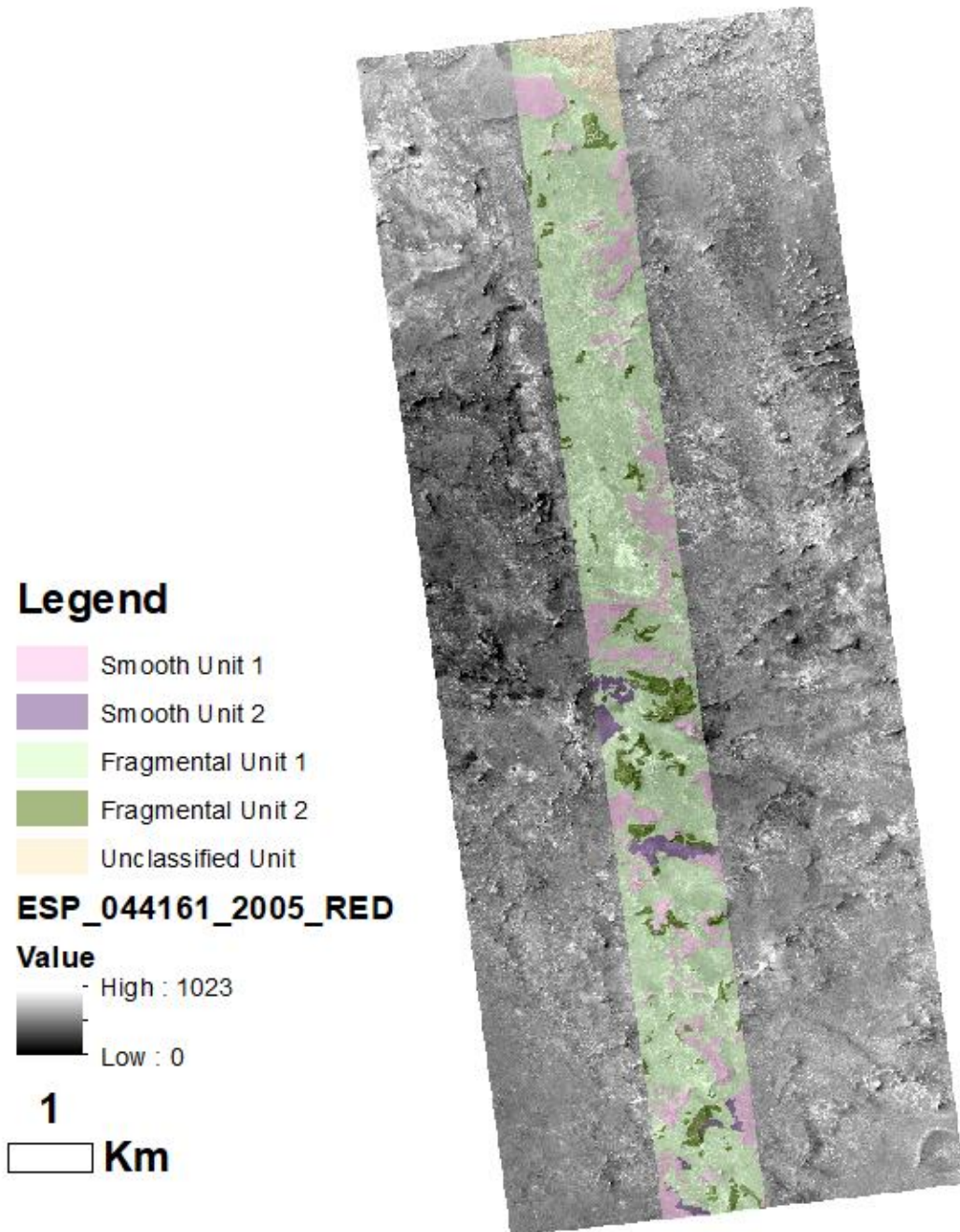
Figure 13 Mapping results for ESP_044161_2005_COLOR overlaid on the RED channel image. Greens show the fragmental unit and underlying bedrock, while pinks and purples indicate the smooth unit. The orange colour shows an as yet unclassified unit confined to the area most proximal to the crater rim. Image courtesy NASA/JPL/UArizona/HiRISE Team.

2.4.1   Fragmental unit

The fragmental unit is the most extensive ejecta unit within the Hargraves Crater ejecta. Overlying regional Noachian surfaces (Tanaka et al., 2005; Mangold et al., 2007; Mustard et al., 2007; Scheller and Ehlmann, 2020), the unit is mapped over the extent of HiRISE image ESP_044161_2005_COLOR (Fig. 13) as well as over Hargraves Crater on a CTX mosaic (Fig. 12). At full scale (Fig. 12), the fragmental unit correlates with the bright night TIR THEMIS signature (Fig. 10D). CTX mapped exposures of the unit are light toned, blocky, and fragmental, suggesting that unit is clastic. At a higher resolution, HiRISE images in Figure 14 show a complex portion of the exposed ejecta blanket, highlighting the unit. The most colour-varied portions are classified and mapped as the fragmental unit (Fig. 14), with measurable resolvable fragments ranging in size from tens to hundreds of meters. Both sub-units are discussed together, though fragmental unit 2 is has a more hummocky appearance than unit 1 and is slightly morphologically different. Locally, the fragmental unit is comparatively light-toned with the most broadly common IRB colours being white/off-white and in some areas are cyan (*c.f.*, Figs. 11, 13, and 14). Fragments shown are sub-angular (Figure 14B) and vary in colour in the colour-infrared image between shades of white, blue, green, and orange. Three different compositions of fragments are identified in Figure 14B. Variation in colour, rather than homogenous fragment colouration, is important to note. Some exposures are highly fragmented with similarly coloured fragments located close by. For example, outcrops identified by the green arrows (Figure 14B) are fragmented, but nearby fragments are similar and nearly homogenous in colour. In contrast, other outcrops show interlocking fragments that vary in colour (red arrow, Figure 14B). The mean exposed discrete clasts size is approximately 10 meters in diameter. The number of measured clasts in each zone (Fig. 15C) was primarily related to exposure and our ability to determine clast boundaries. Many fragmental unit clasts smaller than 3-4 pixels were unresolvable and not measured due to image resolution. A 2-pixel by 2-pixel (0.5 meter by 0.5 meter) box (a total of 4 pixels) represents the limit of resolution, with correlating area equivalent circle diameter 0.56 meters (Figure 15 in green (map of analysed clasts in Appendix A)). Mean sphericity for measured clasts in the fragmental unit was calculated to be 0.64 and no meaningful trend relating location and sphericity was observed in mean calculations for each zone.
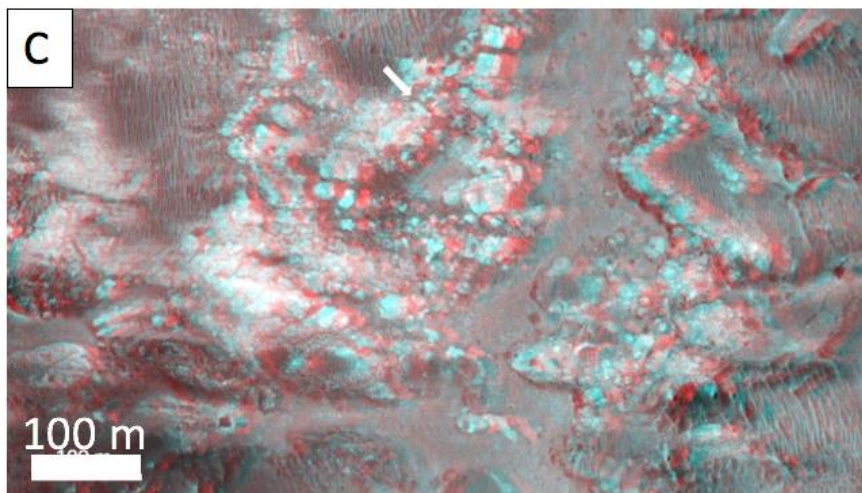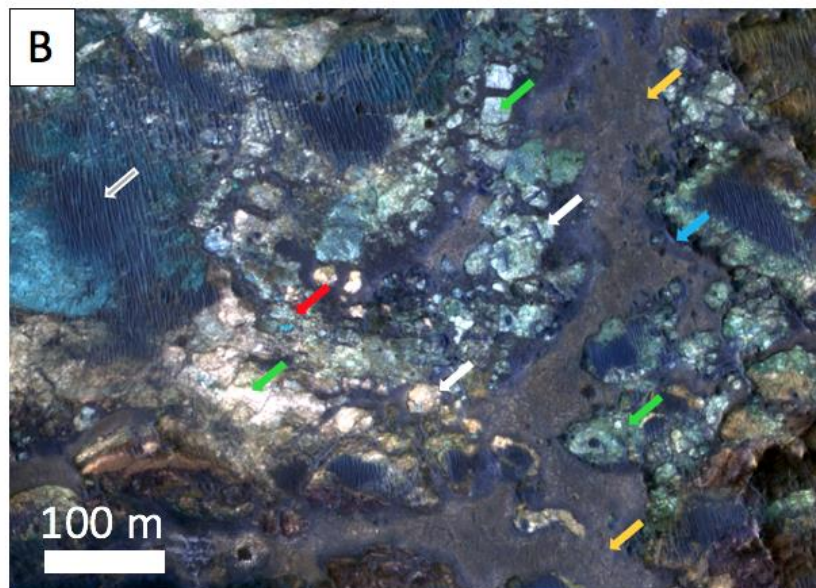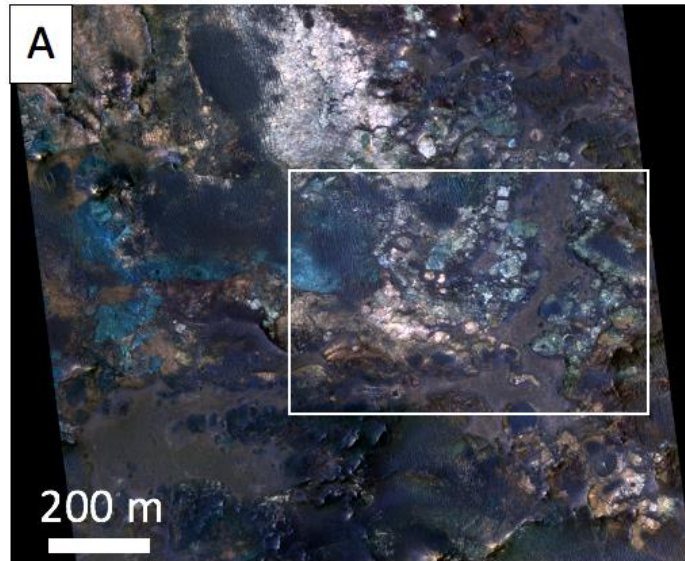
Figure 14 A) Context image showing a portion of ESP_044161_2005_COLOR. White box indicated location of 14B. B) Exposures of the fragmental and smooth units are the focus of the central and lower portions of the image. Green arrows indicate different monomict variations of the fragmental unit. The red arrow shows a portion of the fragmental unit that contains multiple varieties of clasts, a polymict portion. White arrows indicate sections of the fragmental unit that are visible specifically through "windows" in the smooth unit. The orange arrows identify northern and southern centres of the smooth unit while the blue arrow highlights the darker-toned border edge of the smooth unit. The grey arrow shows the presence of aeolian dunes in the scene. C) Anaglyph image of area shown in B. White arrow indicates an area showcasing two size fractions within the fragmental unit. Anaglyph is composed of ESP_044161_2005 and ESP_051321_2005 which were taken as stereo images of the same location.

The fragmental unit is visible in what appear to be "windows" where it is clearly observed to underly the smooth unit (described in full below). Here, we define a "window" as a state in which the underlying fragmental/bedrock unit is completely or partially (>50%) surrounded by the overlying smooth unit (Fig. 14). These windows are quasi-circular in shape and occur primarily at the outer edges of the overlying smooth unit. However, it is notable that some of the most distinct clasts in the exposed fragmental unit are observed in outcrops that host the smooth unit. Many of the measurable clasts, large enough to resolve but small enough that we can observe the full extent of the clast occur as outcrops just outside and below the smooth unit. As shown in an anaglyph view of the area (Fig. 14C), portions of the fragmental unit make up the comparatively more rugged terrain (i.e., higher slopes and topographic highs) that underlies the smooth unit capping the outcrop. In some areas, the fragmental unit is overlain and partially to fully obscured by blue to purple linear positive relief features (Fig. 14), which are clear and consistent examples of aeolian bedforms, in some cases manifesting as excellent examples of transverse aeolian ridges (see below) (e.g., Berman et al. 2018).

A Mean Clast Size by Distance (Zone) - Fragmental Unit

B Mean Clast Size by Distance (Zone) - Smooth Unit
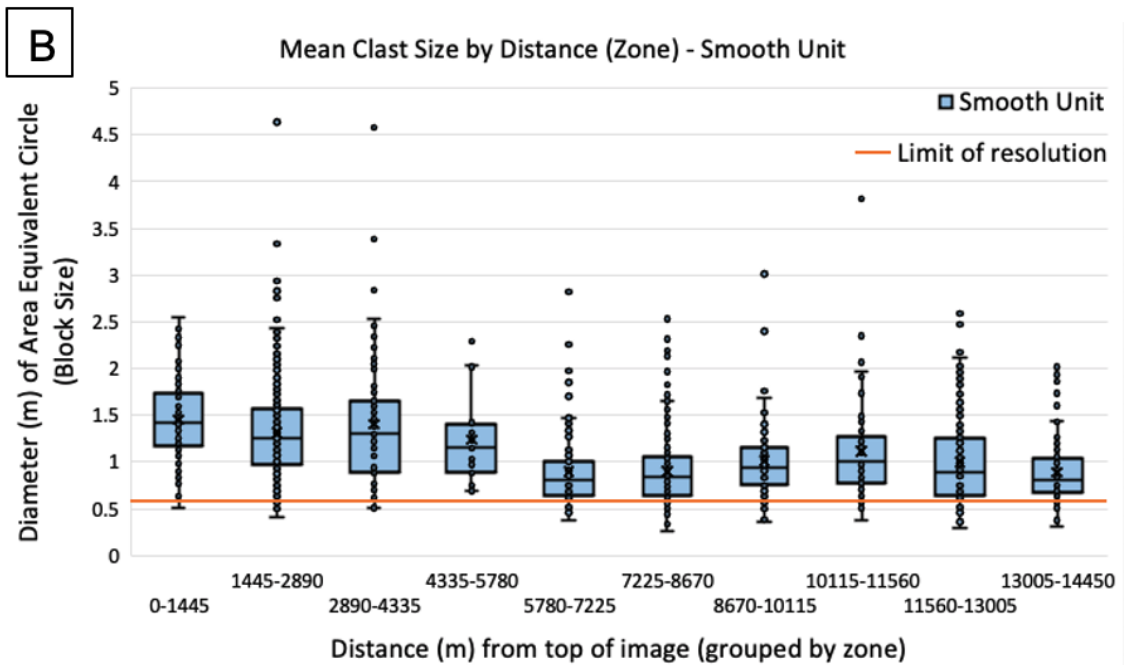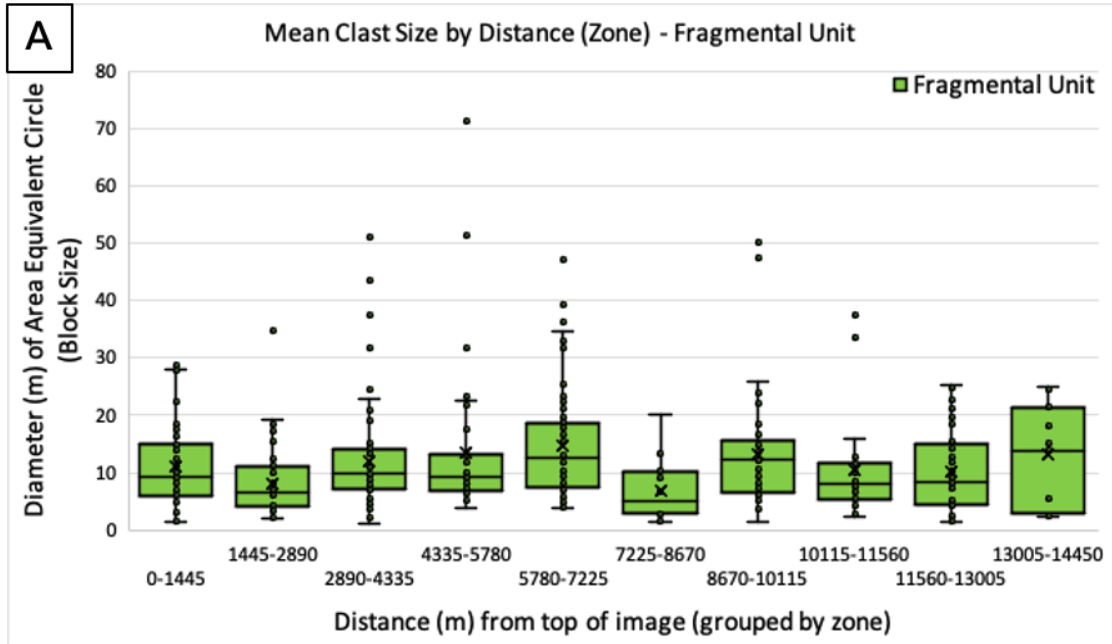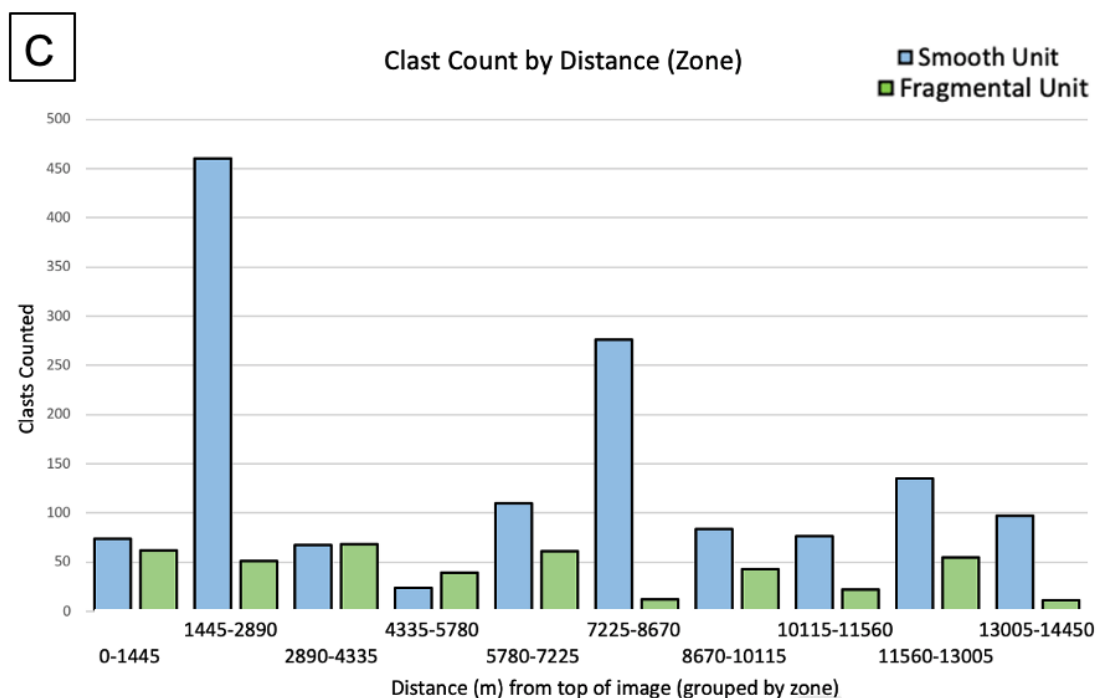
Figure 15 Box and whisker plots for the mean size of measured discrete clasts within (A) the smooth unit (blue) and (B) the fragmental unit (green). Each box plot represents all the measured clasts in one zone. Each zone represents a binned area of the image with zone 1 closest to the crater and zone 10 further from the crater, showing the mean clast size over distance from the crater. The approximate distance from the top of the image has been given in meters for each zone. (A) include a line in orange shows the diameter of the area equivalent circle of the smallest fully resolvable clast. (C) The number of measured clasts in each zone for each unit.

2.4.2   Dark-toned & smooth unit

Characteristically smooth and relatively homogenous darker-toned features (Fig. 16A) are classified as the "smooth unit" and mapped in pink (Fig. 12 and 13). Sub-units smooth 1 and smooth 2 (Fig. 13) are discussed together and are similar for interpretation and observation purposes but are slightly morphologically different for mapping. As shown in the full map of the Hargraves Crater ejecta, the unit extends consistently for approximately 1 crater radius from the crater rim (Fig. 12) and correlates with the dark areas of the THEMIS night TIR mosaic (*c.f.* Fig 10 and 12). At HiRISE high-resolution, the edges of the unit are visible as a blue-purple outline, (Fig. 14) that grades into

shadow. These edges of the unit, while distinct, are generally smooth and rounded (Fig. 16D), although in some areas they exhibit sharp vertical edges (see Fig. 16B). In some areas the unit is also characterized by a subtle polygonal texture that may be comprised of fractures (Fig. 16B and C).

In most cases, this unit occupies topographic highs within the high-resolution study area (see highs within Figure 14C). The smooth unit is notably always observed to stratigraphically overlie the fragmental unit (Fig. 14C, Appendix A Figure 14 for full extent). The outcrop in Figure 14 shows the unit in the more northern and eastern sections of the area and branching toward the south, thinning at the edges where the topography decreases. Edges of the unit are also notably smooth and at the margins of the so-called "windows" into the underlying fragmental unit. We also note that aeolian bedforms and dunes only rarely overlie the smooth unit, likely due to the higher topographic elevation of the smooth unit.

A close analysis of the smooth unit also shows clusters of bright clasts (generally ~3-4 pixels in area) that vary in colour but are similar to the colours observed for the clasts within the fragmental unit (Fig. 16D). The pixels appear to be randomly distributed throughout the smooth unit and are generally constrained to slightly lighter-toned portions of the smooth unit. The smooth unit contains significantly smaller clasts than those of the fragmental unit. These clasts observed in the smooth unit are composed of a few pixels rather than tens to hundreds of pixels when compared to the fragmental unit. The mean pixel size is ~1 meter in diameter (~4 pixels wide), though they are barely resolvable, introducing error into that measurement. There are many more discrete clasts visible in the smooth unit than within the fragmental unit. As the smooth unit outcrops over less area than the fragmental unit, counted clasts are highly contingent on the locations of the unit, though they are highest close to the crater and about a third of the way away down the image. These are locations with clear smooth unit deposits and less erosion to eliminate and obscure clasts. Mean apparent sphericity for measured clasts in the smooth unit was calculated to be 0.68 and no meaningful trend relating location and sphericity was observed in mean calculations for each zone.
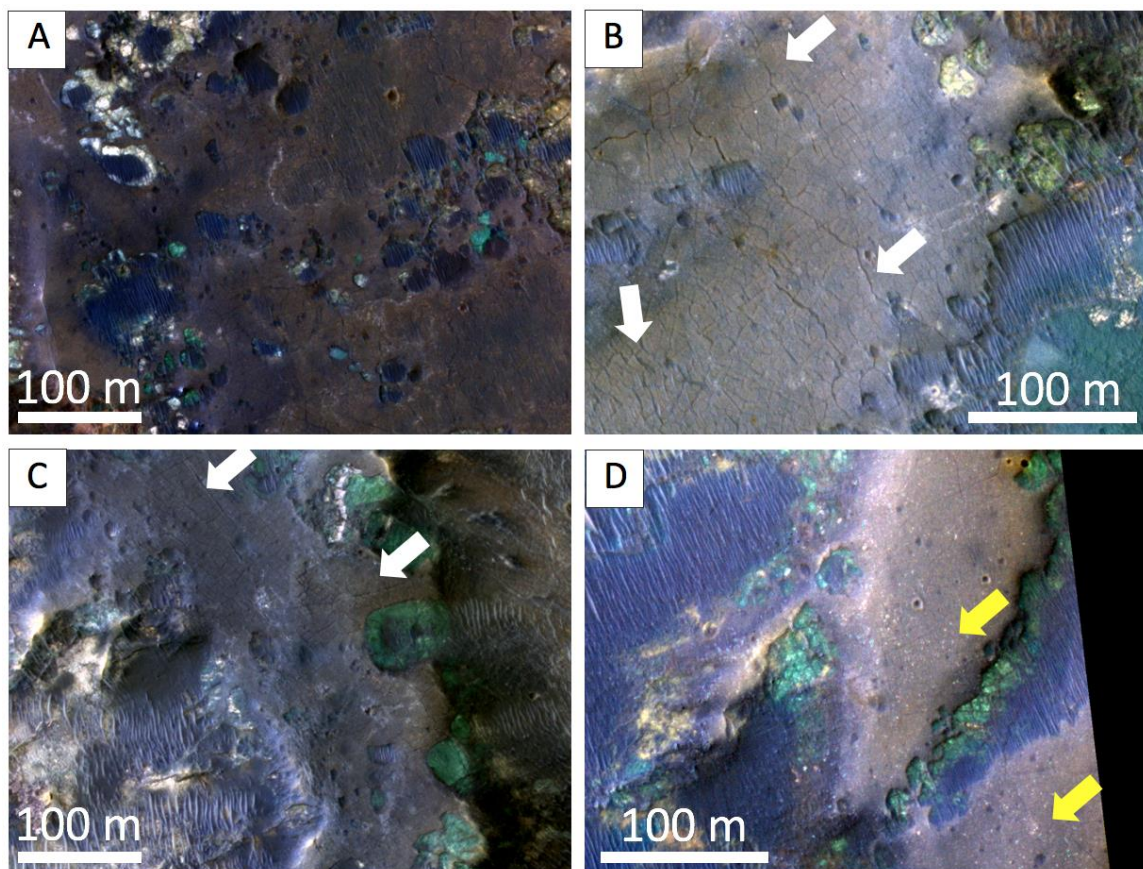
Figure 16 HiRISE images showing dark toned outcrops of the smooth unit. A) and C) show examples where "windows" have formed in the unit. B) and C) show polygonal features in the smooth unit (white arrows). D) shows bright pixels in the smooth unit that are interpreted as clasts of the fragmental unit or target rock (yellow arrows).

Finally, in exposures closest to the crater rim, we observe ~10 m diameter quasi-circular to circular pit features that are often densely clustered, but lack apparent ejecta materials of their own, within the smooth unit (Fig. 17). The pits do not have raised rims above the surrounding surface material and share edges, creating a network of negative relief features. As these features do not have ejecta deposits, raised rims, or any alignment other than clustering, they are inconsistent with an interpretation as clustered primary or secondary craters. In contrast, these clustered quasi-circular features are observed to be consistent with and interpreted as remnant crater related pitted materials (c.f. Tornabene et al., 2012). Pitted material has been observed superposing underlying ejecta units

(Tornabene et al. 2012), as is seen in Figure 17. When observed as a group of pits, this material is comprised of irregularly shaped depressions that may expose underlying material and form polygonal shapes with steep inner walls (Boyce et al., 2012; Tornabene et al., 2012). Pitted material depressions are nearly circular while sharing straight sides as the pits overlap each other (Boyce et al., 2012). Pits observed in the Hargraves Crater ejecta (Fig. 18A) share observable similarities with those identified in Mojave Crater (Fig. 18 B); their shapes as well as their common location within crater related materials, support the interpretation of these features as pitted materials in the smooth unit. While the morphology of the pits is already most consistent with pitted material, other similar features such as aeolian dune features or karst related features require specific environments or materials (Tornabene et al., 2012) that are not shown to be present at Hargraves Crater, making pitted material the most consistent interpretation for the pits observed in the smooth unit.
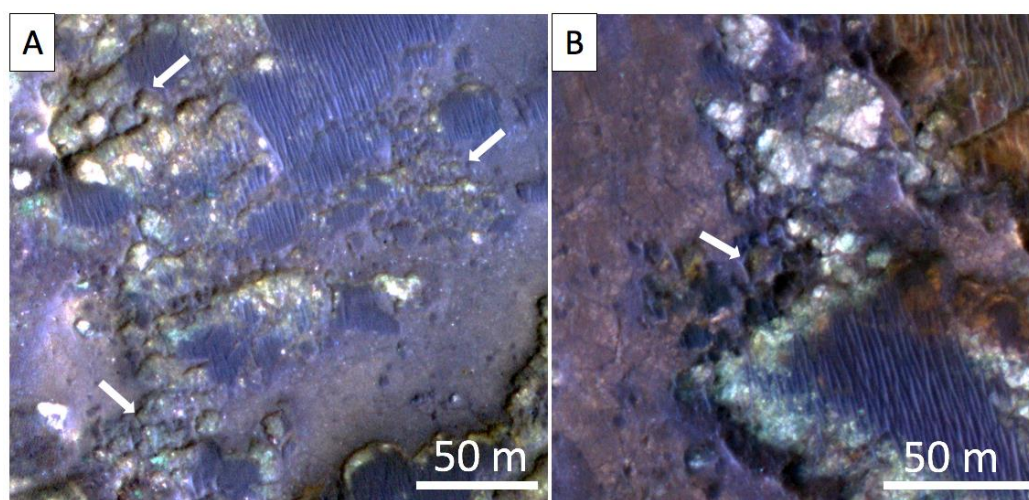
Figure 17 Examples of remnant pitted material at different locations in the smooth unit of the Hargraves Crater ejecta. White arrows indicate the features.
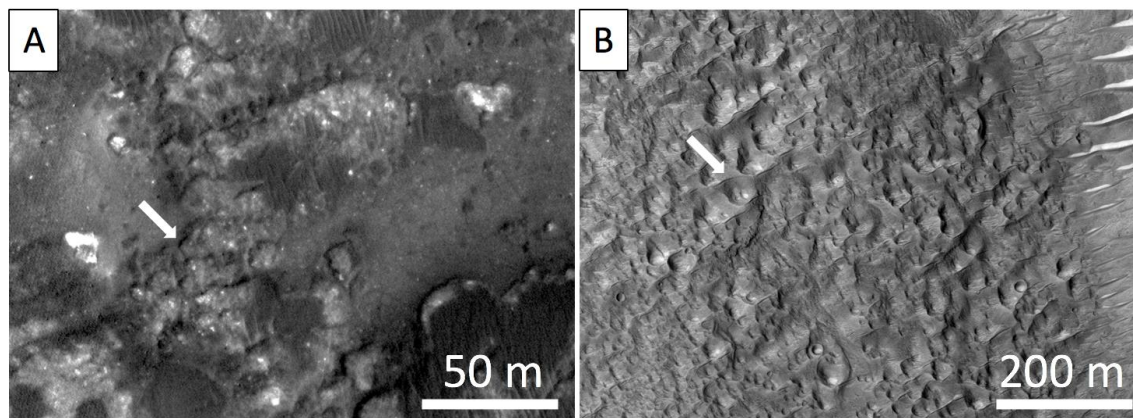
Figure 18 A. Pitted material in the Hargraves Crater ejecta. As shown in the ESP_044161_2005_RED image. B shows pitted material in a melt pool just west of Mojave Crater as a comparison, image ESP_063233_1875.

2.4.3   Aeolian bedforms

Blue/purple dark toned (Fig. 19), and yellowish in some occurrences (Fig. 20A), *en echelon* linear features appear to predominately overlay the fragmental unit and are interpreted as aeolian bedforms. The stratigraphic relationship between the fragmental unit and the bedforms is best observed where these linear features are the least densely concentrated (Fig. 19). The aeolian bedforms are consistently present in the local topographic lows and are oriented NNW-SSE. These aeolian bedforms are specifically interpreted as Transverse Aeolian Ridges (TARS), which are abundant across Mars (Berman et al., 2018). TARs are commonly located in local topographic lows, are locally sourced, and their strike direction is attributed to large scale wind patterns (Berman et al. 2018). TARs are closely spaced with consistent strike directions and sized as large ripples rather than full-scale dunes. They are approximately 1.5 m in height and can only be resolved well with higher resolution instruments such as CTX and HiRISE.
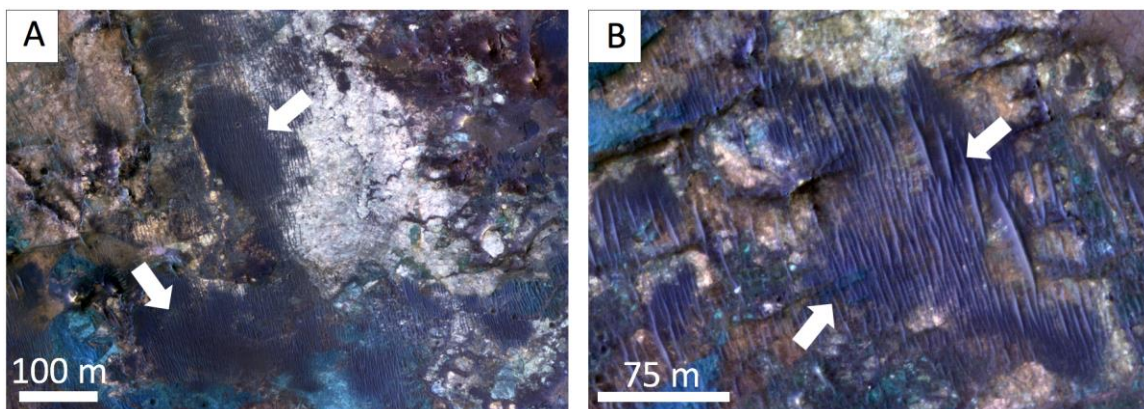
Figure 19 Northwest-southeast striking linear features are interpreted as aeolian dunes. A) shows dunes in topographic lows overlying some outcrop of the fragmental unit. B) is twice the resolution of the left image, showing a separate example of the TARS in more detail.

2.4.4   Superposed and buried craters

Located throughout the southern Hargraves Crater ejecta exposure are singular, non-connected circular features, some with relatively sharp and raised rims. Not to be confused with the interconnected quasi-circular pits described above, these features are consistent with craters (Fig. 20). Divided based on their context, there are both pre-existing craters and overprinting craters within the exposure. Although they generally lack raised rims, pre-existing craters in the area are quite circular and often filled with smooth dark material, sometimes with what appears to be a wrinkled texture, which upon closer inspection may correlate with numerous linear aeolian bedforms (Fig. 20). A small cluster of overprinting craters are visible between the two craters in Figure 20A.

2.4.5   Unclassified Unit

The unclassified unit is observed only singularly around Hargraves Crater. It has a lobed morphology consistent with a flow. It appears fractured to a degree much higher than other units at Hargraves Crater and may be consistent with older surrounding bedrock. We speculate that this unit may be consistent with a mass movement such as a landslide related to the formation of Hargraves Crater. The unit is not discussed further within this thesis due to its singular appearance and inconclusive evidence for interpretation.
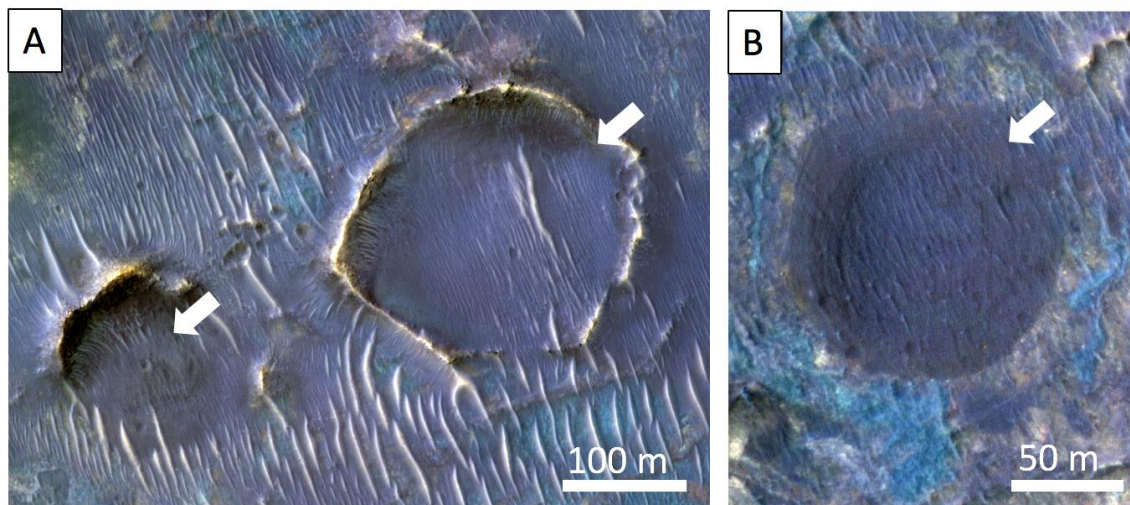
Figure 20 Buried and superposed craters in the image. A) shows 2 filled craters with several smaller more recent craters are visible between the two. B) is twice the resolution of A and shows a filled crater without still visible rims.

2.4.6   The Hargraves Crater ejecta blanket

This study focused on the southern exposure of the Hargraves Crater ejecta blanket because it exemplified the best exposure and preservation of the ejecta. The fragmental unit and underlying fracture bedrock are observed over the full extent of the study site. Bright, distinct clasts and massive deposits of the fragmental units are found closely associated with the overlying smooth deposits. The smooth unit is concentrated toward the eastern side of the image and is distributed extending from the top of the image, the crater rim. The smooth unit is consistently stratigraphically above the fragmental unit but is also observed in some topographic lows. However, as shown in Figure 12, the smooth unit and the fragmental unit are both observed and mapped around all sides of Hargraves Crater. Other portions of the ejecta blanket show a subset of the characteristics observed in the southern Hargraves ejecta (e.g., Fig. 21). Areas of the ejecta in the Nili Fossae trough and to the west (Fig. 21A, B) as well as exposures to the east show the same exposed breccia fragments and overlying smooth impact melt-rich units that are characteristic of the Hargraves Crater ejecta. To the northwest (Fig. 21C), the ejecta is not as obviously separated into the two units, but still shows some signs of underlying fragmental unit. Notably, other areas of the ejecta blanket show example of both the

topographically high draping outcrops of the smooth unit shown in the southern exposure as well as the smooth unit flowing around mounds of the fragmental unit in topographic lows. Overall, exposures of the fragmental unit within the smooth unit are more limited in other areas of the ejecta blanket. However, recent increased HiRISE coverage of more of the Hargraves Crater ejecta blanket may contribute to future studies.
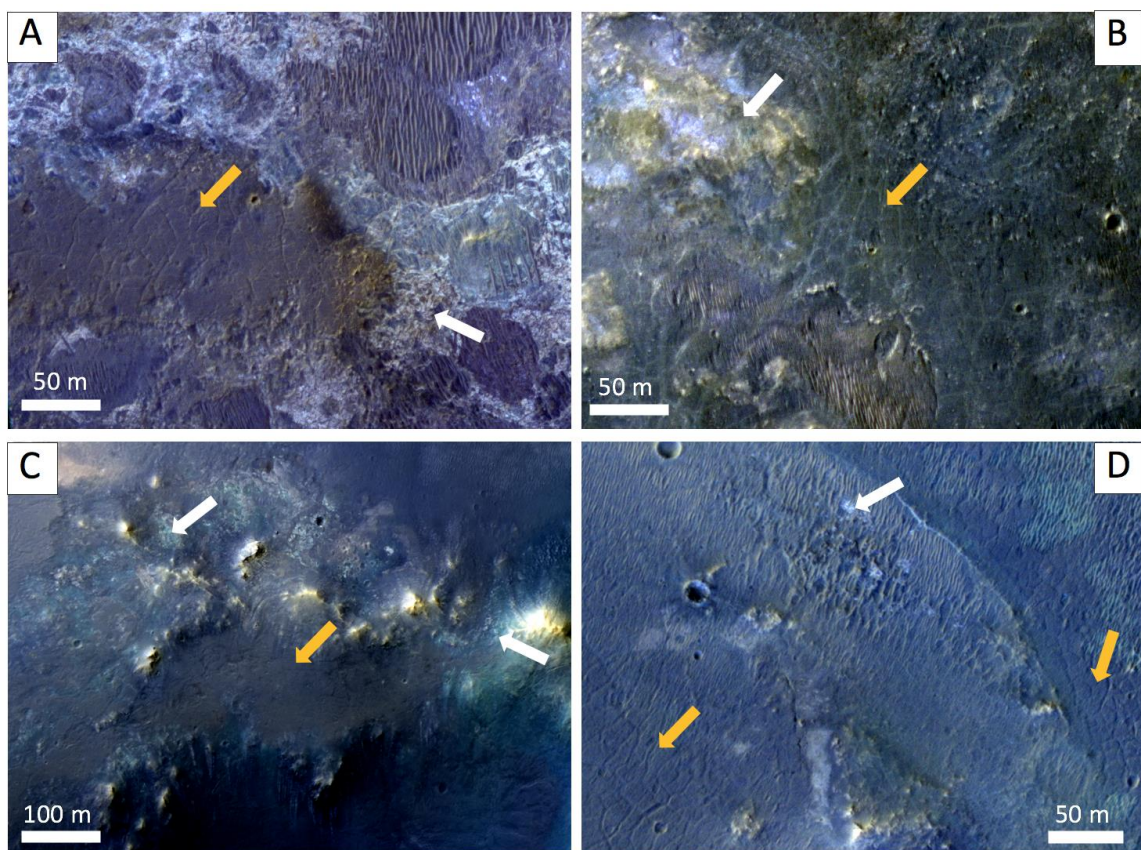
Figure 21 Other examples of ejecta at Hargraves Crater. Orange arrows indicate the smooth unit as well as polygonised texture in A, B, and D. White arrows indicate the fragmental unit. A) is from the Nili Fossae trough to the west of the crater. B) is between the trough and the rim to the west. C) is to the east of the crater. D) is to the north of the crater.

2.5 Discussion

We observed and mapped two distinct units comprising the Hargraves Crater ejecta. Below, we synthesize the morphologic, thermophysical, and stratigraphic observations

with the geologic context of the region as well as terrestrial studies to examine the nature, origin and emplacement of the units. The maps of Hargraves Crater on CTX images (Fig. 12) and of the southern ejecta in HiRISE images (Fig. 13) provide key stratigraphic and morphologic information regarding these units. Correlations with THEMIS TIR mosaics inform on the thermophysical properties of the units. The comparison of these datasets against terrestrial craters such as the Ries impact structure (Horz et al., 1983; Osinski et al., 2011) and the Mistastin Lake impact structure (Mader and Osinski, 2018) inform on the nature of the Hargraves Crater ejecta and ejecta processes as a whole.

2.5.1   Fragmental Unit – Ballistic Lithic Breccia

The fragmental unit is a bright, fragmental, rough unit of ejecta at Hargraves Crater. As shown in the map of the Hargraves Crater ejecta, the fragmental unit is distributed radially around Hargraves Crater (Fig. 12). Outcrops are often surrounded by the smooth unit and are patchy in exposure within one crater radius. The ejecta is distributed relatively symmetrically on all sides, with some preference shown to topographic lows over topographic highs. The mapping shape of the unit ties the ejecta to Hargraves Crater, rather than the local primary stratigraphy and is consistent with emplacement via ballistic sedimentation and radial flow (Oberbeck, 1975). Similar ejecta distributions are visible on Earth, the Moon and Mars. Based on the radial distribution and clast characteristics and content, we interpret the unit as a ballistic lithic breccia.

The clasts of the fragmental unit are similarly consistent with a ballistic breccia. As a whole, the unit is mapped as bright patches of exposed rock. This mapping correlates with bright, warm TIR signatures in the THEMIS night TIR mosaic (*c.f.* Fig. 10 and 12), supporting an interpretation of outcroppings of consolidated rock, such as a lithic breccia. Within the higher resolution southern ejecta exposure, the bright fragmental clasts are consistent with this interpretation. As shown in Figure 14, there is no visible sorting in the fragmental unit that may have indicated a different, perhaps fluvial or sustained aeolian, depositional mechanism and non-crater-related origin. Visible fragments show sub-angular rounding, as evidence of transport and turbulence that is consistent with radial flow after ballistic sedimentation (Horz et al., 1983). Composing the unit are a distinct variety of clast sizes. Some areas show non-resolvable clasts forming a matrix

(Fig. 14C, white arrow) around larger clasts, which dominate much of the visible exposure (Fig. 14). This unsorted, sub-angular, brecciated clast composition is consistent with lithic breccias observed on Earth at the Ries impact structure and the Mistastin impact structure, among others (Horz et al., 1983; Osinski et al., 2011; Mader and Osinski, 2018). Both craters have lithic breccia ejecta units composed of sub-angular to - sub rounded unsorted clasts and both are interpreted to be ballistically emplaced lithic breccias (Horz et al., 1983; Osinski et al., 2011; Mader and Osinski, 2018). The large massive monomict discrete sections of the fragmental unit (Fig. 14), may represent "megablocks" within the unit, which is also consistent with observations of megablocks at the Ries Impact Structure (Horz et al., 1983; Sturm et al., 2015). At the Ries crater, megablocks in the ballistic unit (the Bunte Breccia) were defined to be blocks larger than ~25m (Sturm et al., 2013, 2015) while on Mars they have been defined as larger than ~10m (Weiss et al., 2018). At Hargraves Crater, the massive portions of the fragmental unit are, if considered together by colour to be blocks, much larger than 25 m, up to kilometres in scale. At the Ries impact structure these blocks are interpreted to be of allochthonous origin, and we interpreted a similar origin for those observed at Hargraves Crater and for the entirety of the fragmental unit. It should be noted that the Ries crater (24 km diameter) is a smaller crater than Hargraves Crater (68 km diameter). Thus, the megablocks of Hargraves Crater would be scaled to a substantially larger cut-off for megablocks, as the ejecta velocity generated by the impact would be significantly greater and capable of excavating larger blocks (Housen and Holsapple, 2011). Caudill et al. (2018) similarly suggested large blocky fragments within the Bakhuysen crater ejecta on Mars may be exhumed megablocks and made the same cursory interpretations regarding the Hargraves Crater ejecta. The Hargraves Crater fragmental unit, including both the lithic clasts of variable sizes and the megablocks, is interpreted as a ballistically emplaced lithic breccia, which is consistent with analogous interpretations at the Ries impact structure and the Mistastin Lake impact structure (Horz et al., 1983; Osinski et al., 2011; Mader and Osinski, 2018).

The fragmental unit additionally demonstrates heterogeneity of colour, which has implications for the original target stratigraphy. The colour variety, in HiRISE IRB, indicates differences in the compositions of the fragments, suggesting possibilities of an

original layered or varied stratigraphy composed of multiple units as well as alteration before, during, and even after deposition (e.g., Tornabene et al. 2013; Osinski et al, 2013). Alteration of the rocks, which is consistent with local stratigraphy (Mangold et al., 2007; Mustard et al., 2007; Ehlmann et al., 2009; Ehlmann and Mustard, 2012; Scheller and Ehlmann, 2020), has been correlated with changes from blue and green mafic clasts (in IRB colour) to yellow and orange coloured clasts (in IRB colour) (Delamere et al., 2010). Inconsistent alteration would result in a varied lithology and varied coloration. Regardless of composition, the polymict nature – being composed of multiple lithologies – of the fragmental unit as well as the variation in fragmentation and size, suggests an allochthonous origin (Grieve and Therriault, 2012), as fragments would have to be transported from multiple locations to be deposited adjacent to and entrained with each other, consistent with ballistic sedimentation and radial flow (Hörz et al. 1983). A combination of polymict and monomict sections of breccia are observed at several terrestrial craters, including the Ries crater and the Mistastin Lake crater (Horz et al., 1983; Osinski et al., 2011; Mader and Osinski, 2018). While the polymict portions of the Hargraves Crater ejecta are consistent with an interpretation as a ballistic breccia, the monomict components (Figure 14B, green arrows) help to dismiss an alternative interpretation. The Nili Fossae megabreccia unit associated with the formation of the Isidis Basin (e.g. Mustard et al. 2009; Weiss et al. 2018) comprises pieces of bedrock that are variably banded and brightly coloured (Bramble et al., 2017; Scheller et al., 2020). While the Hargraves Crater ejecta may tap into the local megabreccia as source rock for the ejecta, much of the fragmental unit consists of massive units of monomict breccia in green colours in the HiRISE IRB swath. This coloration and the lack of banding within any of the blocks at Hargraves Crater suggest additional inputs into the ejecta and is not consistent with an interpretation of the fragmental unit as outcroppings of the local megabreccia.

2.5.2   Smooth Unit – Clast-bearing Impact Melt Rock

The smooth unit is dark toned and smooth in surface texture (Fig. 16) with a clast content that varies from clast-poor to clast-rich. The distribution of the unit, shown mapped in Figure 12, correlates with dark, cool areas of the THEMIS night TIR mosaic (*c.f.* Fig. 10

and 12), consistent with melt-bearing rock. Similar to early impact melt deposits identified on the Moon (Hawke and Head, 1977), the smooth unit is distinctly located proximal and radial to the crater and not near a source volcanic vent, making it inconsistent with a volcanic interpretation (Table 1). The Syrtis Volcanics are located nearby and have taken advantage of a topographic low, the Nili Fossae "trough", to spread, but the surface surrounding Hargraves is comparatively topographically higher and is not mapped to include the volcanics (Mangold et al. 2007). Thus, the smooth unit is less consistent with an interpretation as lava flows or pyroclastic deposit and consistent with an interpretation as melt-bearing impact melt. Thus, we interpret the smooth unit as a clast-bearing impact melt unit.

The surface characteristics and texture of the smooth unit is also consistent with an impact-melt bearing unit interpretation. The dark tone and smooth texture are similar to many known impact melt deposits on the moon (Table 1) (Bray et al. 2010, Hawke and Head 1977, Howard and Wilshire 1975). The polygonal features shown in Figures 16B and 16C are interpreted as cooling-contraction fractures. This texture is indicative of the high temperature nature of the unit during emplacement. Cooling cracks have been previously associated with impact melt on the Moon, Mars, and Earth including at the Mistastin Lake impact structure (Table 1) (Mouginis-Mark and Garbeil, 2007; Bray et al., 2010; Tornabene et al., 2012; Mader and Osinski, 2018). Similarly, the visible sharp contacts between the smooth unit and the underlying fragmental unit (Fig. 14 and 16) suggest both the emplacement of a superheated distinct unit and a change between the deposition of the fragmental unit and that of the smooth unit (Osinski et al. 2011) showing two stages of deposition. This is consistent with a melt-rich unit and is also seen terrestrially at the Ries impact structure (Horz et al., 1983; Osinski et al., 2011) and the Mistastin Lake impact structure (Mader and Osinski, 2018). Alternative interpretations of the unit such as an airfall or a grain flow are unlikely to show the distinct sharp contact visible at Hargraves Crater. An airfall deposit may occur over a longer period of time (Fisher and Schmincke, 1984) and would then be unlikely to produce the sharper contact visible at Hargraves Crater. A grain flow unit separate from the initial ejecta would likely still blend in with the contact with the underlying breccia unit. Finally, we interpret the circular features within the smooth unit as pitted material (Fig. 17 and 18) which are

consistent with impact melt units (Tornabene et al., 2012), corroborating the interpretation of this unit as a clast-rich impact melt rock. Vents that have been compared to pitted material have been identified at the Ries impact crater (Caudill et al., 2018). While lava flow pits and wind scoops may have similar pit-shaped features, they are morphologically different from those seen at Hargraves (Tornabene et al., 2012).

The clast content of the smooth unit is also most consistent with impact melt-rich rock. Specifically, as shown in Figure 16D, the unit contains fragments of target rock in small variously coloured, but not resolved, pixels within the unit. These clusters of pixels are likely lithic clasts close to the resolution limits of HiRISE (on the order of 0.56 meters in diameter or less) (Fig. 15 and 16D). The incorporation of clasts into the melt rock is common in impact melt rock as seen in the impact melt layer and the suevite layer respectively at the Mistastin Lake crater and the Ries crater (Horz et al., 1983; Osinski et al., 2011; Mader and Osinski, 2018). However, these clasts are too large to be xenoliths or pyroclastic bombs and too extensively distributed for a volcanic lava like the Syrtis Volcanics. Additionally, the meter-scale clasts observed within the smooth unit of Hargraves together with the thin atmosphere of Mars are not consistent with the clast sizes of airfall deposits (Fisher and Schmincke, 1984). We also do not observe grading and sorting within the unit, which would be consistent with a pyroclastic flow or airfall deposit (Fisher and Schmincke 1984). Both an airfall hypothesis and a grain flow hypothesis would also be consistent with sorting and grading (Lowe, 1976; Fisher and Schmincke, 1984). While it is possible that these patterns are not resolvable, the visibility of the larger clasts within the smooth unit are not consistent with the organization of either hypothesis. The visibility of the meter-scale clasts suggests a lack of sorting within the smooth unit that is more consistent with an impact-melt hypothesis.

Table 1 Hargraves Crater Smooth Unit Characteristics and Characteristics of Possible Interpretations

	Stratigraphy	Morphology	Contact w. Underlying Unit	Surface Texture	Clast Composition	Pitted Material	Location	References
Hargraves Crater	2 layers, smooth unit consistently overlying fragmental breccia unit	Lobed and branchy, draping in some places and sharp walls in others.	Clear, distinct contact between two separate units	Smooth, few craters, polygonal texture	Meter-scale clasts within much finer-grained matrix, various composition, no visible sorting	Yes. Interpreted as crater-related pitted material.	Proximal to the crater, distribution appears directly crater related	This study, Ryan et al. (2016, 2017)
Impact Melt	Impact melt over continuous ejecta, fills in depressions	Lobed morphology, flows, ponds, veneers	Distinct sharp edges against surrounding and underlying ejecta	Smooth, cooling cracks, tension cracks, lineation, flow textures, may preserve more recent craters	Some clast bearing, some not.	Yes. On Mars, Ceres, and Vesta.	Proximal to the crater, crater interior, crater terraces.	Bray et al., 2010, 2018; Hawke and Head, 1977; Howard and Wilshire, 1975; Tornabene et al., 2012, Osinski et al 2011, Hörz et al. 1983
Syrtis Volcanic Lavas	Lava over jarosite ridges and layered sulfates, fills in depressions	Flat and smooth	Sharp contact, chilled margins	Smooth, preserves craters, levees, polygonal texture	No clasts of large size, possibly xenoliths	Yes - but differing morphology to crater-related pitted material	Low topography areas in Nili Fossae, Syrtis Major Planum primarily. Near source vents.	Scheller et al., 2020; Ehlmann et al., 2009; Bramble et al., 2017; Mustard et al., 2007, 2009, Fisher and Schmincke, 1984
Pyroclastics	Could overlie anything, fills in depressions	Flat	Sharp contact, cooling margins		Clastic, sorted, and graded	Yes	Near a source vent.	Fisher and Schmincke, 1984
Grain Flow	Could overlie anything	Rubbly	Non-distinct	Rubbly on a small scale	Clastic, sorted, and graded	No.	Near crater	
Airfall	Does not fill in depressions	Rubbly	Non-distinct	Rubbly on a small scale	Clastic, sorted, and graded	No.	Near crater	

While the smooth unit in the southern ejecta at Hargraves Crater is consistently found on topographic highs, it does occupy lows in other areas of the ejecta blanket, and it is important to note that it always remains stratigraphically higher than the fragmental unit. While melt-bearing deposits typically occupy topographic lows (e.g. Hawke and Head 1977; Bray et al., 2010; Osinski et al., 2011; Tornabene et al., 2012) the erosional environment observed in the southern exposure suggests that the current topographic highs may have once been lows. Inverted topographic features are common on Earth and Mars in settings where a more competent material fills in a depression or a low such as a channel, graben or crater surrounded by less competent surrounding or country rock (e.g. Newsom et al., 2010). The more competent melt-bearing rock is less susceptible to erosion than the underlying or surrounding melt-poor fragmental unit. While the more readily erodible surrounding fragmental material is removed, erosion leaves the more difficult to erode material (and whatever lies directly below it) as a local topographic high. Such inverted topography has been observed at terrestrial impact structures, such as at the Mistastin Lake Impact Structure Discovery Hill outcrop (Mader and Osinski, 2018).   This outcrop, interpreted as a melt-pool, remains as a topographic high capping an underlying melt-poor lithic breccia layer, while the surroundings have been glacially eroded away (Mader and Osinski, 2018). In impact ejecta, the overlying melt unit would be inherently a more competent material as a result of the "melting" and then cooling of the parent rock compared to the underlying less competent fractured rock fused into a breccia.

2.5.3   A Two-Layer Stratigraphy

One of the unique features of the Hargraves Crater ejecta blanket is the visibility of the inner structure of the ejecta through the windows in the smooth unit. These windows can be easily mistaken as clasts themselves rather than gaps in the smooth unit but can be distinguished with careful observations. Nonetheless, such occurrences often impede our ability to measure the clast or fragment characteristics. This is especially true where the margins of the clast cannot be completely observed due to obscuration by the overlying smooth unit or, in some cases, insufficient size of the so-called windows through the smooth unit or extensive aeolian bedforms/deposits. Even so, the windows allow for

high-resolution examination of the contact between the overlying smooth unit with the underlying fragmental unit.

These two units at Hargraves Crater are interpreted as an underlying ballistic clast rich impact breccia and an overlying clast rich impact melt rock, reminiscent of the two layers of ejecta observed at both the Ries impact structure and the Mistastin Lake Impact structure (Fig. 22). The suevite unit at the Ries crater is interpreted as a high temperature melt-bearing flow emplaced directly on top of the underlying ballistic lithic Bunte Breccia. At Hargraves Crater we see evidence of these same characteristics, as well as a high impact melt content, similar to that of the suevite unit at the Ries. At the Mistastin Lake Impact Structure, similar outcrops of preserved brecciated and fragmented material underlie impact melt bearing layers (Mader and Osinski, 2018). Discovery Hill, one such outcrop, is interpreted to showcase at least two stages of emplacement- a ballistic fragmental layer followed by an impact melt-bearing layer. The surrounding material of that layer has since been eroded away. These terrestrial craters and the field observations of their characteristics, particularly from Hörz et al. (1983) and Mader and Osinski (2018) help to interpret the top down observations from Hargraves Crater and provide insight into the cratering process. Hargraves Crater provides an orbital, map view Martian complement to these field studies of craters on Earth.
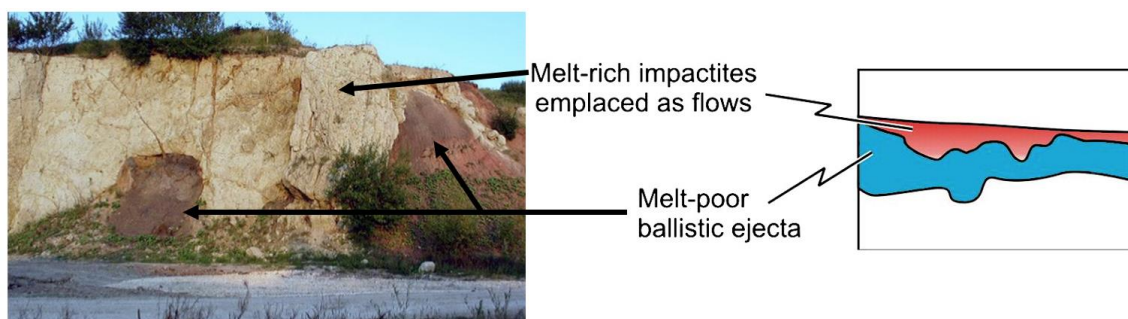

Figure 22 Shows an image of crater ejecta at the Ries crater with two distinct layers linked to the corresponding types of ejecta layers. Image and figure modified from Osinski et al. (2011).

The Hargraves Crater ejecta appears to be an excellent orbital example of the superposition of a melt-bearing unit on a brecciated, ballistically emplaced unit that is

observed in the field at Mistastin Lake and the Ries and supports the two-stage ejecta emplacement model posited by Osinski et al. (2011). These results further support that any explanation for ejecta emplacement will need to account for the two units – one melt-bearing and one melt-poor – shown clearly at Hargraves Crater (Fig. 12, 13, 14, 16). This visibility of the inner structure of the ejecta blanket is one of the unique properties offered by Hargraves Crater. Elevating its value for emplacement studies, the presence of remnant pitted material showcases the preservation state of the Hargraves Crater ejecta. While not pristine, the visible pitted material does show that some of the surface morphology is still present in the Hargraves Crater ejecta. As the erosion is crucial to the level of exposure observed of the lower layers of Hargraves Crater ejecta, this balance between erosion and preservation is one of the advantages to studying Hargraves Crater. It is possible that further erosion of these pits is the origin for the windows seen in other locations. This uncommon visibility and balance between preservation and excavation is important to future impact studies. By finding and analysing other examples of such "Hargraves-type" ejecta blankets we can significantly enhance our knowledge of ejecta formation and emplacement and have a stronger understanding and basis for sampling and mission studies on Mars.

Chapter 3

3   Discussion

The impact ejecta deposits of Hargraves Crater represent a unique opportunity to study crater ejecta formation and emplacement on Mars and by proxy Earth. Martian craters are more analogous to terrestrial craters than lunar craters due to similarities between the two planets. Both planets have significant crustal volatile content, atmospheres, and active surface processes such as erosion. Thus, the opportunities provided by craters such as Hargraves Crater are significant to furthering our understanding of impact cratering. In this chapter, we define and explore the significance of Hargraves-type ejecta as showcased by Hargraves Crater and a sample of craters bearing similar features. Further work and a survey to locate other examples of Hargraves-type ejecta deposits is essential to future cratering studies.

At Hargraves Crater, the value of studying the ejecta lies in the unusual combination of preservation and exposure that reveals the interior characteristics of the ejecta. In Chapter 2, data was provided for the presence of a distinct impact melt bearing rock layer overlying lithic impact breccia, which constrains potential mechanisms for impact ejecta emplacement. The Hargraves Crater ejecta blanket shows two distinct units of ejecta, each with distinctly different properties, demonstrating that there must be at least two phases of ejecta emplacement. The overlying layer, interpreted as an impact melt layer, is a darker tone and is mapped as the "smooth unit" of this study (Chapter 2, Fig. 16). The impact melt layer has a smooth texture but includes polygonal fracturing (Chapter 2, Fig. 16), interpreted as a cooling pattern. Small clasts (less than 2 meters in diameter) are imbedded in this smooth unit. Any emplacement mechanism must account for these characteristics and based on these observations and others presented in Chapter 2, we interpret the smooth unit as an impact melt-bearing rock unit, emplaced as an overland flow as suggested by Osinski et al. (2011).

Similarly, the underlying unit also establishes constraints on ejecta mechanisms. As a whole, the Hargraves Crater ejecta is heterogeneous, polymict, even as megablocks of homogenous colour, comprise some monomict areas. Both variations of the unit show

variation in the reflectance within individual clasts that may be suggestive of internal, non-resolvable brecciation within the clast. The polymict nature, large "megablocks," lack of visible sorting and sub-angular rounding on the distinct clasts, and a thermophysical signature similar to that of bedrock are all consistent with a lithic breccia, emplaced via ballistic sedimentation and radial flow (Oberbeck, 1975; Horz et al., 1983).

Finally, the characteristics of the relationship between the two units provide further constraints. The distinct contact between the two units suggest that they were emplaced as distinct stages, one after the other. The consistent stratigraphy, lithic impact breccia underlying impact-melt bearing rock, regardless of topography, corroborates this observation. The clear contact, within the constraints of orbital observation, additionally supports the suggestion of overland flow for emplacement of the impact melt bearing layer, as it shows a comparatively undisturbed ballistic layer rather than a churned layer as might be seen with aerial emplacement of the melt rock (Osinski et al. 2011; Hörz et al. 1983). The relationship between these two layers taken together is consistent with a ballistic lithic breccia deposited prior to the emplacement of an impact melt-bearing unit via overland flow. All of these characteristics and the views of the ejecta blanket visible at Hargraves Crater are integral to further emplacement mechanism and impact studies. The connections drawn in Chapter 2, between the layers seen terrestrially and the two units at Hargraves demonstrate the importance of Hargraves Crater to our understanding of cratering studies. The Hargraves Crater ejecta offers a map view, orbital perspective to the ejecta that we see on Earth.

Hargraves Crater is the best-known representation of the balance of exposure and preservation that allows us to view the interior of the ejecta blanket, revealing a lithic breccia unit underlying an impact melt-bearing unit, that we term Hargraves-type ejecta. To continue studying impact cratering processes it is important to both study other craters that have these characteristics and to understand why they exist. The Hargraves Crater ejecta blanket is one of few craters with such features but is not alone. The thermophysical signature of the fragmental unit at Hargraves Crater, indicative of bedrock, was used to identify similar exposures in the ejecta blankets of other craters. A small number of other craters share many of the characteristics observed at Hargraves

Crater. In particular, there are three excellent examples of "Hargraves-type" ejecta worth mentioning: Kontum crater (-32.04°N, 292.93°) (Fig. 23C), an unnamed crater in the Hellas region (-16.18°N, 74.40°) (Fig. 23D) and another unnamed crater in Noachis Terra (-24.60°N, 26.16°) (Fig. 23B). Kontum Crater has a diameter of ~22 km and is located on the edge of Bosporos Planum, south of Valles Marineris. The unnamed crater located in the Hellas Basin region, north of Saheki Crater, is ~3.8 km in diameter. Finally, the Noachis Terra crater is ~26 km in diameter and is located just southwest of Murray Crater and some distance east of Bakhuysen Crater. A THEMIS brightness temperature mosaic based specifically on night-time Thermal Infrared (TIR) observations for each of the discussed craters compares to that of Hargraves Crater and the exposure that is the main focus of Chapter 2 (Fig. 23). The bright signature is a proxy for the outcrop possessing a high thermal inertia, specifically it shows that at night, the outcrop retains heat in spots that were cool and dark during the day. This type of thermophysical signature is common to bedrock and other compacted bodies of rock (e.g. Edwards et al., 2009). Similarly, in Figures 23B, 23C, and 23D, the Noachis Terra, Kontum, and Hellas region craters, respectively, have ejecta blankets with bright THEMIS Night TIR signatures. The ballistic lithic breccia layer of the ejecta is preserved due to the overlying melt layer yet exposed through erosion and the "windows" in the ejecta. There are corresponding cooler zones in the THEMIS TIR mosaic as well that correlate in a number or locations with the smooth unit (Fig. 23) While these thermophysical signatures are not unique to Hargraves-type craters, the correlation with the mapped units is unusual and they aid in attempts to understand the processes by which this type of ejecta forms rather than more typical ejecta blankets.
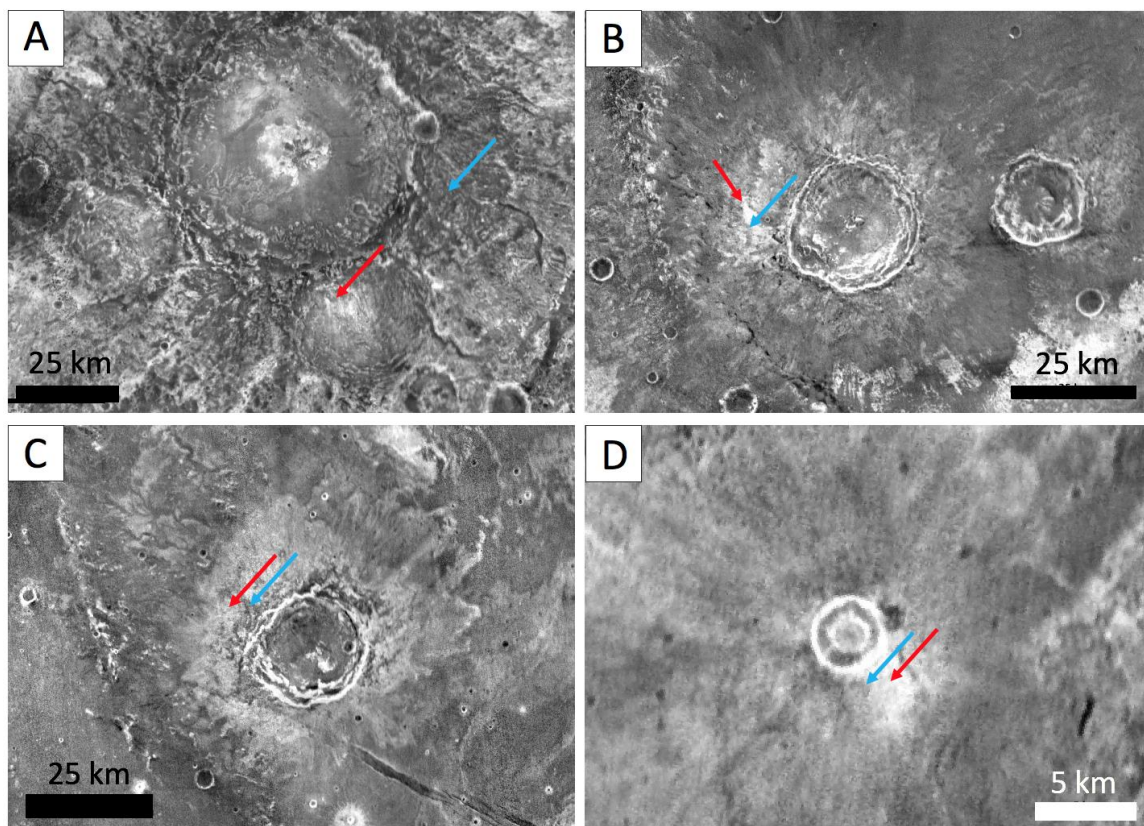
Figure 23 Images from the THEMIS Night Infrared Global Mosaic. Hargraves Crater (A), An unnamed crater in Noachis Terra (B), Kontum Crater (C), and an unnamed crater in the Hellas region (D). In each image, a red arrow indicates a location with a bright Night IR signature in the ejecta blanket of the crater. Blue arrows indicate cooler signatures.

When examined in visible light images, the ejecta blankets of these three craters exhibit further similar characteristics to those seen at Hargraves Crater; namely, the ejecta can be divided into a fragmental brecciated unit underlying a dark toned smooth unit. Figures 24, 25, and 26, show a sample of images from Kontum Crater, the Noachis Terra crater, and the Hellas crater, respectively. Some areas within the images indicate areas interpreted as lithic impact breccia while others show outcrops interpreted as impact melt-rich material. In all three figures at all three locations, the units suggestive of the fragmental unit are fragmented, shown by variation in the reflectance, have a brightness suggestive of bedrock or breccia, and have some angularity in shape. None appear to

have visible layering or sorting. The breccia units at each of the three craters share visual and morphological similarities with the breccia visible at Hargraves Crater; likewise, with the dark toned smooth units.
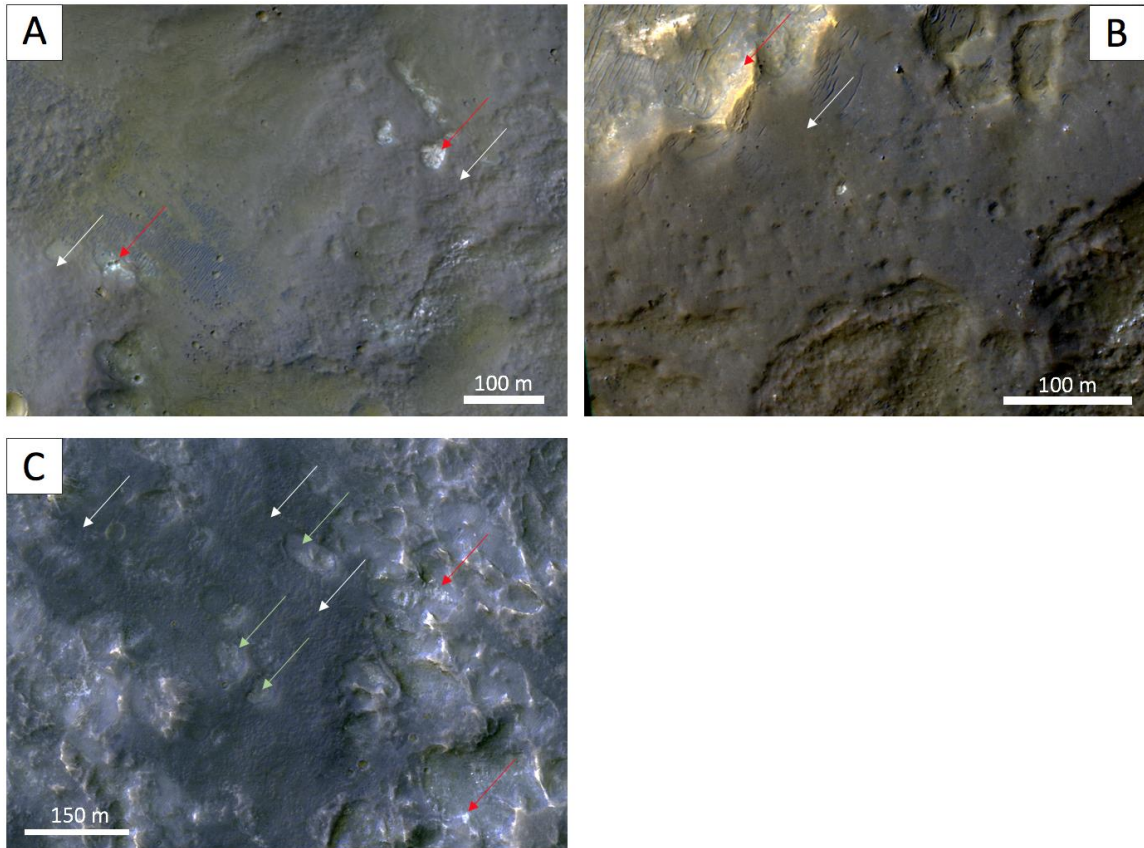

Figure 24 A collection of scenes from the ejecta blanket of Kontum Crater. Smooth units interpreted as impact melt-rich are indicated with white arrows while brecciated fragmental units are indicated with red arrows. Windows within the impact melt-rich unit are indicated with green arrows in Figure C. Taken from HiRISE images: A/B: ESP_059397_1480_COLOR and C: ESP_058962_1480_COLOR, Courtesy NASA/JPL/UA-LPL
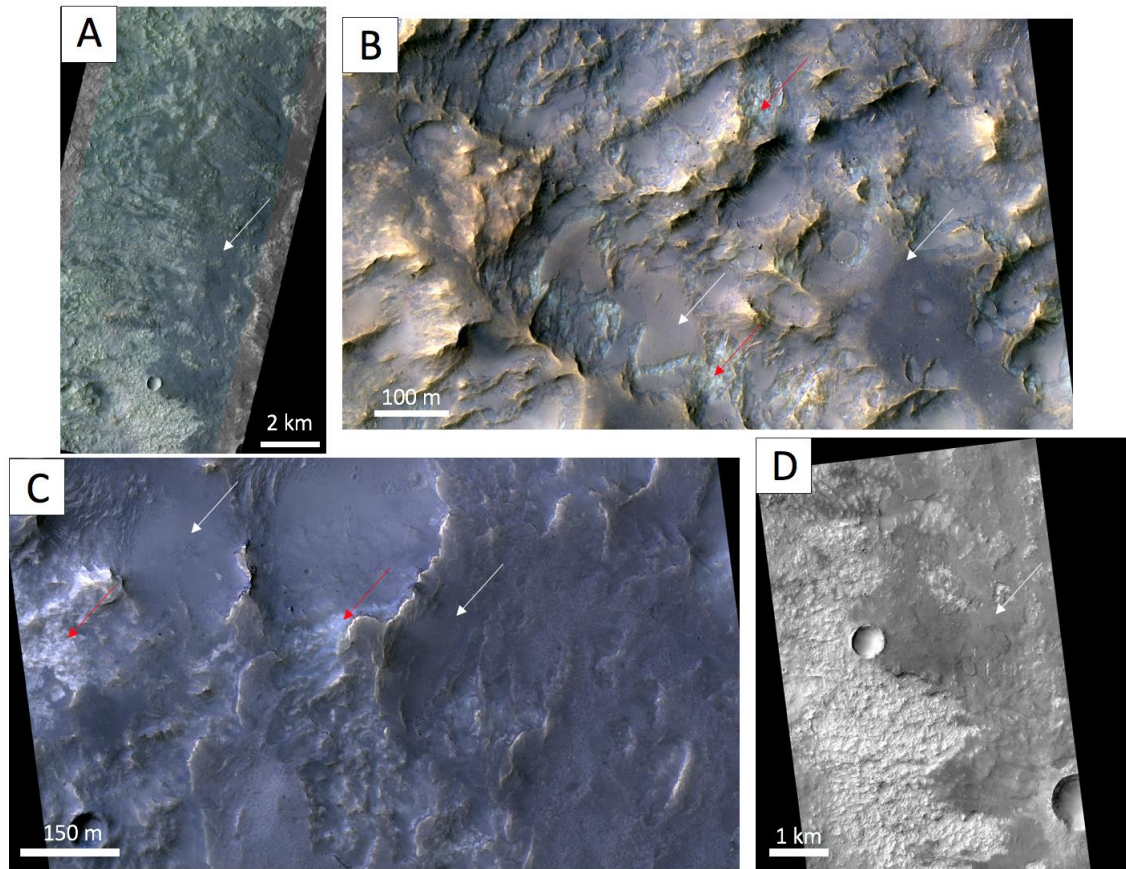
Figure 25 A sample of images of the ejecta blanket of a crater located in Noachis Terra at –24.60°N, 26.16°. Figure A shows a CaSSIS image while Figures B-D are taken from HiRISE images. White arrows shown the impact melt-bearing unit, while red indicate the breccia unit. B also showcases the impact melt-bearing unit in a topographic low but eroding away such that it is topographically higher than the underlying breccia unit. Figures A and D are zoomed out and show more of the ejecta blanket as a whole. The crater is located to the right-hand side, the East, of each of those two images. Images are CaSSIS: A: MY34_004723_334_1_NPBwPAN and HiRISE: B: ESP_050321_1550_COLOR C: ESP_050176_1550_COLOR and D: ESP_050176_1550_RED. Courtesy NASA/JPL/HiRISE Team and ESA/Roscosmos/ExoMars/UniBe-CaSSIS
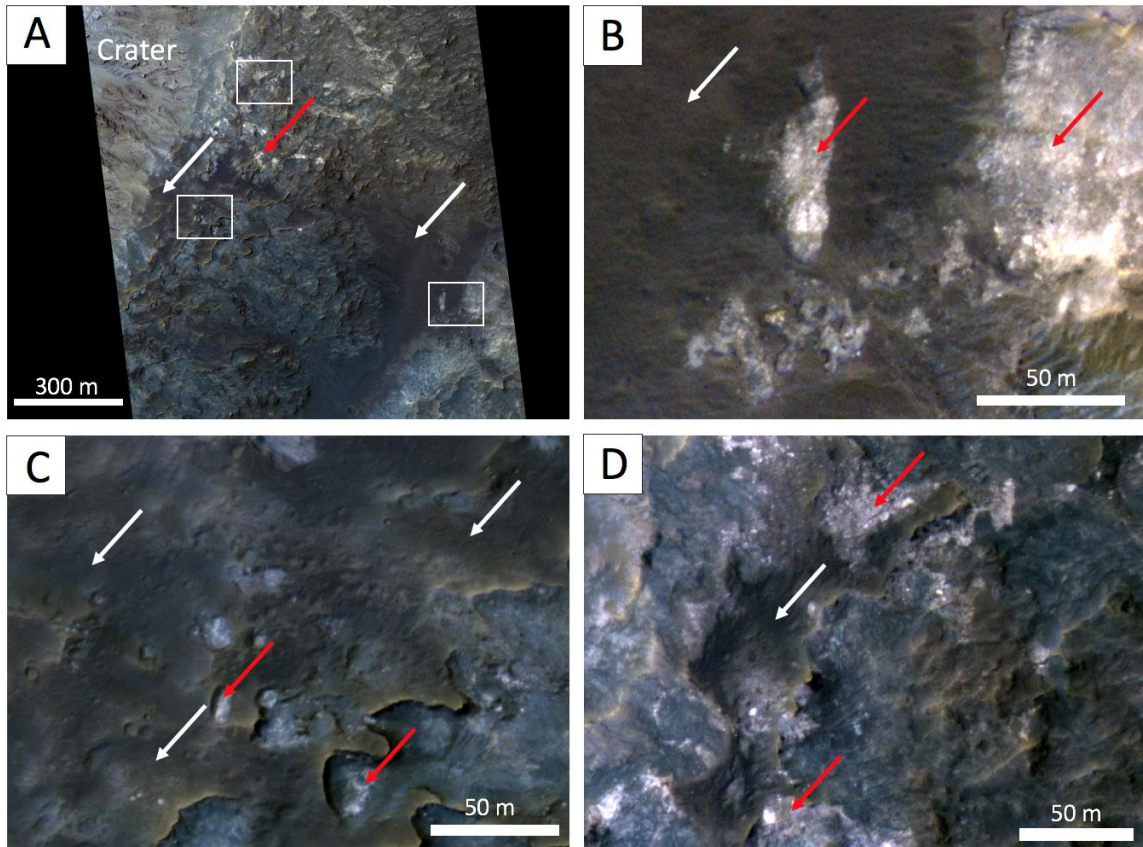
Figure 26 Scenes from the ejecta blanket of a crater in the Hellas Basin region (-16.18°N, 74.40°). The white arrows indicate smooth areas that are interpreted as an impact melt-bearing ejecta layer overlying a brecciated ballistic layer, indicated by red arrows. Large clasts are visible in the lower left corner of C. Taken from HiRISE image: ESP_050306_1635_COLOR. Courtesy NASA/JPL/HiRISE Team.

The impact melt units in Figures 24, 25, and 26 are all dark toned homogenous, low textured. Visible textures are reminiscent of ponds, flows and/or of crater-related pitted material, as discussed in Chapter 2, section 4.2. These three impact melt units also show evidence of clasts, much like at Hargraves Crater (Figure 26C). Figure 26C shows a good example with large clasts. The relationship between the two units is maintained across all of the craters, analogous to that observed at Hargraves Crater. The impact-melt rich unit consistently overlies the underlying breccia unit where visible. Furthermore, like Hargraves, there is a sharp and distinct contact between those units. This relationship is observed in some locations through the "windows" in the impact melt-bearing layer.

Examples of these windows are most clearly shown in Figures 24A, 26B, and 26C. Not all of the brecciated material is covered by impact melt rock, but it is never found overlying the impact melt rock either. This relationship between these two units across multiple craters is important to understanding the impact ejecta emplacement process. By seeing the inner structure of the ejecta, we have been able to connect the impact processes on Earth and Mars. We also are able to confirm that there are multiple phases of ejecta emplacement. Further study of these Hargraves-type craters and an exhaustive survey to locate other examples is necessary to develop our understanding of impact processes further.

One of the outstanding questions regarding Hargraves-type ejecta that will need to be addressed in future work, is the origin of these characteristics and features. Hargraves Crater, Kontum Crater, the unnamed Hellas region Crater, and the unnamed Noachis Terra crater have a number of collective characteristics that may help to explain the extent of exposure and preservation observed in these ejecta blankets. Part of what makes Hargraves-type ejecta blankets notable are the balance between preservation and exposure that allows for an overhead view of the "anatomy" of an ejecta blanket. The preservation of these craters has left the smooth impact layers of the ejecta visible, which have in turn protected the underlying ballistic layers. Erosion has concurrently exposed the sides of both layers and made them visible to orbital imagers. The low levels of deposition in Hargraves Crater also contribute to the exposure of the units. While there are a few bedforms present, there is not enough coverage to obscure the ejecta. Understanding the factors that result in this balance and consequently produce Hargraves-type ejecta blankets will help to find other examples of craters for further study of cratering processes. We note that additional examples need to be found for further analysis. But here we provide a preliminary examination of these four examples of Hargraves-type ejecta and provide speculation on the possible factors that may have provided the conditions for these craters to possess sufficient balance between preservation, exposure, deposition, and degradation.
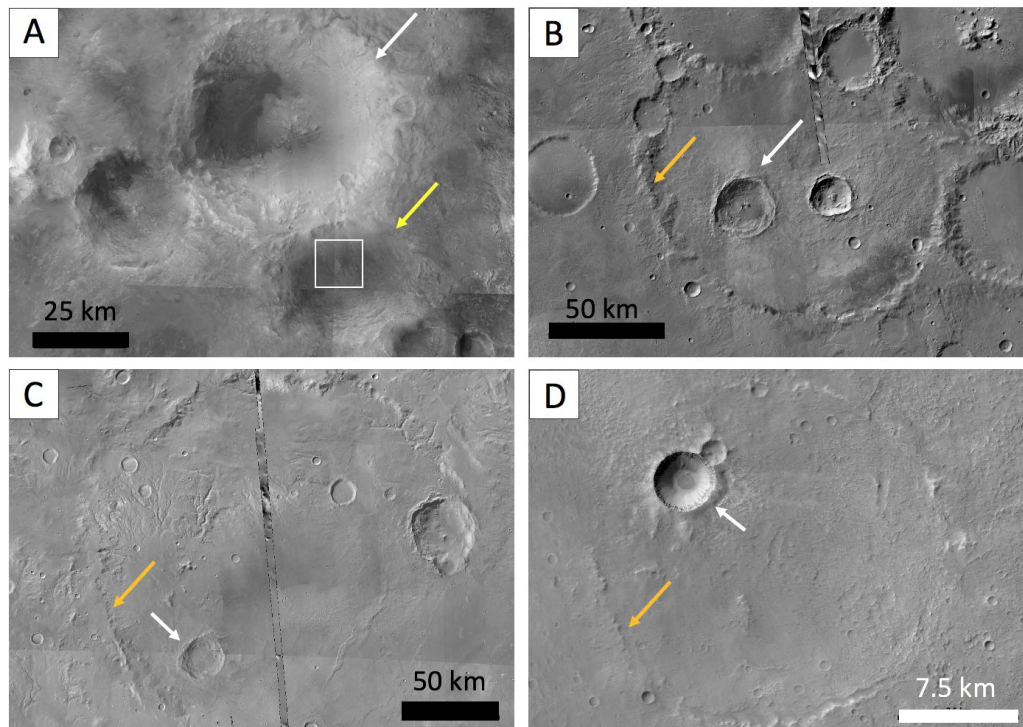
Figure 27 A collection of shots from the Murray Lab CTX Mosaic, overlain on the MOLA Global Mosaic to fill in data gaps. A is Hargraves Crater, B is a crater in Noachis Terra, C is Kontum Crater, and D is a crater in the Hellas region. Each crater is indicated with a white arrow. In A, the older crater on which Hargraves in superimposed is indicated with a yellow arrow, while a white box shows the location of the ejecta outcrop that is the focus of chapter 2. In B-D, an orange arrow indicates the rim of an older crater in which each crater formed. Courtesy Murray Lab and the CTX Team.

First, three of these impacts occur within depressions or in pre-existing degraded and infilled craters, depositing the ejecta blankets into the lower lying topography (Figure 27). The other crater, Hargraves Crater, has several features into which ejecta is deposited as well, including the older crater hosting the best-exposed outcrop. These shallow topographic depressions may be linked to the development of these features. We speculate that the protection offered by the pre-existing topography may contribute to the preservation of the ejecta and of the impact-melt layer. Funnelling of abrasive wind within these shallow topographic lows may contribute to both the erosion and

preservation of the ejecta, even as the topography protects the blanket as a whole. Previous studies have suggested that negative relief topographic features such as a crater or trough can accelerate winds and lead to increased, directed abrasion (Laity, 1987). There is also evidence that in the past, such as closer to when the ejecta at Hargraves Crater was deposited, there was greater aeolian activity on Mars (Edgett and Malin, 2000; Greeley et al., 2006). As a consequence, the less competent material, the fragmental unit is likely to have broken and easily been eroded away. While, it's possible that other means of erosion, such as glaciation or lacustrine influences, could be responsible for these characteristics, there is no conclusive evidence suggesting such an interpretation. Aeolian erosion is both precedented and the most consistent explanation for these features with the evidence presented. Beyond the location of the craters there are a few common characteristics that are not unexpected but are still present across all four craters and others that have been identified. All of the craters are large enough to produce impact melt, though certainly the smaller Hellas region crater produced less (Grieve and Cintala, 1992; Abramov et al., 2012). Additionally, the layered nature of the Hargrave-type ejecta is found relatively proximal to the crater, within the continuous ejecta deposits. The examples shown in Figures 24, 25, and 26 are all well within 2 crater radii of the crater rim.

For future work, a full survey of Mars identifying additional craters is necessary to continue studying Hargraves-type ejecta. The thermophysical signatures of these ejecta blankets, while not always diagnostic of Hargraves-type ejecta – this is due to being sensitive on the order of 10s of centimetres into the subsurface with TIR (e.g. Fergason et al., 2006) – can be also used to identify potential Hargraves-type ejecta blankets elsewhere on the surface of Mars. Additionally, more extensive use the HiRISE and CaSSIS imagers (see Chapter 1 for instrument description) are integral to identifying Hargraves-type crater ejecta. The colour capabilities of both imagers allow for the darker toned impact melt layers to be identified. While not yet utilized at Hargraves Crater in this study due to lack of data, the wider (9.5 km x 45 km), multiple colour CaSSIS image swath covers a large footprint and highlights the dark tones of impact melt, helping to reveal the relationship between the units and their place in the crater ejecta as a whole. The higher resolution (~25 cm/px) and colours of HiRISE allow for the identification of

individual breccia fragments and the observation of clasts within the impact melt layer, the largest of which are barely resolvable. Then, examining these common factors and others should be explored further, comparing across the different examples of Hargraves-type ejecta and considering evidence of aeolian patterns and topographic factors. One starting place might be to examine the THEMIS TIR mosaic patterns and compare for evidence of degradation or wind patterns that are common across the example craters. Additionally, at Hargraves Crater itself, tying the high-resolution images to any available compositional data, such as THEMIS, may lead to a better understanding of the Hargraves units within the context of the local geology, which would lead to a deeper understanding of the crater ejecta and its origins. These ideas for further study are integral to future space studies on Mars. Both orbital and rover missions study the heavily cratered surface of Mars. The unique insight into the interior of ejecta blankets offered by this study and future studies of Hargraves-type ejecta deposits provides invaluable knowledge to those missions and our understanding of Mars geology as a whole.

References

Abramov, O., Wong, S.M., Kring, D.A., 2012. Differential melt scaling for oblique impacts on terrestrial planets. Icarus 218, 906–916. https://doi.org/https://doi.org/10.1016/j.icarus.2011.12.022

Ahrens, T.J., O'Keefe, J.D., 1972. Shock melting and vaporization of lunar rocks and minerals. Moon 4, 214–249. https://doi.org/10.1007/BF00562927

Artemieva, N.A., Wünnemann, K., Krien, F., Reimold, W.U., Stöffler, D., 2013. Ries crater and suevite revisited-Observations and modeling Part II: Modeling. Meteorit. Planet. Sci. 48, 590–627. https://doi.org/10.1111/maps.12085

Barlow, N.G., 2005. A review of Martian impact crater ejecta structures and their implications for target properties, in: Kenkmann, T., Hörz, F., Deutsch, A. (Eds.), Large Meteorite Impacts III. Geological Society of America, p. 0. https://doi.org/10.1130/0-8137-2384-1.433

Barlow, N.G., Boyce, J.M., Costard, F.M., Craddock, R.A., Garvin, J.B., Sakimoto, S.E.H., Kuzmin, R.O., Roddy, D.J., Soderblom, L.A., 2000. Standardizing the nomenclature of Martian impact crater ejecta morphologies. J. Geophys. Res. Planets 105, 26733–26738. https://doi.org/10.1029/2000JE001258

Barnouin-Jha, O.S., Schultz, P.H., 1999. Interactions between an impact generated ejecta curtain and an atmosphere. Int. J. Impact Eng. 23, 51–62. https://doi.org/https://doi.org/10.1016/S0734-743X(99)00061-5

Barnouin-Jha, O.S., Schultz, P.H., Lever, J.H., 1999. Investigating the interactions between an atmosphere and an ejecta curtain 1. Wind tunnel tests. J. Geophys. Res. E Planets 104, 27105–27115. https://doi.org/10.1029/1999JE001026

Berger, J.A., Schmidt, M.E., Gellert, R., Campbell, J.L., King, P.L., Flemming, R.L., Ming, D.W., Clark, B.C., Pradler, I., VanBommel, S.J. V, Minitti, M.E., Fairén, A.G., Boyd, N.I., Thompson, L.M., Perrett, G.M., Elliott, B.E., Desouza, E., 2016. A global Mars dust composition refined by the Alpha-Particle X-ray Spectrometer in Gale Crater. Geophys. Res. Lett. 43, 67–75. https://doi.org/10.1002/2015GL066675

Berman, D.C., Balme, M.R., Michalski, J.R., Clark, S.C., Joseph, E.C.S., 2018. High-resolution investigations of Transverse Aeolian Ridges on Mars. Icarus 312, 247–266. https://doi.org/https://doi.org/10.1016/j.icarus.2018.05.003

Boyce, J., Barlow, N., Mouginis-Mark, P., Stewart, S., 2010. Rampart craters on Ganymede: Their implications for fluidized ejecta emplacement. Meteorit. Planet. Sci. 45, 638–661. https://doi.org/10.1111/j.1945-5100.2010.01044.x

Boyce, J.M., Garbeil, H., 2007. Geometric relationships of pristine Martian complex impact craters, and their implications to Mars geologic history. Geophys. Res. Lett. 34. https://doi.org/10.1029/2007GL029731

Boyce, J.M., Wilson, L., Mouginis-Mark, P.J., Hamilton, C.W., Tornabene, L.L., 2012. Origin of small pits in martian impact craters. Icarus 221, 262–275. https://doi.org/https://doi.org/10.1016/j.icarus.2012.07.027

Bramble, M.S., Mustard, J.F., Salvatore, M.R., 2017. The geological history of Northeast Syrtis Major, Mars. Icarus 293, 66–93. https://doi.org/https://doi.org/10.1016/j.icarus.2017.03.030

Bray, V.J., Atwood-Stone, C., Neish, C.D., Artemieva, N.A., McEwen, A.S., McElwaine, J.N., 2018. Lobate impact melt flows within the extended ejecta blanket of Pierazzo crater. Icarus 301, 26–36. https://doi.org/https://doi.org/10.1016/j.icarus.2017.10.002

Bray, V.J., Tornabene, L.L., Keszthelyi, L.P., McEwen, A.S., Hawke, B.R., Giguere, T.A., Kattenhorn, S.A., Garry, W.B., Rizk, B., Caudill, C.M., Gaddis, L.R., van der Bogert, C.H., 2010. New insight into lunar impact melt mobility from the LRO camera. Geophys. Res. Lett. 37. https://doi.org/10.1029/2010GL044666

Carr, M.H., 1995. The Martian drainage system and the origin of valley networks and fretted channels. \jgr 100, 7479–7508. https://doi.org/10.1029/95JE00260

Carr, M.H., Crumpler, L.S., Cutts, J.A., Greeley, R., Guest, J.E., Masursky, H., 1977. Martian impact craters and emplacement of ejecta by surface flow. J. Geophys. Res. 82, 4055–4065. https://doi.org/10.1029/JS082i028p04055

Carr, M.H., Head, J.W., 2010. Geologic history of Mars. Earth Planet. Sci. Lett. 294, 185–203. https://doi.org/https://doi.org/10.1016/j.epsl.2009.06.042

Catling, D.C., 2014. Chapter 16 - Mars Atmosphere: History and Surface Interactions, in: Spohn, T., Breuer, D., Johnson, T.V.B.T.-E. of the S.S. (Third E. (Eds.), . Elsevier, Boston, pp. 343–357. https://doi.org/https://doi.org/10.1016/B978-0-12-415845-0.00016-5

Caudill, C.M., Osinski, G.R., Tornabene, L.L., Longstaffe, F.J., 2018. Degassing Pipes at the Ries Impact Structure as an Analogue for Crater-Related Pitted Materials, in: Lunar and Planetary Science Conference, Lunar and Planetary Science Conference. p. 2765.

Chao, E.C.T., 1976. Mineral-Produced High-Pressure Striae and Clay Polish: Key Evidence for Nonballistic Transport of Ejecta from Ries Crater. Science (80-.). 194, 615 LP – 618. https://doi.org/10.1126/science.194.4265.615-a

Christensen, P.R., Engle, E., Anwar, S., Dickenshied, S., Noss, D., Gorelick, N., Weiss-Malik, M., 2009. JMARS - A Planetary GIS, in: AGU Fall Meeting Abstracts. AA(Airzona State University, Tempe, AZ, USA), AB(Airzona State University, Tempe, AZ, USA), AC(Airzona State University, Tempe, AZ, USA), AD(Airzona State University, Tempe, AZ, USA), AE(Airzona State University, Tempe, AZ, USA), AF(Google Inc, Mountain V, pp. IN22A-06.

Christensen, P.R., Jakosky, B.M., Kieffer, H.H., Malin, M.C., McSween, H.Y., Nealson, K., Mehall, G.L., Silverman, S.H., Ferry, S., Caplinger, M., Ravine, M., 2004. The Thermal Emission Imaging System (THEMIS) for the Mars 2001 Odyssey Mission. Space Sci. Rev. 110, 85–130. https://doi.org/10.1023/B:SPAC.0000021008.16305.94

Delamere, W.A., Tornabene, L.L., McEwen, A.S., Becker, K., Bergstrom, J.W., Bridges, N.T., Eliason, E.M., Gallagher, D., Keszthelyi, L., Mattson, S., McArthur, G.K., Mellon, M.T., Milazzo, M., Russell, P.S., Thomas, N., 2010. Color imaging of Mars

by the High Resolution Imaging Science Experiment (HiRISE). Icarus 205, 38–52. https://doi.org/10.1016/J.ICARUS.2009.03.012

Dickson, J.L., Kerber, L.A., Fassett, C.I., Ehlmann, B.L., 2018. A Global, Blended CTX Mosaic of Mars with Vectorized Seam Mapping: A New Mosaicking Pipeline Using Principles of Non-Destructive Image Editing, in: Lunar and Planetary Science Conference.

Edgett, K.S., Cantor, B.A., Harrison, T.N., Kennedy, M.R., Lipkaman, L.J., Malin, M.C., Posiolova, L. V., Shean, D.E., 2010. Active and Recent Volcanism and Hydrogeothermal Activity on Mars, in: AAS/Division for Planetary Sciences Meeting Abstracts #42, AAS/Division for Planetary Sciences Meeting Abstracts. p. 34.06.

Edgett, K.S., Malin, M.C., 2000. New views of Mars eolian activity, materials, and surface properties: Three vignettes from the Mars Global Surveyor Mars Orbiter Camera. J. Geophys. Res. Planets 105, 1623–1650. https://doi.org/10.1029/1999JE001152

Edwards, C.S., Bandfield, J.L., Christensen, P.R., Fergason, R.L., 2009. Global distribution of bedrock exposures on Mars using THEMIS high-resolution thermal inertia. J. Geophys. Res. Planets 114. https://doi.org/10.1029/2009JE003363

Edwards, C.S., Nowicki, K.J., Christensen, P.R., Hill, J., Gorelick, N., Murray, K., 2011. Mosaicking of global planetary image datasets: 1. Techniques and data processing for Thermal Emission Imaging System (THEMIS) multi-spectral data. J. Geophys. Res. Planets 116. https://doi.org/10.1029/2010JE003755

Ehlmann, B.L., Mustard, J.F., 2012. An in-situ record of major environmental transitions on early Mars at Northeast Syrtis Major. Geophys. Res. Lett. 39. https://doi.org/10.1029/2012GL051594

Ehlmann, B.L., Mustard, J.F., Swayze, G.A., Clark, R.N., Bishop, J.L., Poulet, F., Des Marais, D.J., Roach, L.H., Milliken, R.E., Wray, J.J., Barnouin-Jha, O., Murchie, S.L., 2009. Identification of hydrated silicate minerals on Mars using MRO-CRISM: Geologic context near Nili Fossae and implications for aqueous alteration. J. Geophys. Res. Planets 114. https://doi.org/10.1029/2009JE003339

Engelhardt, W. V, Arndt, J., Fecker, B., Pankau, H.G., 1995. Suevite breccia from the Ries crater, Germany: Origin, cooling history and devitrification of impact glasses. Meteoritics 30, 279–293. https://doi.org/10.1111/j.1945-5100.1995.tb01126.x

Engelhardt, W. von, 1990. Distribution, petrography and shock metamorphism of the ejecta of the Ries crater in Germany—a review. Tectonophysics 171, 259–273. https://doi.org/https://doi.org/10.1016/0040-1951(90)90104-G

Engelhardt, W. von, Graup, G., 1984. Suevite of the ries crater, Germany: Source rocks and implications for cratering mechanics. Geol. Rundschau 73, 447–481. https://doi.org/10.1007/BF01824968

Fergason, R.L., Christensen, P.R., Kieffer, H.H., 2006. High-resolution thermal inertia derived from the Thermal Emission Imaging System (THEMIS): Thermal model and applications. J. Geophys. Res. Planets 111.

https://doi.org/10.1029/2006JE002735

Fisher, R. V, Schmincke, H.-U., 1984. Subaerial Fallout Tephra, in: Pyroclastic Rocks. Springer Berlin Heidelberg, Berlin, Heidelberg, pp. 125–162. https://doi.org/10.1007/978-3-642-74864-6_6

French, B.M., 1998. Traces of catastrophe: A handbook of shock-metamorphic effects in terrestrial meteorite impact structures. Lunar and Planetary Institute, Houston.

Frey, H., Sakimoto, S.E., Roark, J., 1998. The MOLA Topographic signature at the crustal dichotomy boundary zone on Mars. Geophys. Res. Lett. 25, 4409–4412. https://doi.org/10.1029/1998GL900095

Goudge, T.A., Mustard, J.F., Head, J.W., Fassett, C.I., Wiseman, S.M., 2015. Assessing the mineralogy of the watershed and fan deposits of the Jezero crater paleolake system, Mars. J. Geophys. Res. Planets 120, 775–808. https://doi.org/10.1002/2014JE004782

Grau Galofre, A., Jellinek, A.M., Osinski, G.R., 2020. Valley formation on early Mars by subglacial and fluvial erosion. Nat. Geosci. https://doi.org/10.1038/s41561-020-0618-x

Greeley, R., Arvidson, R.E., Barlett, P.W., Blaney, D., Cabrol, N.A., Christensen, P.R., Fergason, R.L., Golombek, M.P., Landis, G.A., Lemmon, M.T., McLennan, S.M., Maki, J.N., Michaels, T., Moersch, J.E., Neakrase, L.D. V, Rafkin, S.C.R., Richter, L., Squyres, S.W., de Souza Jr., P.A., Sullivan, R.J., Thompson, S.D., Whelley, P.L., 2006. Gusev crater: Wind-related features and processes observed by the Mars Exploration Rover Spirit. J. Geophys. Res. Planets 111. https://doi.org/10.1029/2005JE002491

Grieve, R.A.F., Ames, D.E., Morgan, J. V, Artemieva, N., 2010. The evolution of the Onaping Formation at the Sudbury impact structure. Meteorit. Planet. Sci. 45, 759–782. https://doi.org/10.1111/j.1945-5100.2010.01057.x

Grieve, R.A.F., Cintala, M.J., 1992. An Analysis of Differential Impact Melt-crater Scaling and Implications for the Terrestrial Impact Record. Meteoritics 27, 526. https://doi.org/10.1111/j.1945-5100.1992.tb01074.x

Grieve, R.A.F., Therriault, A.M., 2012. Impactites: Their Characteristics and Spatial Distribution. Impact Cratering, Wiley Online Books. https://doi.org/doi:10.1002/9781118447307.ch7

Hawke, B.R., Head, J.W., 1977. Impact melt on lunar crater rims., in: Roddy, D.J., Pepin, R.O., Merrill, R.B. (Eds.), Impact and Explosion Cratering: Planetary and Terrestrial Implications. pp. 815–841.

Head, J.W., Mustard, J.F., Kreslavsky, M.A., Milliken, R.E., Marchant, D.R., 2003. Recent ice ages on Mars. Nature 426, 797–802. https://doi.org/10.1038/nature02114

Hirt, C., Claessens, S.J., Kuhn, M., Featherstone, W.E., 2012. Kilometer-resolution gravity field of Mars: MGM2011. Planet. Space Sci. 67, 147–154. https://doi.org/https://doi.org/10.1016/j.pss.2012.02.006

Hörz, F., 1982. Ejecta of the Ries crater, Germany, in: Geological Implications of

Impacts of Large Asteroids and Comets on the Earth. Geological Society of America Boulder, pp. 39–55.

Horz, F., Ostertag, R., Rainey, D.A., 1983. Bunte Breccia of the Ries: Continuous Deposits of Large Impact Craters. Rev. Geophys. Sp. Phys. 21, 1667–1725.

Housen, K.R., Holsapple, K.A., 2011. Ejecta from impact craters. Icarus 211, 856–875. https://doi.org/10.1016/j.icarus.2010.09.017

Howard, K.A., Wilshire, H.G., 1975. Flows of impact melt at lunar craters. U. S. Geol. Surv. J. Res. 3, 237–251.

Kieffer, S.W., Simonds, C.H., 1980. The role of volatiles and lithology in the impact cratering process. Rev. Geophys. 18, 143–181. https://doi.org/10.1029/RG018i001p00143

Komatsu, G., Ori, G.G., Di Lorenzo, S., Rossi, A.P., Neukum, G., 2007. Combinations of processes responsible for Martian impact crater "layered ejecta structures" emplacement. J. Geophys. Res. Planets 112. https://doi.org/10.1029/2006JE002787

Kraal, E.R., Wong, M.P., Grosfils, E.B., Gilmore, M.S., Kozak, S.J., Reinen, L.A., 1998. The origin and modification of a trough in the Nili Fossae, Mars. Lunar Planet. Sci., XXIX.

Kremer, C.H., Mustard, J.F., Bramble, M.S., 2019. A widespread olivine-rich ash deposit on Mars. Geology 47, 677–681. https://doi.org/10.1130/G45563.1

Laity, J.E., 1987. Topographic Effects on Ventifact Development, Mojave Desert, California. Phys. Geogr. 8, 113–132. https://doi.org/10.1080/02723646.1987.10642315

Levy, J., Head, J., Marchant, D., 2009. Thermal contraction crack polygons on Mars: Classification, distribution, and climate implications from HiRISE observations. J. Geophys. Res. Planets 114. https://doi.org/10.1029/2008JE003273

Levy, J.S., Fassett, C.I., Head, J.W., Schwartz, C., Watters, J.L., 2014. Sequestered glacial ice contribution to the global Martian water budget: Geometric constraints on the volume of remnant, midlatitude debris-covered glaciers. J. Geophys. Res. Planets 119, 2188–2196. https://doi.org/10.1002/2014JE004685

Lowe, D.R., 1976. Grain flow and grain flow deposits. J. Sediment. Res. 46, 188–199. https://doi.org/10.1306/212F6EF1-2B24-11D7-8648000102C1865D

Mader, M.M., Osinski, G.R., 2018. Impactites of the Mistastin Lake impact structure: Insights into impact ejecta emplacement. Meteorit. Planet. Sci. 53, 2492–2518. https://doi.org/10.1111/maps.13173

Malin, M.C., Bell III, J.F., Cantor, B.A., Caplinger, M.A., Calvin, W.M., Clancy, R.T., Edgett, K.S., Edwards, L., Haberle, R.M., James, P.B., Lee, S.W., Ravine, M.A., Thomas, P.C., Wolff, M.J., 2007. Context Camera Investigation on board the Mars Reconnaissance Orbiter. J. Geophys. Res. Planets 112. https://doi.org/10.1029/2006JE002808

Mangold, N., Poulet, F., Mustard, J.F., Bibring, J.-P., Gondet, B., Langevin, Y., Ansan,

V., Masson, P., Fassett, C., Head III, J.W., Hoffmann, H., Neukum, G., 2007. Mineralogy of the Nili Fossae region with OMEGA/Mars Express data: 2. Aqueous alteration of the crust. J. Geophys. Res. Planets 112. https://doi.org/10.1029/2006JE002835

McCauley, J.F., 1973. Mariner 9 evidence for wind erosion in the equatorial and mid-latitude regions of Mars. J. Geophys. Res. 78, 4123–4137. https://doi.org/10.1029/JB078i020p04123

McEwen, A.S., Banks, M.E., Baugh, N., Becker, K., Boyd, A., Bergstrom, J.W., Beyer, R.A., Bortolini, E., Bridges, N.T., Byrne, S., Castalia, B., Chuang, F.C., Crumpler, L.S., Daubar, I., Davatzes, A.K., Deardorff, D.G., DeJong, A., Alan Delamere, W., Dobrea, E.N., Dundas, C.M., Eliason, E.M., Espinoza, Y., Fennema, A., Fishbaugh, K.E., Forrester, T., Geissler, P.E., Grant, J.A., Griffes, J.L., Grotzinger, J.P., Gulick, V.C., Hansen, C.J., Herkenhoff, K.E., Heyd, R., Jaeger, W.L., Jones, D., Kanefsky, B., Keszthelyi, L., King, R., Kirk, R.L., Kolb, K.J., Lasco, J., Lefort, A., Leis, R., Lewis, K.W., Martinez-Alonso, S., Mattson, S., McArthur, G., Mellon, M.T., Metz, J.M., Milazzo, M.P., Milliken, R.E., Motazedian, T., Okubo, C.H., Ortiz, A., Philippoff, A.J., Plassmann, J., Polit, A., Russell, P.S., Schaller, C., Searls, M.L., Spriggs, T., Squyres, S.W., Tarr, S., Thomas, N., Thomson, B.J., Tornabene, L.L., Van Houten, C., Verba, C., Weitz, C.M., Wray, J.J., 2010. The High Resolution Imaging Science Experiment (HiRISE) during MRO's Primary Science Phase (PSP). Icarus 205, 2–37. https://doi.org/10.1016/j.icarus.2009.04.023

McEwen, A.S., Eliason, E.M., Bergstrom, J.W., Bridges, N.T., Hansen, C.J., Delamere, W.A., Grant, J.A., Gulick, V.C., Herkenhoff, K.E., Keszthelyi, L., kirk, R.L., Mellon, M.T., Squyres, S.W., Thomas, N., Weitz, C.M., 2007. Mars reconnaissance orbiter's high resolution imaging science experiment (HiRISE). J. Geophys. Res. E Planets 112, 1–40. https://doi.org/10.1029/2005JE002605

Melosh, H.J., 1989. Impact cratering : a geologic process, New York : Oxford University Press ; Oxford : Clarendon Press. Tucson.

Mouginis-Mark, P.J., Garbeil, H., 2007. Crater geometry and ejecta thickness of the Martian impact crater Tooting. Meteorit. Planet. Sci. 42, 1615–1625. https://doi.org/10.1111/j.1945-5100.2007.tb00594.x

Mustard, J.F., Ehlmann, B.L., Murchie, S.L., 2009. Hydrothermal Alteration Constrained by Mineral Assemblages on Mars: Evidence from Craters Near Syrtis Major, in: AGU Fall Meeting Abstracts. pp. P13C-05.

Mustard, J.F., Poulet, F., Head, J.W., Mangold, N., Bibring, J.P., Pelkey, S.M., Fassett, C.I., Langevin, Y., Neukum, G., 2007. Mineralogy of the Nili Fossae region with OMEGA/Mars Express data: 1. Ancient impact melt in the Isidis Basin and implications for the transition from the Noachian to Hesperian. J. Geophys. Res. Planets 112. https://doi.org/10.1029/2006JE002834

Neumann, G.A., Zuber, M.T., Wieczorek, M.A., McGovern, P.J., Lemoine, F.G., Smith, D.E., 2004. Crustal structure of Mars from gravity and topography. J. Geophys. Res. Planets 109. https://doi.org/10.1029/2004JE002262

Newsom, H.E., Lanza, N.L., Ollila, A.M., Wiseman, S.M., Roush, T.L., Marzo, G.A.,

Tornabene, L.L., Okubo, C.H., Osterloo, M.M., Hamilton, V.E., Crumpler, L.S., 2010. Inverted channel deposits on the floor of Miyamoto crater, Mars. Icarus 205, 64–72. https://doi.org/https://doi.org/10.1016/j.icarus.2009.03.030

Oberbeck, V.R., 1975. The role of ballistic erosion and sedimentation in lunar stratigraphy. Rev. Geophys. 13, 337–362. https://doi.org/10.1029/RG013i002p00337

Oberbeck, V.R., Morrison, R.H., Horz, F., 1975. Transport and emplacement of crater and basin deposits, in: The Moon. D. Reidel Publishing Company, pp. 9–26.

Osinski, G.R., Grieve, R.A.F., Bleacher, J.E., Neish, C.D., Pilles, E.A., Tornabene, L.L., 2018. Igneous rocks formed by hypervelocity impact. J. Volcanol. Geotherm. Res. 353, 25–54. https://doi.org/https://doi.org/10.1016/j.jvolgeores.2018.01.015

Osinski, G.R., Grieve, R.A.F., Chanou, A., Sapers, H.M., 2016. The "suevite" conundrum, Part 1: The Ries suevite and Sudbury Onaping Formation compared. Meteorit. Planet. Sci. 51, 2316–2333. https://doi.org/10.1111/maps.12728

Osinski, G.R., Grieve, R.A.F., Spray, J.G., 2004. The nature of the groundmass of surficial suevite from the Ries impact structure, Germany, and constraints on its origin. Meteorit. Planet. Sci. 39, 1655–1683. https://doi.org/10.1111/j.1945-5100.2004.tb00065.x

Osinski, G.R., Grieve, R.A.F., Tornabene, L.L., 2012. Excavation and Impact Ejecta Emplacement. Impact Cratering, Wiley Online Books. https://doi.org/doi:10.1002/9781118447307.ch4

Osinski, G.R., Pierazzo, E., 2012. Impact Cratering: Processes and Products. Impact Cratering, Wiley Online Books. https://doi.org/doi:10.1002/9781118447307.ch1

Osinski, G.R., Silber, E.A., Clayton, J., Grieve, R.A.F., Hansen, K., Johnson, C.L., Kalynn, J., Tornabene, L.L., 2019. Transitional impact craters on the Moon: Insight into the effect of target lithology on the impact cratering process. Meteorit. Planet. Sci. 54, 573–591. https://doi.org/10.1111/maps.13226

Osinski, G.R., Tornabene, L.L., Grieve, R.A.F., 2011. Impact ejecta emplacement on terrestrial planets. Earth Planet. Sci. Lett. 310, 167–181. https://doi.org/10.1016/j.epsl.2011.08.012

Pike, R.J., 1980. Control of crater morphology by gravity and target type: Mars, Earth, Moon. Lunar Planet. Sci. Conf. Proc. 3, 2159–2189.

Robbins, S.J., Hynek, B.M., 2012. A new global database of Mars impact craters ≥1 km: 2. Global crater properties and regional variations of the simple-to-complex transition diameter. J. Geophys. Res. Planets 117. https://doi.org/10.1029/2011JE003967

Roberts, W.A., 1966. Shock-A process in extraterrestrial sedimentology. Icarus 5, 459–477. https://doi.org/10.1016/0019-1035(66)90059-5

Ryan, C.H., Tornabene, L.L., Cannon, K.M., Mustard, J.F., Sapers, H.M., Osinski, G.R., 2017. Geomorphological mapping of Hargraves ejecta in the Nili Fossae Trough: Insight into impact processes at potential Mars 2020 landing site. 48th Lunar Planet.

Sci. Conf. 2861.

Ryan, C.H., Tornabene, L.L., Osinski, G.R., Cannon, K.M., Mustard, J.F., MacRae, R.A., Corney, R., Sapers, H.M., 2016. Geomorphological Mapping of the Hargraves Ejecta and Polygonal Terrain Associated with the Candidate Mars 2020 Landing Site, Nili Fossae Trough. 47th Lunar Planet. Sci. Conf. Abstract #2524.

Scheller, E.L., Ehlmann, B.L., 2020. Composition, Stratigraphy, and Geological History of the Noachian Basement Surrounding the Isidis Impact Basin. J. Geophys. Res. Planets n/a, e2019JE006190. https://doi.org/10.1029/2019JE006190

Schneider, C.A., Rasband, W.S., Eliceiri, K.W., 2012. NIH Image to ImageJ: 25 years of image analysis. Nat. Methods 9, 671–675. https://doi.org/10.1038/nmeth.2089

Siegert, S., Branney, M.J., Hecht, L., 2017. Density current origin of a melt-bearing impact ejecta blanket (Ries suevite, Germany). Geology 45, 855–858. https://doi.org/10.1130/G39198.1

Stöffler, D., 1977. Research drilling Nördlingen 1973: Polymict breccias, crater basement, and cratering model of the Ries impact structure. Geol. Bavarica 75, 443–458.

Sturm, S., Kenkmann, T., Willmes, M., Pösges, G., Hiesinger, H., 2015. The distribution of megablocks in the Ries crater, Germany: Remote sensing, field investigation, and statistical analyses. Meteorit. Planet. Sci. 50, 141–171. https://doi.org/10.1111/maps.12408

Sturm, S., Wulf, G., Jung, D., Kenkmann, T., 2013. The ries impact, a double-layer rampart crater on earth. Geology 41, 531–534. https://doi.org/10.1130/G33934.1

Szwast, M.A., Richardson, M.I., Vasavada, A.R., 2006. Surface dust redistribution on Mars as observed by the Mars Global Surveyor and Viking orbiters. J. Geophys. Res. Planets 111. https://doi.org/10.1029/2005JE002485

Tanaka, K.L., Skinner, J.A., Hare, T.M., 2005. Geologic Map of the Northern Plains of Mars., U.S. Geological Survey Geologic Investigations. USGS. https://doi.org/10.3133/sim2888

Thomas, N., Cremonese, G., Ziethe, R., Gerber, M., Brändli, M., Bruno, G., Erismann, M., Gambicorti, L., Gerber, T., Ghose, K., Gruber, M., Gubler, P., Mischler, H., Jost, J., Piazza, D., Pommerol, A., Rieder, M., Roloff, V., Servonet, A., Trottmann, W., Uthaicharoenpong, T., Zimmermann, C., Vernani, D., Johnson, M., Pelò, E., Weigel, T., Viertl, J., De Roux, N., Lochmatter, P., Sutter, G., Casciello, A., Hausner, T., Ficai Veltroni, I., Da Deppo, V., Orleanski, P., Nowosielski, W., Zawistowski, T., Szalai, S., Sodor, B., Tulyakov, S., Troznai, G., Banaskiewicz, M., Bridges, J.C., Byrne, S., Debei, S., El-Maarry, M.R., Hauber, E., Hansen, C.J., Ivanov, A., Keszthelyi, L., Kirk, R., Kuzmin, R., Mangold, N., Marinangeli, L., Markiewicz, W.J., Massironi, M., McEwen, A.S., Okubo, C., Tornabene, L.L., Wajer, P., Wray, J.J., 2017. The Colour and Stereo Surface Imaging System (CaSSIS) for the ExoMars Trace Gas Orbiter. Space Sci. Rev. 212, 1897–1944. https://doi.org/10.1007/s11214-017-0421-1

Tornabene, L., Ryan, C., Cannon, K., Mustard, J., Osinski, G., Sapers, H., Pontefract, A.,

Bina, A., 2017. The Hargraves Ejecta Blanket: Opportunities for sampling diverse target and impact-related materials in the NFT landing ellipse, in: 3rd Landing Site Workshop for the Mars 2020 Rover Mission.

Tornabene, L.L., Osinski, G.R., McEwen, A.S., Boyce, J.M., Bray, V.J., Caudill, C.M., Grant, J.A., Hamilton, C.W., Mattson, S., Mouginis-Mark, P.J., 2012. Widespread crater-related pitted materials on Mars: Further evidence for the role of target volatiles during the impact process. Icarus 220, 348–368. https://doi.org/10.1016/j.icarus.2012.05.022

Tornabene, L.L., Watters, W.A., Osinski, G.R., Boyce, J.M., Harrison, T.N., Ling, V., McEwen, A.S., 2018. A depth versus diameter scaling relationship for the best-preserved melt-bearing complex craters on Mars. Icarus 299, 68–83. https://doi.org/https://doi.org/10.1016/j.icarus.2017.07.003

Wada, K., Barnouin-Jha, O.S., 2006. The formation of fluidized ejecta on Mars by granular flows. Meteorit. Planet. Sci. 41, 1551–1569. https://doi.org/10.1111/j.1945-5100.2006.tb00435.x

Weiss, B.P., Scheller, E., Gallegos, Z., Ehlmann, B.L., Lanza, N., Newsom, H.E., 2018. Field studies and numerical modeling., in: 49th Lunar and Planetary Science Conference. p. 1385.

Werner, S.C., 2005. Major aspects of the chronostratigraphy and geologic evolutionary history of Mars. Cuvillier Verlag.

Wichman, R., Schultz, P., 1989. Sequence and mechanisms of deformation around the Hellas and Isidis Impact Basins on Mars. J. Geophys. Res. Solid Earth 94, 17333–17357. https://doi.org/10.1029/JB094iB12p17333

Zuber, M.T., Solomon, S.C., Phillips, R.J., Smith, D.E., Tyler, G.L., Aharonson, O., Balmino, G., Banerdt, W.B., Head, J.W., Johnson, C.L., Lemoine, F.G., McGovern, P.J., Neumann, G.A., Rowlands, D.D., Zhong, S., 2000. Internal Structure and Early Thermal Evolution of Mars from Mars Global Surveyor Topography and Gravity. Science (80-.). 287, 1788 LP – 1793. https://doi.org/10.1126/science.287.5459.1788

Zurek, R.W., Smrekar, S.E., 2007. An overview of the Mars Reconnaissance Orbiter (MRO) science mission. J. Geophys. Res. Planets 112. https://doi.org/10.1029/2006JE002701

4

Appendices

Below are appendices A, B, and C. Appendix A shows coverage of two datasets relevant to this study. Appendix B contains records of the mapping of both units and clasts across the southern exposure of Hargraves Crater. Appendix C shows two of the full images used for the mapping of the southern exposure.

Appendix A: Publicly available HiRISE and CRISM (Compact Reconnaissance Imaging Spectrometer for Mars) coverage around Hargraves Crater of 08/04/2020. HiRISE is shown in cyan blue and CRISM coverage in white. Background mosaic is the Murray Lab CTX mosaic (Dickson et al. 2018). There is little overlap, making compositional analysis of higher resolution images difficult.
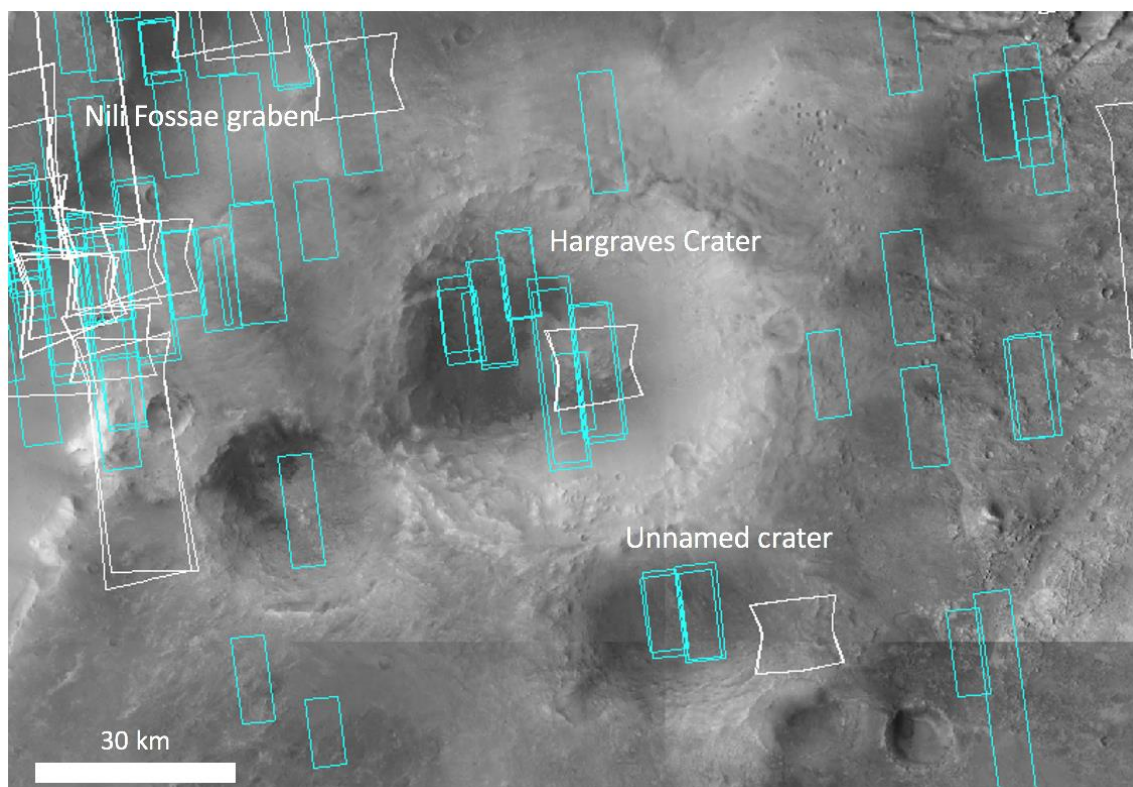
Appendix B1: Ten zones used to group measured clasts by distance. Green and blue polygons are clasts in the fragmental and smooth units respectively and the figure shows the distribution of measured clasts across the full image. The measured clasts are also overlain on the grayscale image of ESP_044161_2005 to show context and a closer version of the polygons. The image is ~1.2 km wide, for reference. The left image is the first five zones, the right is the second five zones.

~600 m
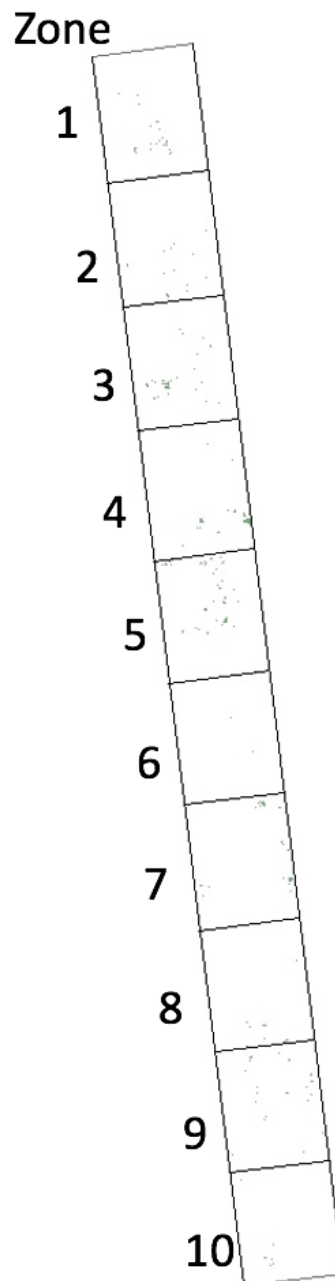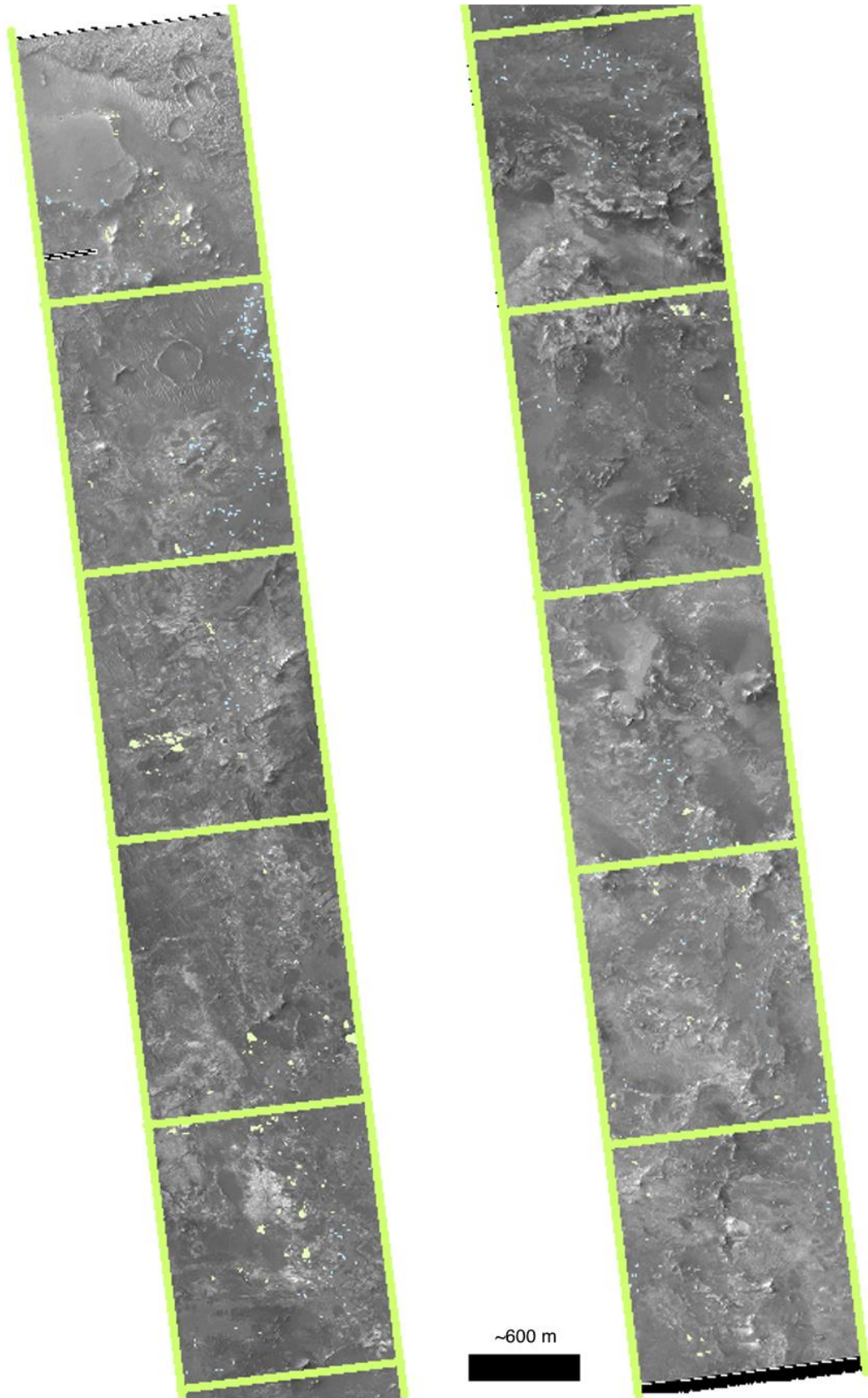
Appendix B2-B11: Left images indicate measured clasts in a given zone while right images overlay measured clasts on mapped units. Greens are the fragmental unit while pinks and purples are the smooth unit. Orange is an as yet unclassified unit. Green lines denote zone boundaries. Zones appear below in order from 1 to 10.

B2. Zone 1.
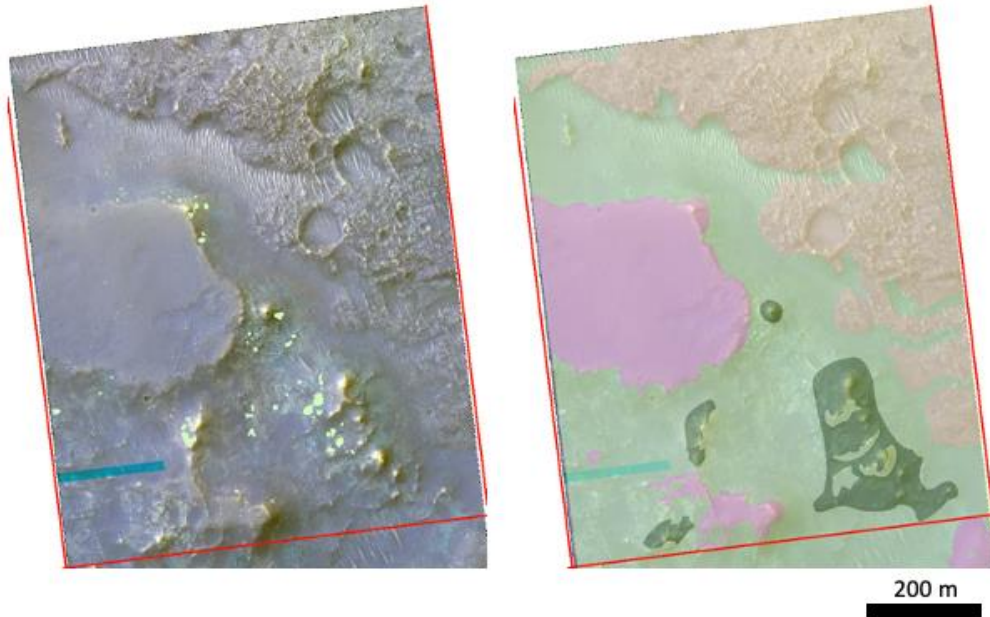
B3. Zone 2.
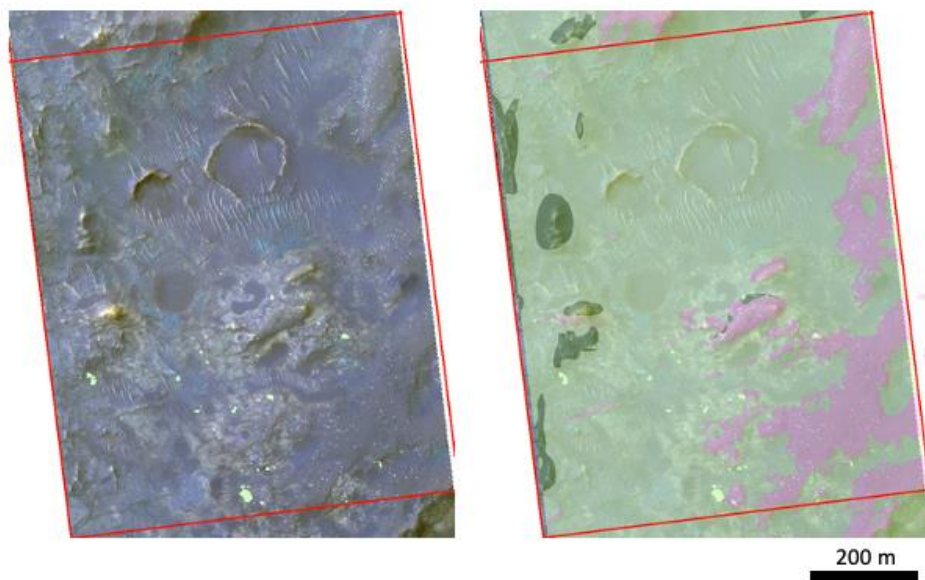
B4. Zone 3.
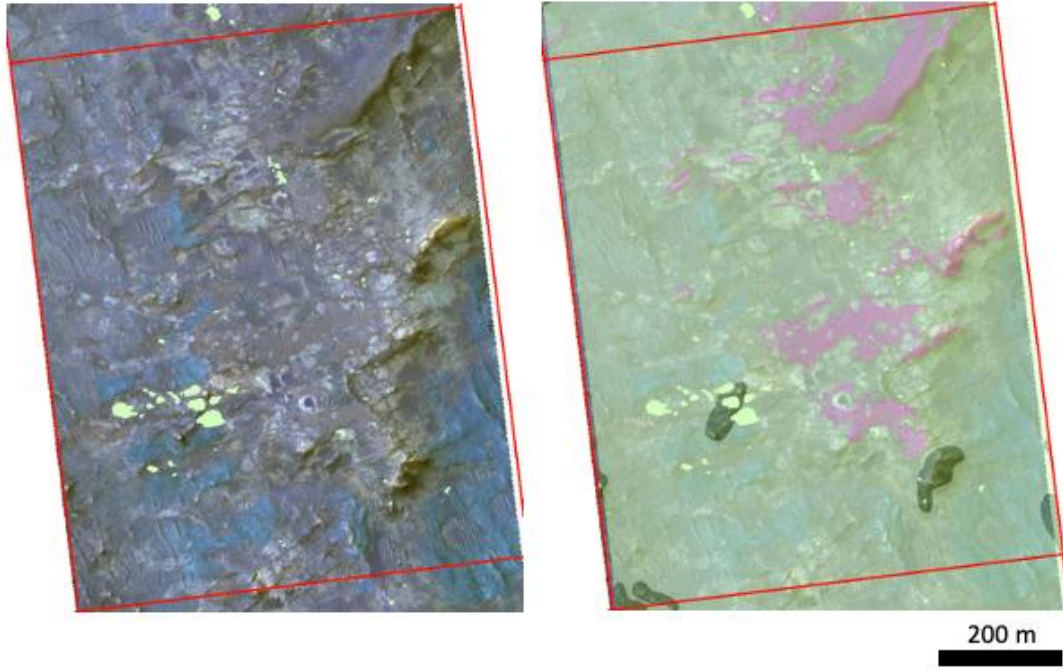
200 m

B5. Zone 4.
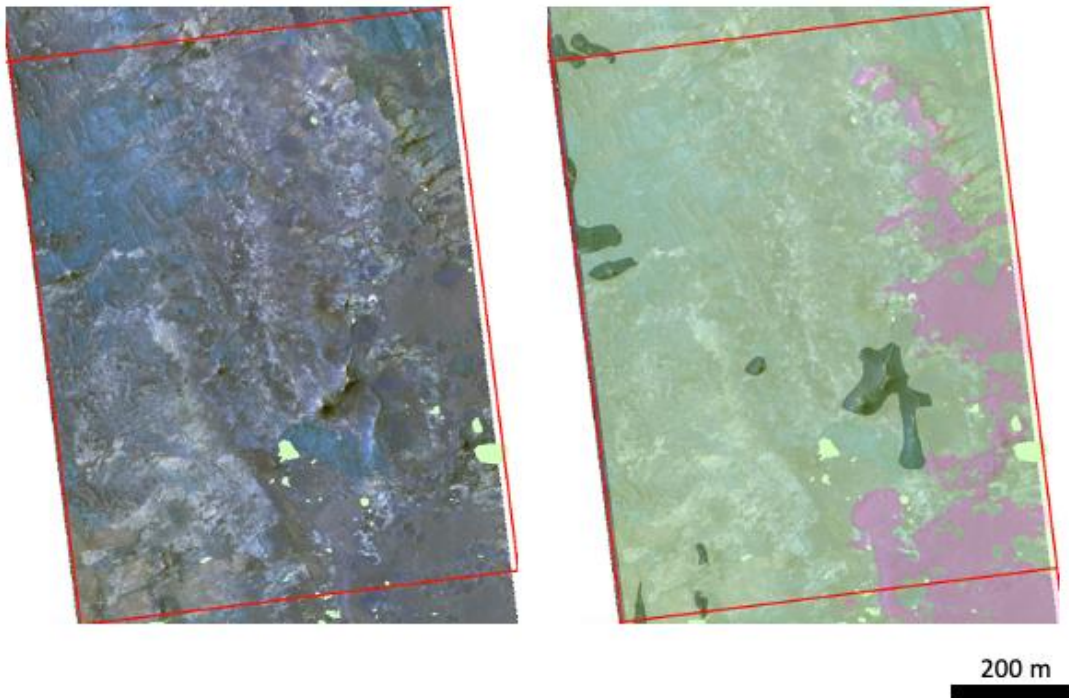
200 m

B6. Zone 5.
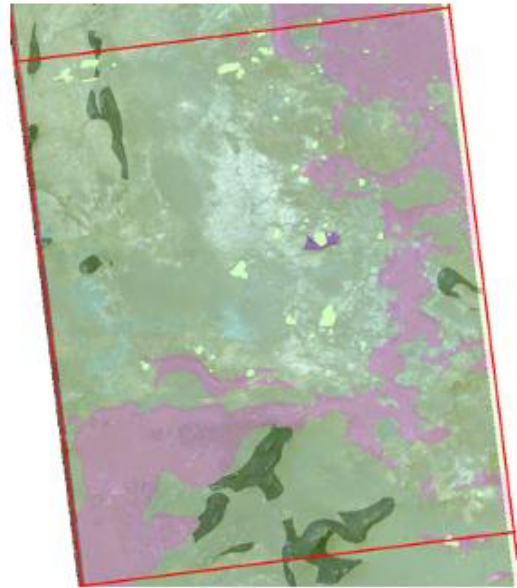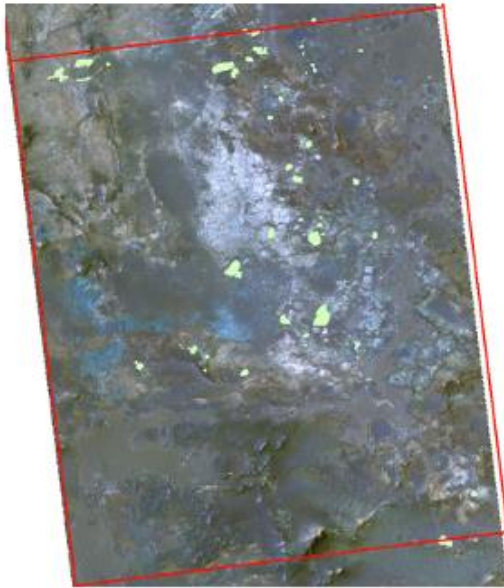
200 m

B7. Zone 6.
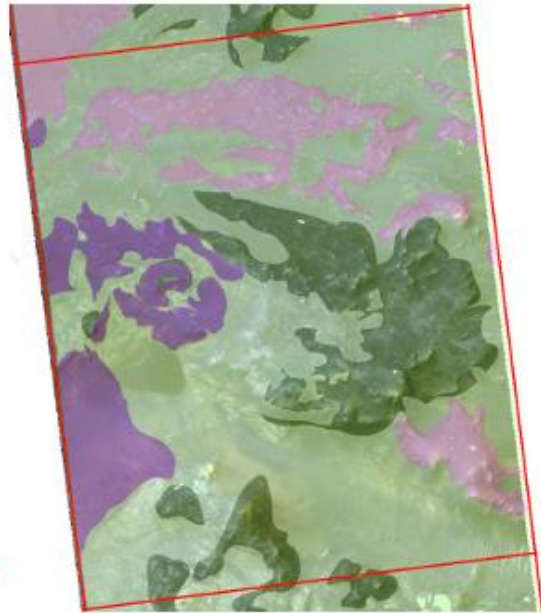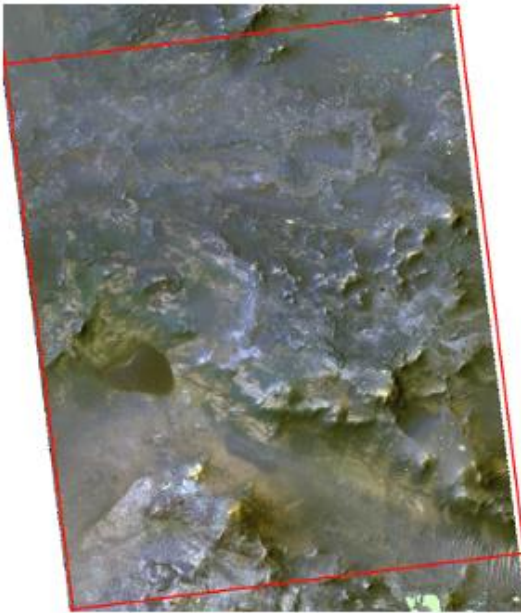
200 m

B8. Zone 7.

200 m

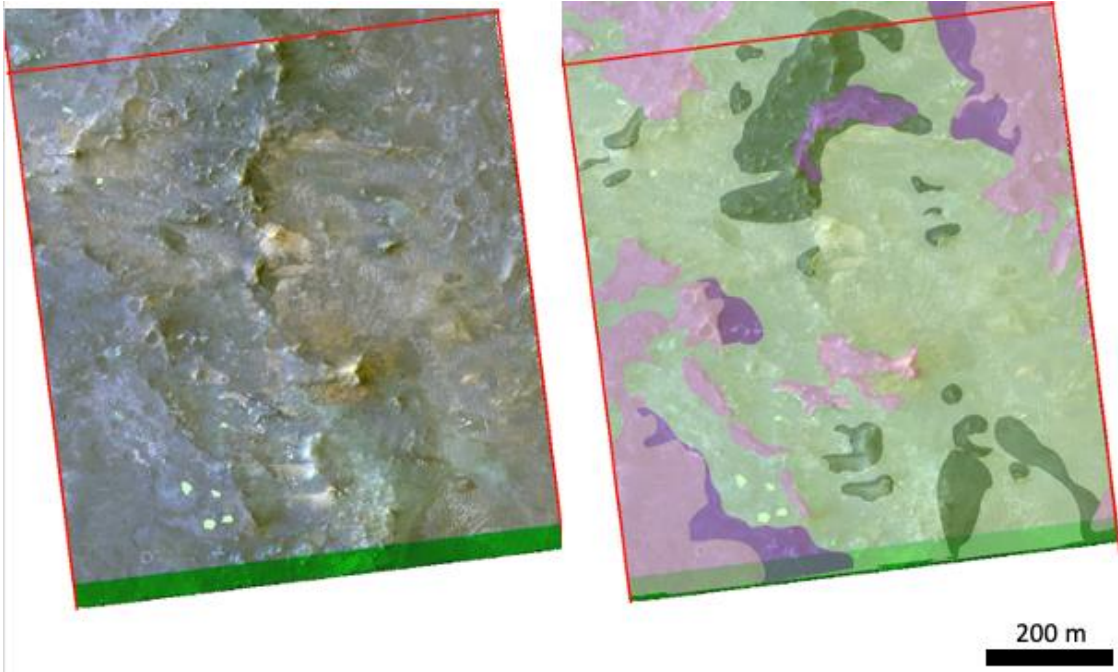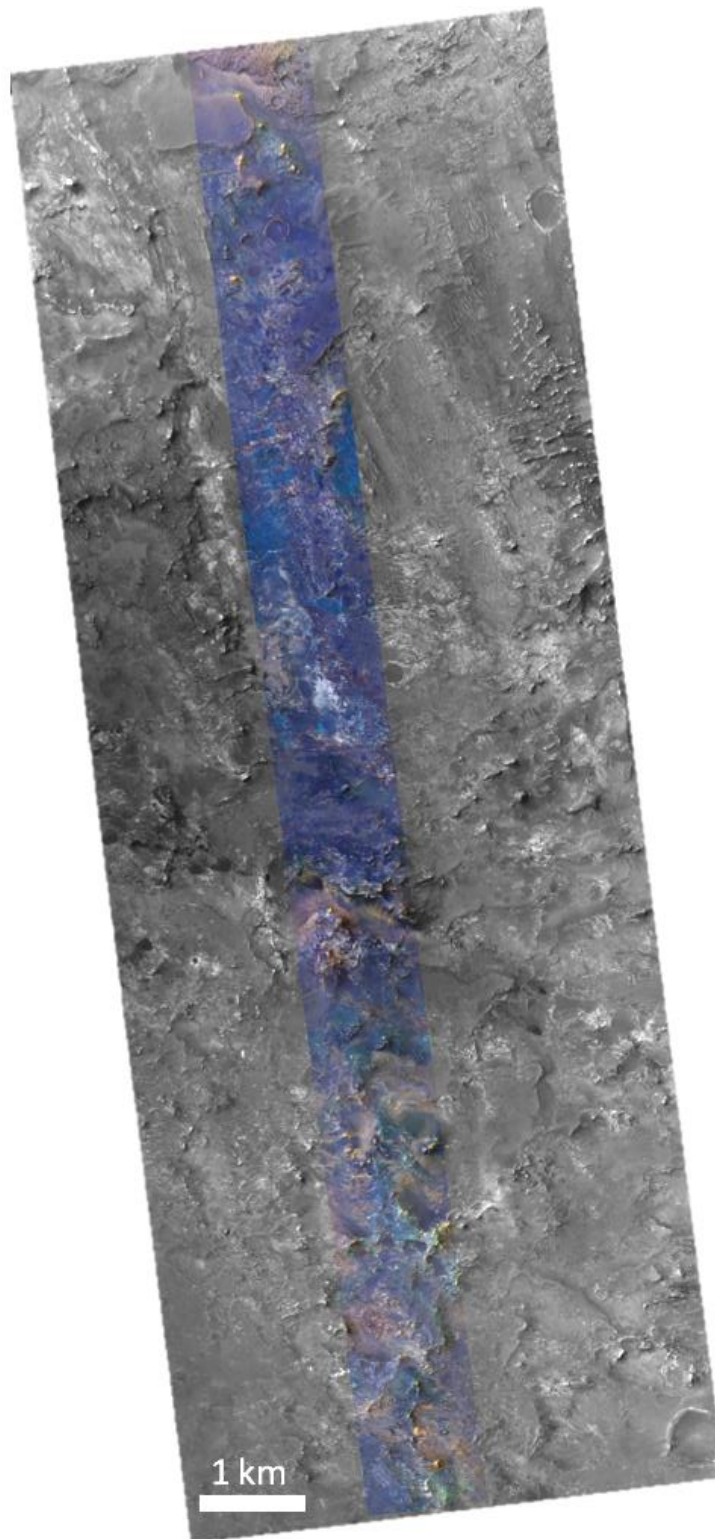**B9. Zone 8.**

200 m

B10. Zone 9.

200 m

B11. Zone 10.

200 m
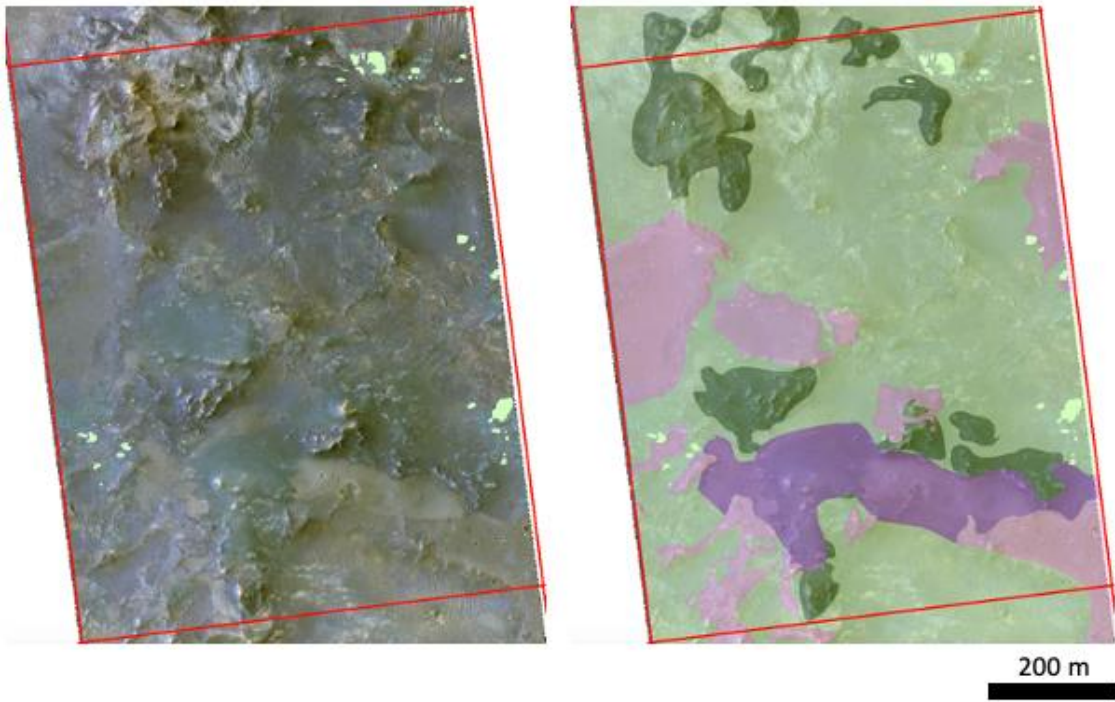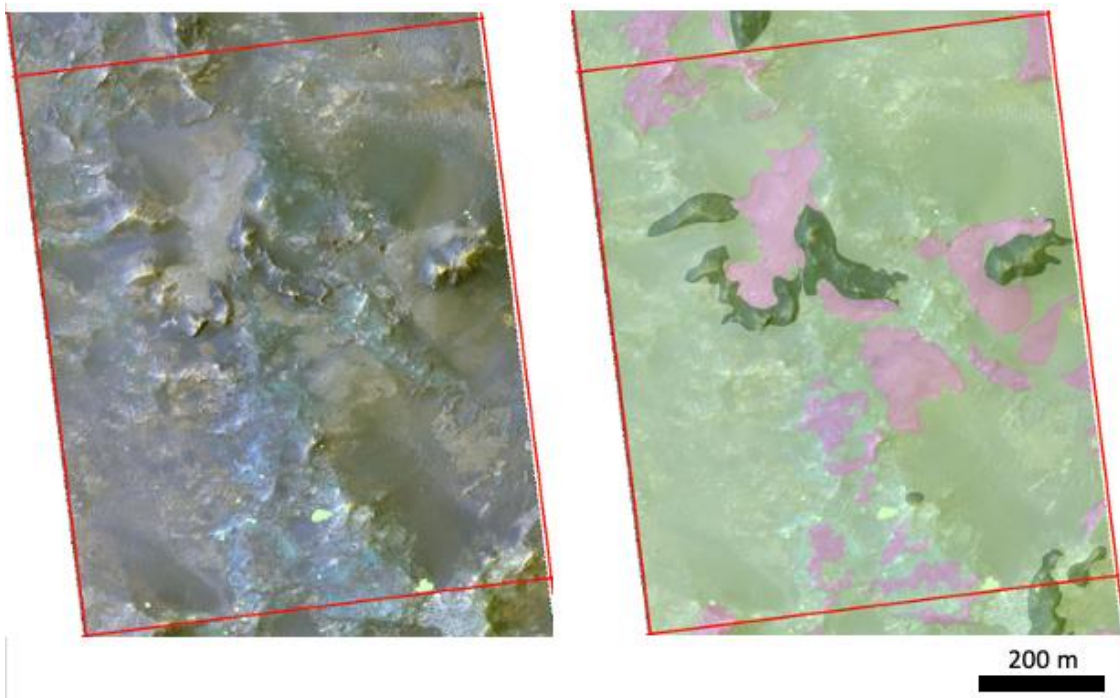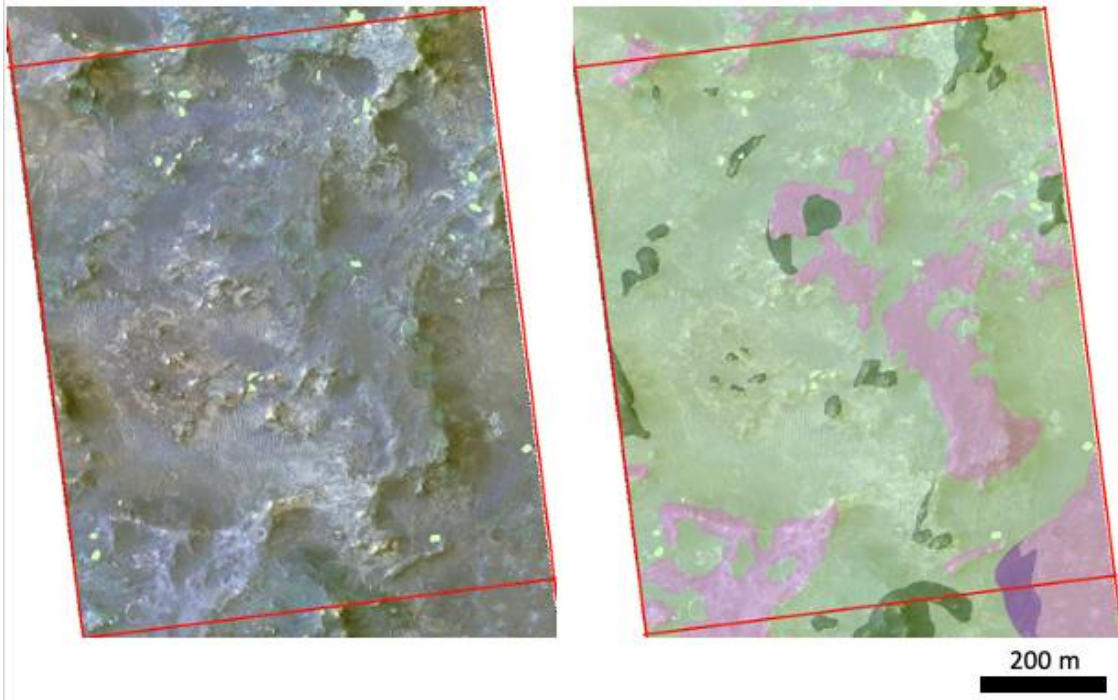
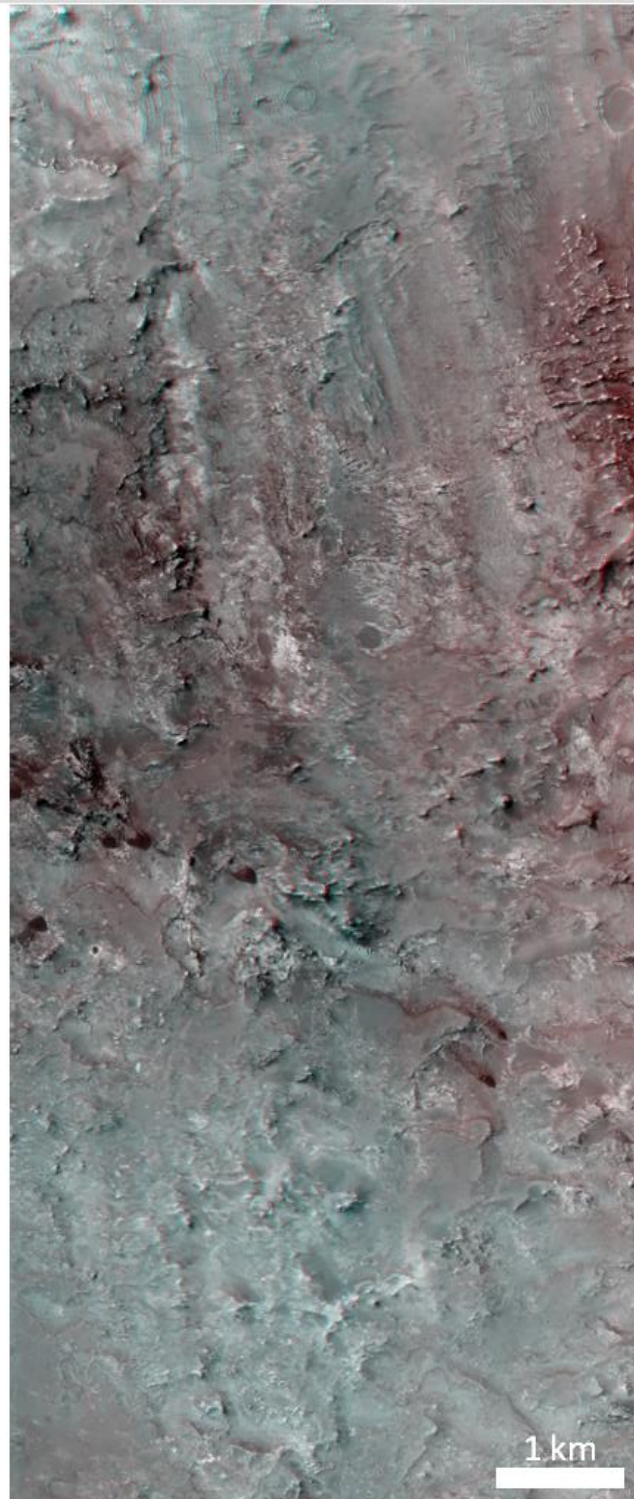**Appendix C: HiRISE MIRB (Merged Infrared – Red – Blue/Green) Image shows the IRB colour strip overlaid on the RED image for ESP_044161_2005.**

1 km

Appendix D: Anaglyph image made from HiRISE images ESP_044161_2005 and ESP_051321_2005. View with 3D glasses.

1 km

Curriculum Vitae

Name:	Leah Sacks
Post-secondary Education and Degrees:	Carleton College Northfield, Minnesota, United States of America 2013-2017 B.A. in Geology The University of Western Ontario London, Ontario, Canada 2018-2020 M.Sc. in Geology and Planetary Science *In Progress*
Honours and Awards:	Western Global Opportunities Scholarship 2020
Related Work Experience	Teaching Assistant The University of Western Ontario 2018-2020 Teaching Assistant Carleton College 2017 Summer Research Student USGS Astrogeology Science Centre 2016

Publications:

Edwards, C.S., Piqueux, S., Hamilton, V.E., Fergason, R.L., Herkenhoff, K.E., Vasavada, A.R., Bennett, K.A., **Sacks, L.,** Lewis, K., Smith, M.D., 2018. The Thermophysical Properties of the Bagnold Dunes, Mars: Ground-Truthing Orbital Data. J. Geophys. Res. Planets 123, 1307–1326. https://doi.org/10.1029/2017JE005501

Hill, P.J.A., Simpson, S.L., Xie, T., Morse, Z.R., **Sacks, L.E.,** Osinski, G.R., Cloutis, E.A., Caudill, C.M., Christoffersen, P., Marion, C.L., Newman, J.D., Pilles, E.A., Tornabene, L.L., 2020. CanMoon Science Interpretation Team: Insights into Volcanic Flows in Lanzarote, Spain, in: Lunar and Planetary Science Conference. p. 2152.

Morse, Z.R., Tornabene, L.L., **Sacks, L.E.,** Andres, C.N., Yingling, W.A., Osinski, G.R., Cloutis, E.A., Marion, C.L., Christoffersen, P.A., 2020. CanMoon Analogue Mission Pre-Mission Remote Sensing and Traverse Planning, in: Lunar and Planetary Science Conference. p. 1254.

Sacks, L.E., Edgar, L.A., Edwards, C.S., Anderson, R.B., 2017. Grain Scale Analyses of the Murray and Stimson Formations Using Data from the Mars Science Laboratory Mars Hand Lens Imager and the ChemCam Remote Micro Imager, in: Lunar and Planetary Science Conference. p. 2595.

Sacks, L.E., Edgar, L.A., Edwards, C.S., Anderson, R.B., 2016. Grain-Scale Analyses of Curiosity Data at Marias Pass, Gale Crater, Mars: Methods Comparison and Depositional Interpretation, in: AGU Fall Meeting Abstracts. AA(Carleton College, Northfield, MN, United States USGS Astrogeology Science Center, Flagstaff, AZ, United States), AB(USGS Astrogeology Science Center, Flagstaff, AZ, United States), AC(Department of Physics and Astronomy, Northern Arizona University, Fl, pp. P23B-2166.

Sacks, L.E., Tornabene, L.L., Osinski, G.R., McEwen, A.S., Sopoco, R.M., 2020. HiRISE Band Ratios and CRISM Spectral Results at Hargraves Crater, in: Lunar and Planetary Science Conference. p. 3014.

Sacks, L.E., Tornabene, L.L., Osinski, G.R., Sopoco, R., McEwen, A.S., 2019. Hargraves-Type Ejecta on Mars: Implications for Impact Ejecta Processes, in: Lunar and Planetary Science Conference.